https://ntrs.nasa.gov/search.jsp?R=19840004596 2020-03-21T01:38:04+00:00Z

General Disclaimer

One or more of the Following Statements may affect this Document

- This document has been reproduced from the best copy furnished by the organizational source. It is being released in the interest of making available as much information as possible.

- This document may contain data, which exceeds the sheet parameters. It was furnished in this condition by the organizational source and is the best copy available.

- This document may contain tone-on-tone or color graphs, charts and/or pictures, which have been reproduced in black and white.

- This document is paginated as submitted by the original source.

- Portions of this document are not fully legible due to the historical nature of some of the material. However, it is the best reproduction available from the original submission.

Produced by the NASA Center for Aerospace Information (CASI)

UNIVERSITY OF ILLINOIS
URBANA

AERONOMY REPORT NO. 111

OBSERVATIONS OF THE UPPER TROPOSPHERE AND LOWER STRATOSPHERE USING THE URBANA COHERENT-SCATTER RADAR

by
L. D. Goss
S. A. Bowhill

July 1, 1983

Library of Congress ISSN 0568-0581

(NASA-... 174594) OBSERVATIONS OF THE UPPER TROPOSPHERE AND LOWER STRATOSPHERE USING THE URBANA COHERENT-SCATTER RADAR (Illinois Univ.) 117 p HC A06/MF A01 CSCL 04A N84-12664
Uncias
G3/46 42944

Aeronomy Laboratory
Department of Electrical Engineering
University of Illinois
Urbana, Illinois

Supported by
National Aeronautics and Space Administration

UILU-ENG-83-2503

A E R O N O M Y R E P O R T

N O. 111

OBSERVATIONS OF THE UPPER ATMOSPHERE AND LOWER STRATOSPHERE USING THE URBANA COHERENT-SCATTER RADAR

by

L. D. Goss
S. A. Bowhill

July 1, 1985

Supported by
National Aeronautics
and Space Administration
Grant NSG 7506

Aeronomy Laboratory
Department of Electrical Engineering
University of Illinois
Urbana, Illinois

ABSTRACT

The Urbana coherent-scatter radar has been used to observe the upper troposphere and lower stratosphere, and 134 hours of data have been collected thus far. Horizontal wind measurements show good agreement with balloon-measured winds. Gravity waves are frequently observed, and are enhanced during convective activity. Updrafts and downdrafts are observed within thunderstorms. Power returns are related to hydrostatic stability, and changes in echo specularity are shown.

PRECEDING PAGE BLANK NOT FILMED

TABLE OF CONTENTS

LIST OF FIGURES

Figure | Page

1. INTRODUCTION

1.1 VHF Radar Probing of the Upper Troposphere and Lower Stratosphere

During the past few years, substantial progress has been made in radar-based studies of the dynamics of the middle atmosphere (approximately 10-100 km altitude). Much of this progress is due to the development of the MST (mesosphere-stratosphere-troposphere) radar technique. Many thorough reviews of the MST technique have appeared recently [Gage and Balsley, 1978; Green et al., 1979; Balsley and Gage, 1980; Rottger, 1980a; Harper and Gordon, 1980]. What follows are a short history of this technique and a discussion of some of its advantages over other atmospheric sensing techniques.

Radar-based investigation of the atmosphere has its historical roots in the early tropospheric radio propagation experiments of the 1930s. With the help of these experiments, it was recognized that atmospheric phenomena were responsible for the observed long distance propagation [duCastel, 1966]. Many of these observations were explained through the theory of tropospheric scatter propagation, developed by Booker and Gordon [1950].

The development of radar during World War II yielded radars sensitive enough to probe the structure of the troposphere. Much of this work depended upon backscatter from hydrometers at microwave frequencies. Unexplainable echoes from the clear air, known then as "angels," were also observed, however. Some of these echoes were subsequently explained by Hardy et al. [1966] as being caused by scattering from turbulent irregularities.

In the early 1960s, high-power VHF and UHF radars were designed and built primarily for ionospheric research. These radars measured backscatter

due to thermal motions of electrons. This type of scattering process is known as Thomson scatter or incoherent scatter. Several facilities were constructed, including: Arecibo, Puerto Rico, Millstone Hill (at Westford Massachusetts), and Jicamarca, Peru.

Mesospheric observations made at these facilities indicated the presence of backscatter which was too large to be caused by Thomson scatter alone. Bowles [1964] suggested that these returns were due to turbulence-induced scatter because of their similarity to ionospheric-scatter propagation signals. In 1974, the first measurements of winds and turbulence in the stratosphere and mesosphere were reported by Woodman and Guillen [1974], using the 50 MHz Jicamarca radar. They calculated the complex autocorrelation function of the scattered signal to obtain the Doppler shift, which in turn gives a measurement of the line-of-sight velocity of the scattering layer. The short-period fluctuations observed in these velocity measurements were attributed to gravity-wave activity. Since this radar technique uses phase information to calculate velocities, it is known as the coherent-scatter technique.

Since 1974, many other incoherent-scatter radars have been used to study the neutral atmosphere. In addition, many VHF radars have been designed and built primarily for coherent-scatter studies. These include: the Sunset radar in Colorado [Green et al., 1975]; the Platteville radar, also in Colorado [Ecklund et al., 1979]; the Poker Flat radar in Alaska [Balsley et al., 1980]; the SOUSY radar in Germany [Czechowsky et al., 1976]; the Urbana radar in Illinois [Miller et al., 1978]; and the MU radar in Japan [Fukao et al., 1980]. As of this writing, several other facilities are now in the planning stage.

Much attention has been focused on the MST technique because of its

advantages over other techniques in investigating the atmosphere. For the upper troposphere and lower stratosphere, comparisons of wind velocities have been made primarily with measurements by radiosondes. It has been shown by many investigators that these winds are in excellent agreement. However, radiosonde data are generally available only twice daily, while radar-measured winds are available on at least an hourly basis. This improvement in temporal resolution has several implications.

First, jet streams and fronts can be studied on a near-real-time basis. This information may be helpful for improving the accuracy of short-term local forecasts [Little, 1972]. The jet stream information may also be used by the commercial airlines to lower fuel consumption on flights. A recent paper by Carlson and Sundararaman [1982] reports an estimated 1-3% savings ($100-300 million) in fuel cost per year with improved wind data and flight planning.

Second, vertical velocities can be measured. These velocities have applications in studying convective development, cloud physics, turbulence, and transport of minor constituents. Studies of gravity waves and atmospheric stability are also possible, as discussed later in this work (e.g. Sections 3.3 and 4.1). The first operational wind profiling system, called PROFS (Prototype Regional Observations and Forecast System), is currently undergoing testing in Colorado [Strauch et al., 1982; Gage, 1983a].

1.2 Scattering Mechanisms

It is now recognized that several scattering mechanisms are responsible for clear-air radar backscatter at lower VHF frequencies with near-vertical antenna beams. These mechanisms can be divided into two major groups, those being turbulent scatter and Fresnel (or partial) reflection. Recent reviews

have covered these two groups quite thoroughly [Rottger, 1980b; Gage and Balsley, 1980]. Details of scattering theory are beyond the scope of this work. Instead, a short qualitative description of several possible scattering mechanisms is given below. These mechanisms are treated in more detail by Gage [1983b].

Two types of turbulent scattering are thought to contribute to clear-air echoes: isotropic and anisotropic. Isotropic turbulent scattering relies on active turbulence generating gradients of the refractive index. In addition, the probing radar wavelength must be sensitive to the scales of these gradients. The relevant theory was developed by Booker and Gordon [1950] to explain over-the-horizon VHF radio propagation, as discussed earlier. The largest scales of turbulence can become anisotropic, particularly in a density-stratified medium. Its horizontal correlation distance may become much larger than that in the vertical direction, producing an azimuthal dependence in echo strength.

When the radar beam is directed almost vertically, coherent structure in stable layers of the atmosphere produces additional returns. Reflection from a single thin layer (refractivity gradient) is known as Fresnel (or partial) reflection. This mechanism was also well-known from early propagation experiments. The term Fresnel reflection came about since these layers are thought to extend horizontally over a Fresnel zone. When more than one of these layers is present in the scattering volume (a random structure in the vertical), we have what is termed Fresnel scattering.

1.3 Objectives and Scope of This Study

The major objectives of this study are as follows:

1) To use the Urbana coherent-scatter radar to obtain power, velocity, and correlation time information from as much of the troposphere and

stratosphere as possible.

2) To relate the information obtained to many types of meteorological phenomena.

3) To provide a basis from which much more detailed studies can be undertaken.

Brief descriptions of both the Urbana radar and the various stages of data analysis are given in Chapter 2. Chapter 3 shows observations of clear-air winds and thunderstorms. Power levels and velocities over a 36-hour period are also shown. Further discussion of specific aspects of these observations appear in Chapter 4. Conclusions and suggestions for future research are given in Chapter 5.

2. EXPERIMENTAL TECHNIQUE

2.1 The Urbana MST Radar

2.1.1 Radar hardware. The Urbana radar is a monostatic, pulsed VHF radar. The radar transmitter has a peak pulse output power rating of 5 MW, although for this study it was operated at approximately 1 MW. The operating frequency is 40.92 MHz. Normal pulse widths are 10 μs and 20 μs, with 10 μs used predominantly for this work, at a pulse repetition frequency (PRF) of 400 Hz. More detailed descriptions of the transmitter subsystems can be found in Gibbs and Bowhill [1979], Hess and Geller [1976], and Herrington and Bowhill [1983].

The coherent-scatter antenna is a large array composed of 1008 half-wave dipoles divided into six groups. It has a physical aperture of 11,000 square meters and a half-power beamwidth of 3.6 x 4.8°. The antenna is connected to both the transmitter and receiver via a gas discharge transmit/receiver (T/R) switch, permitting monostatic operation. The normal pointing direction of the antenna is 1.5° off-vertical toward 36° south of east. A more detailed description of the antenna system can be found in Allman and Bowhill [1976].

2.1.2 Receiver recovery considerations. The monostatic operation of the Urbana radar results in a theoretical limit as to what the lowest observable altitude is. There are many factors which contribute to the determination of this altitude. By far the most important of these factors is the recovery time of the T/R switch. Gibbs and Bowhill [1979] report a 400 μsec recovery time for the T/R switch. Since $R = ct/2$, where R is the range, c is the speed of light, and t is the propagation time, the lowest observable altitude becomes 60 km (assuming range ≈ altitude for a 1.5°

zenith angle). Royrvik et al. [1982] report a lowest observable altitude of 40 km from these considerations.

With this information in mind, it was decided to construct a bistatic arrangement for low altitude observations. A 13-element Yagi antenna was strapped in a vertical position to a telephone pole which is used to support the antenna for the partial-reflection experiment at Urbana. A long coaxial cable connected the antenna directly to the blanker/preamplifier unit, bypassing the T/R switch. The lowest observable altitude for this system was found to be 6 km. The recovery time was due primarily to receiver saturation caused by the blanker pulse.

Power and velocity plots of data obtained using this system are shown in Figures 2.1 and 2.2, respectively. It is apparent from the amount of missing data in the velocity plot that the system is not sensitive enough. Another indication of lack of signal strength is the lack of power returns at stratospheric altitudes. As explained previously in Section 1.2, stratospheric returns should be stronger due to specular reflections from horizontally stratified layers. However, these returns were not present above 15 km.

Several investigations were then undertaken to determine if the usual monostatic operation of the radar could be adapted to collect low altitude data. It was found that the T/R switch recovery time was not as long as previously believed. Also, the scattered signal strength between 10 km and 20 km was found to be higher than that of the mesosphere, particularly near the tropopause. This large scattered power managed to overcome the attenuation caused by the T/R switch.

On June 17, 1982, data were taken with both the Yagi system and the monostatic system in consecutive 2 hour intervals. Data from the monostatic

ORIGINAL PAGE IS
OF POOR QUALITY

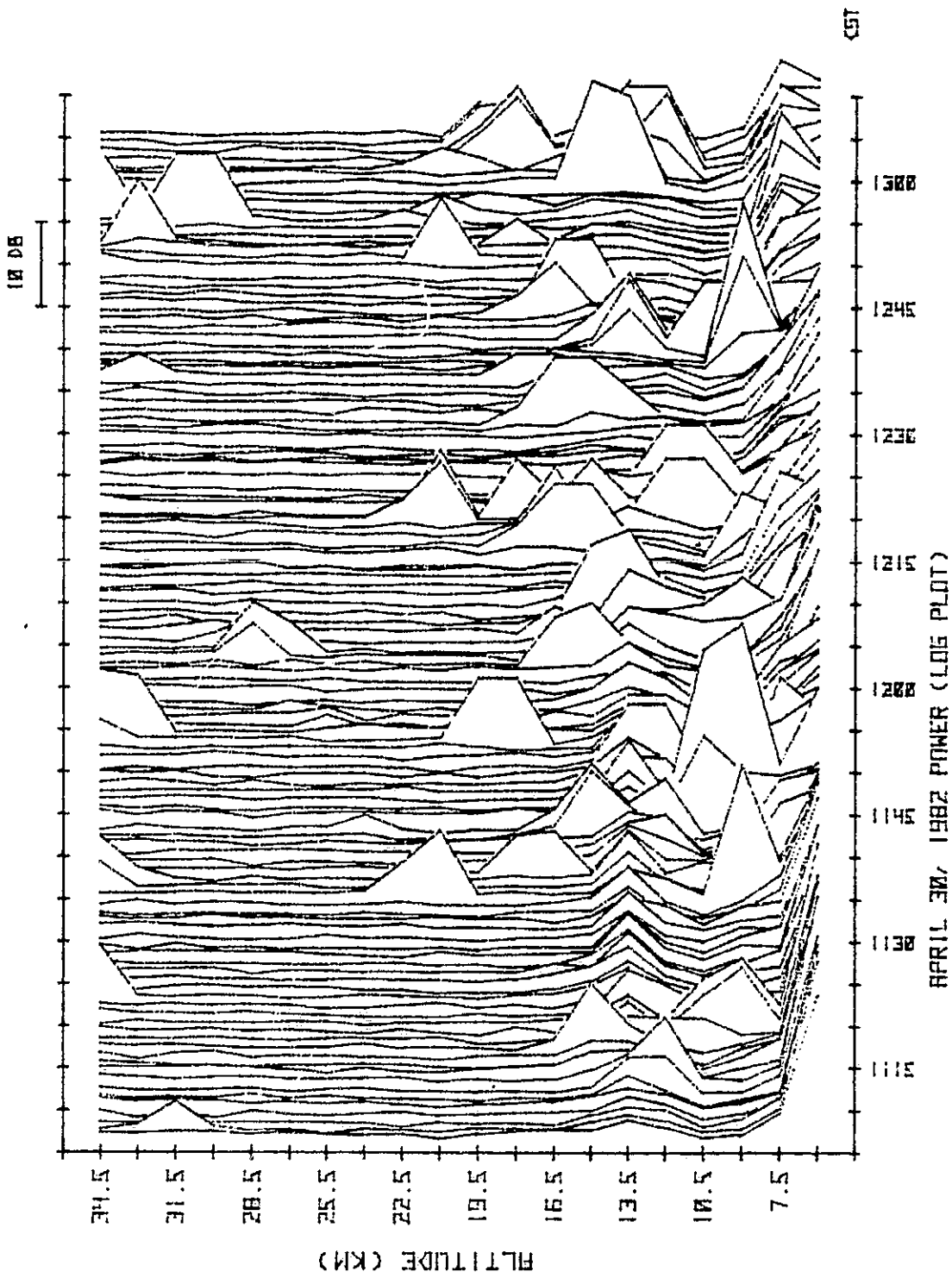

Figure 2.1 Vertical profile of scattered power beginning at 1106 CST on April 30, 1982 using Yagi system.

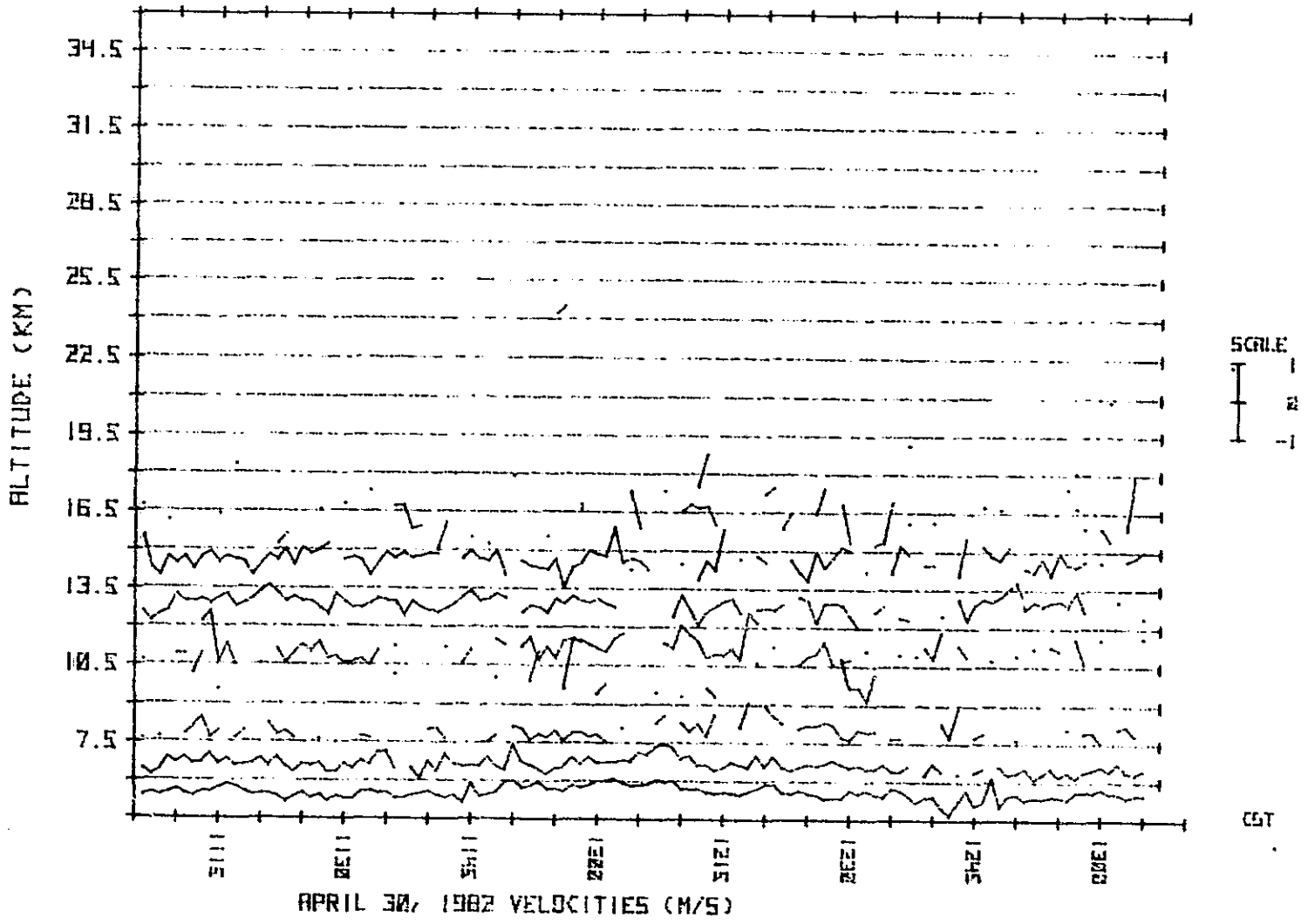

Figure 2.2 Line-of-sight velocity beginning at 1106 CST on April 30, 1982 using Yagi system.

ORIGINAL PAGE IS
OF POOR QUALITY

system is shown in Figure 2.3 and data from the Yagi system in 2.4. Velocities below 12 km in Figure 2.3 are contaminated with interference from the blanker and transmitter pulses. Comparison of the two figures clearly demonstrates the greater sensitivity of the monostatic system.

To be able to observe the lowest altitude possible, the transmitted pulse width was decreased from 20 μsec to 10 μsec, and the blanker pulse width was decreased from 70 μsec to 30 μsec, where the former values correspond to those used for mesospheric observation.

The monostatic system is capable of observing as low as 9 km. Scattered power and line-of-sight velocities are routinely obtained up to an altitude of 24 km. Figures 2.5 and 2.6 are plots of power and line-of-sight velocity, respectively, using the monostatic system. When compared to Figures 2.1 and 2.2 above, it is clear that the monostatic system provides a much greater amount of useful data.

2.2 Data Analysis Techniques

2.2.1 Autocorrelation function. The desired echo power and velocity data can be obtained through the use of either time domain or frequency domain techniques. At Urbana, the time domain technique is used. Therefore the autocorrelation function, formed from samples of the phase detector outputs, provides the foundation from which all other data are derived.

Details of how the power and velocity data are derived from the autocorrelation function, as well as how the function itself is computed are given by Gibbs and Bowhill [1979]. What follows herein are examples of the various stages of analysis which are available in plotted form.

2.2.2 Echo power. Scattered power at each of the 20 sample heights is obtained with one minute time resolution. These data are both collected and plotted in two-hour blocks. For all of the stratospheric data, scat-

ORIGINAL PAGE IS
OF POOR QUALITY

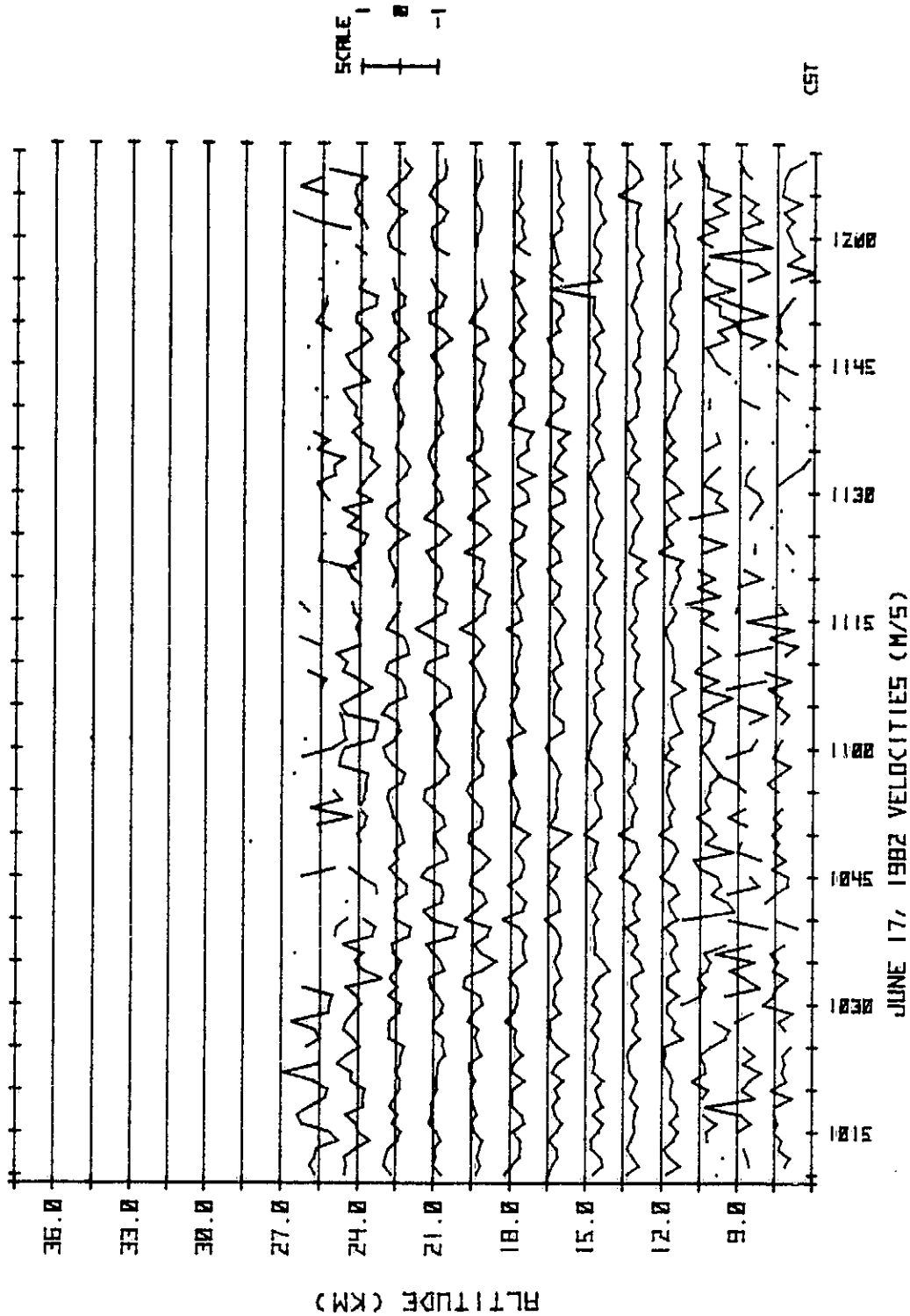

Figure 2.3 Line-of-sight velocity beginning at 1010 CST on June 17, 1982 using monostatic system.

ORIGINAL PAGE IS
OF POOR QUALITY

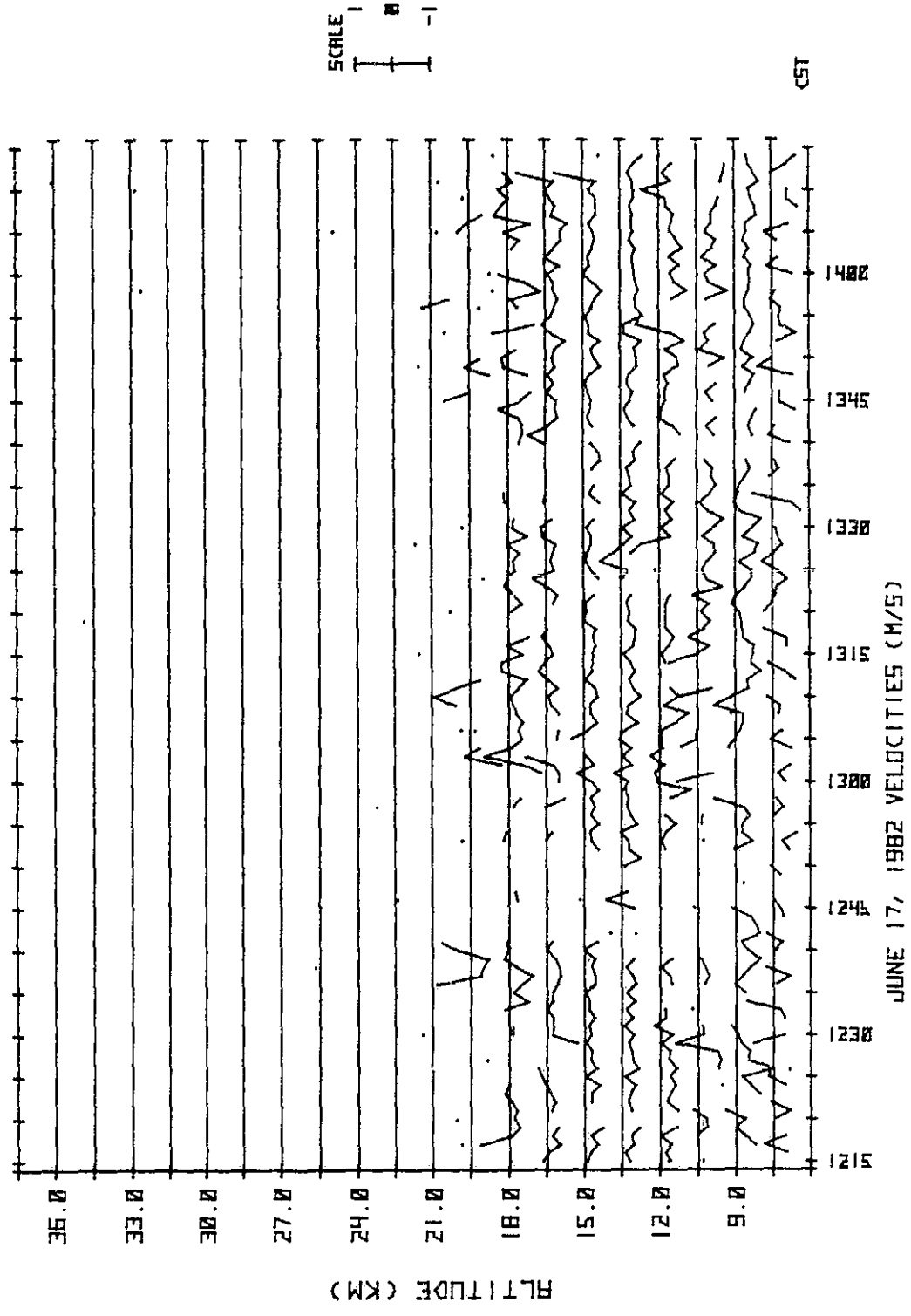

Figure 2.4 Line-of-sight velocity beginning at 1215 CST on June 17, 1982 using Yagi system.

ORIGINAL PAGE IS
OF POOR QUALITY

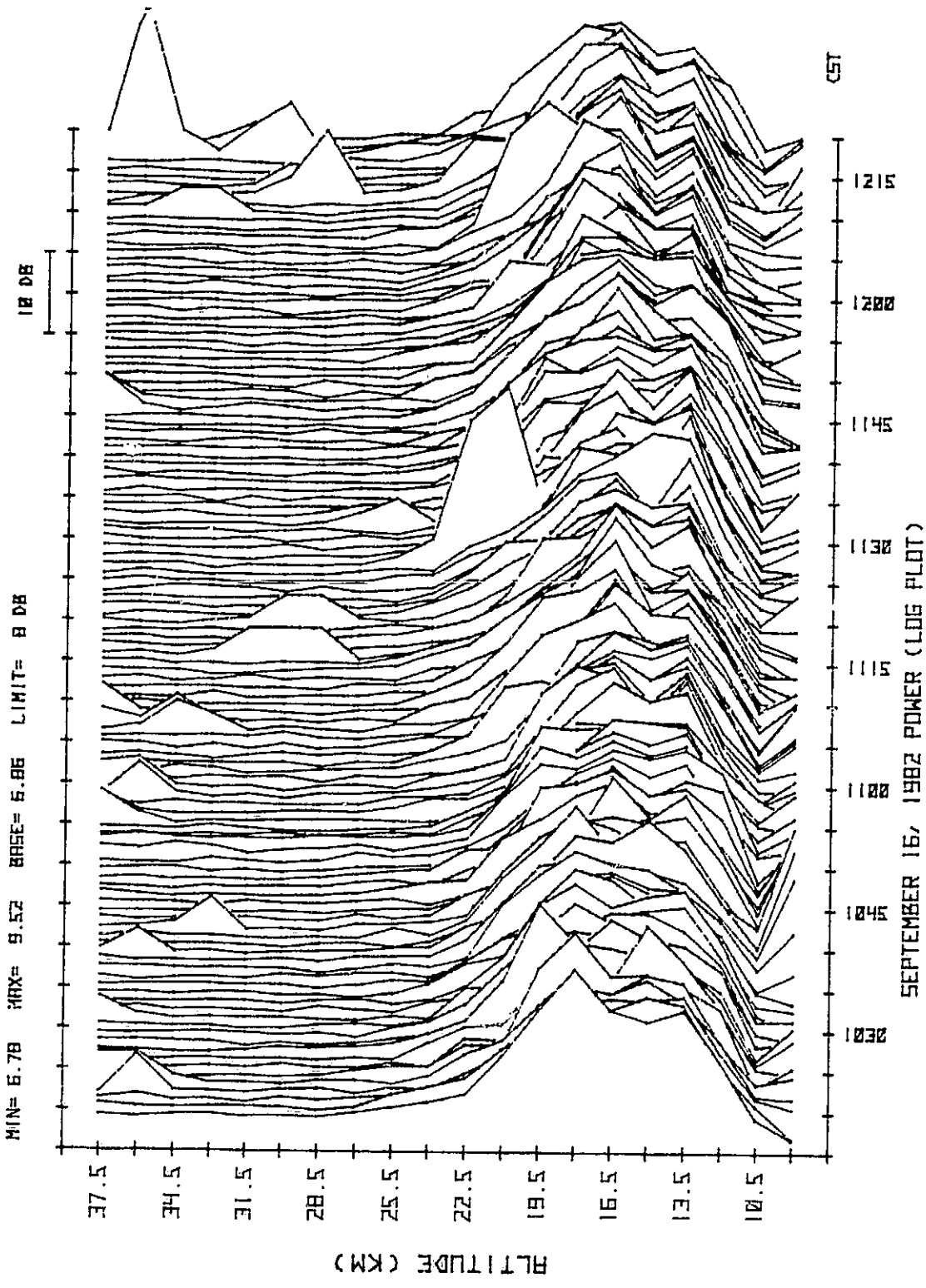

Figure 2.5 Vertical profile of scattered power beginning at 1016 CST on September 16, 1982 using monostatic system.

ORIGINAL PAGE IS
OF POOR QUALITY

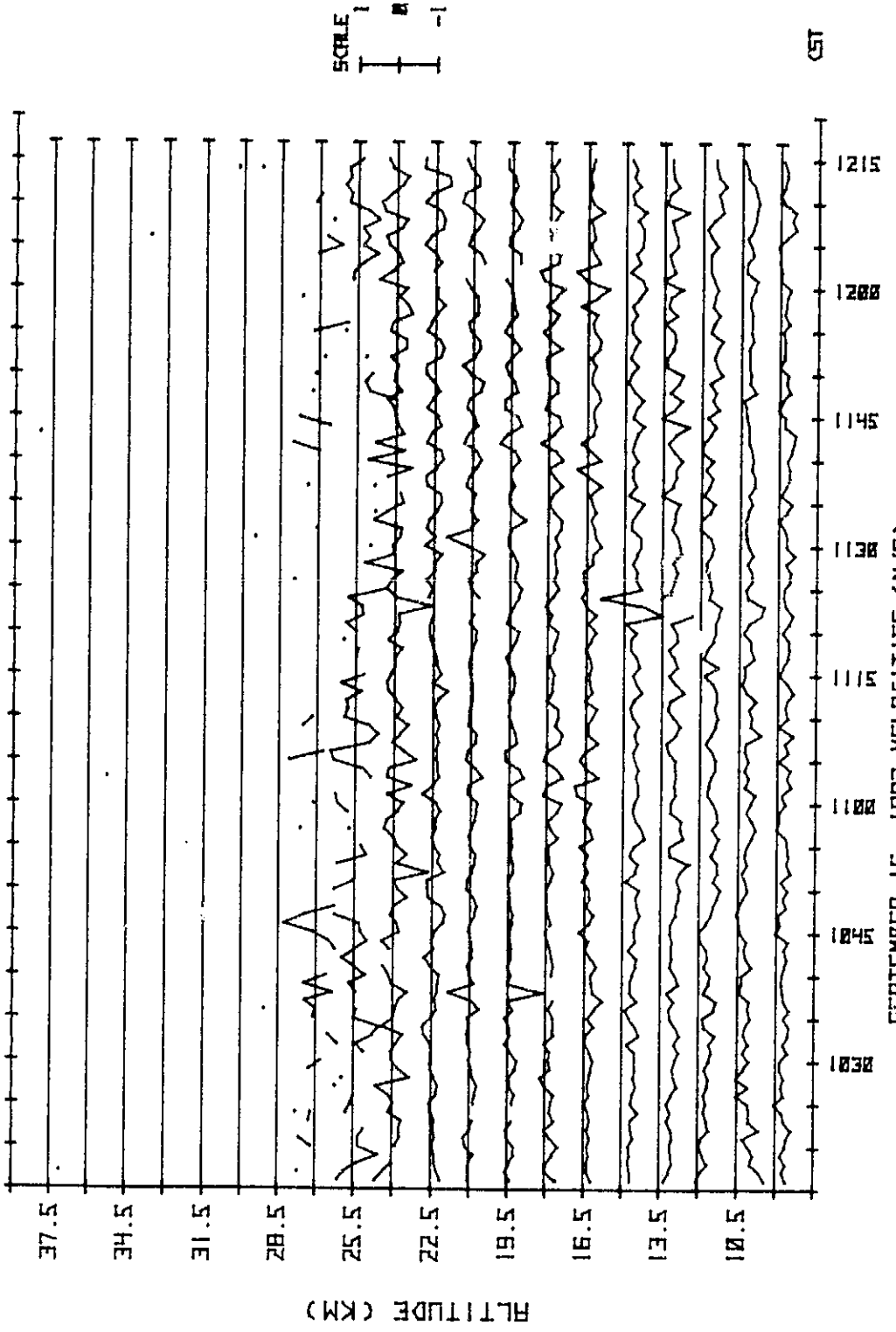

Figure 2.6 Line-of-sight velocity beginning at 1016 CST on September 16, 1982 using monostatic system.

tered power levels are below the noise floor in the region above 25 km. This highest observable altitude has two determining factors. First, echo power is know to decrease rapidly with altitude. Balsley and Gage [1980] report a 2 dB/km decrease with altitude in hourly-averaged echo power at Jicamarca, Peru. Second, the peak pulse power of the Urbana radar is limited to approximately 1 MW. The combined effect of these two factors produces a highest observable altitude of 25 km. Occasionally, however, there will be a spike return at ranges greater than 25 km lasting for 1 or 2 minutes. These are almost certainly caused by airplanes passing through sidelobes of the antenna pattern.

Two types of scattered power plots are available. The first gives scattered power at each sample altitude versus time. An example of this plot is shown in Figure 2.7. A 10 dB scale is shown at right. Note that the plotting algorithm for this diagram uses a hiding routine. For any two adjacent altitudes, the hiding routine is such that the curve for the higher altitude is plotted only if the power at that altitude exceeds an amount equal to 5 dB less than the power at the lower altitude.

The second type of scattered power plot gives the scattered power each minute versus altitude. This plot uses a hiding routine similar to the routine discussed above. In this case, however, the previous minute has priority instead of the lower altitude; the higher minute is plotted only if the power at that minute exceeds an amount equal to 1 dB less than the power at the previous minute. An example of this plot is shown in Figure 2.8.

2.2.3 Line-of-sight velocity. Velocities in the direction of the radar beam are also obtained on a minute-by-minute basis up to about 25 km. On these plots, a negative velocity at any altitude corresponds to motion away from the radar, and vice versa. The scale shown at right is usually

ORIGINAL PAGE IS
OF POOR QUALITY

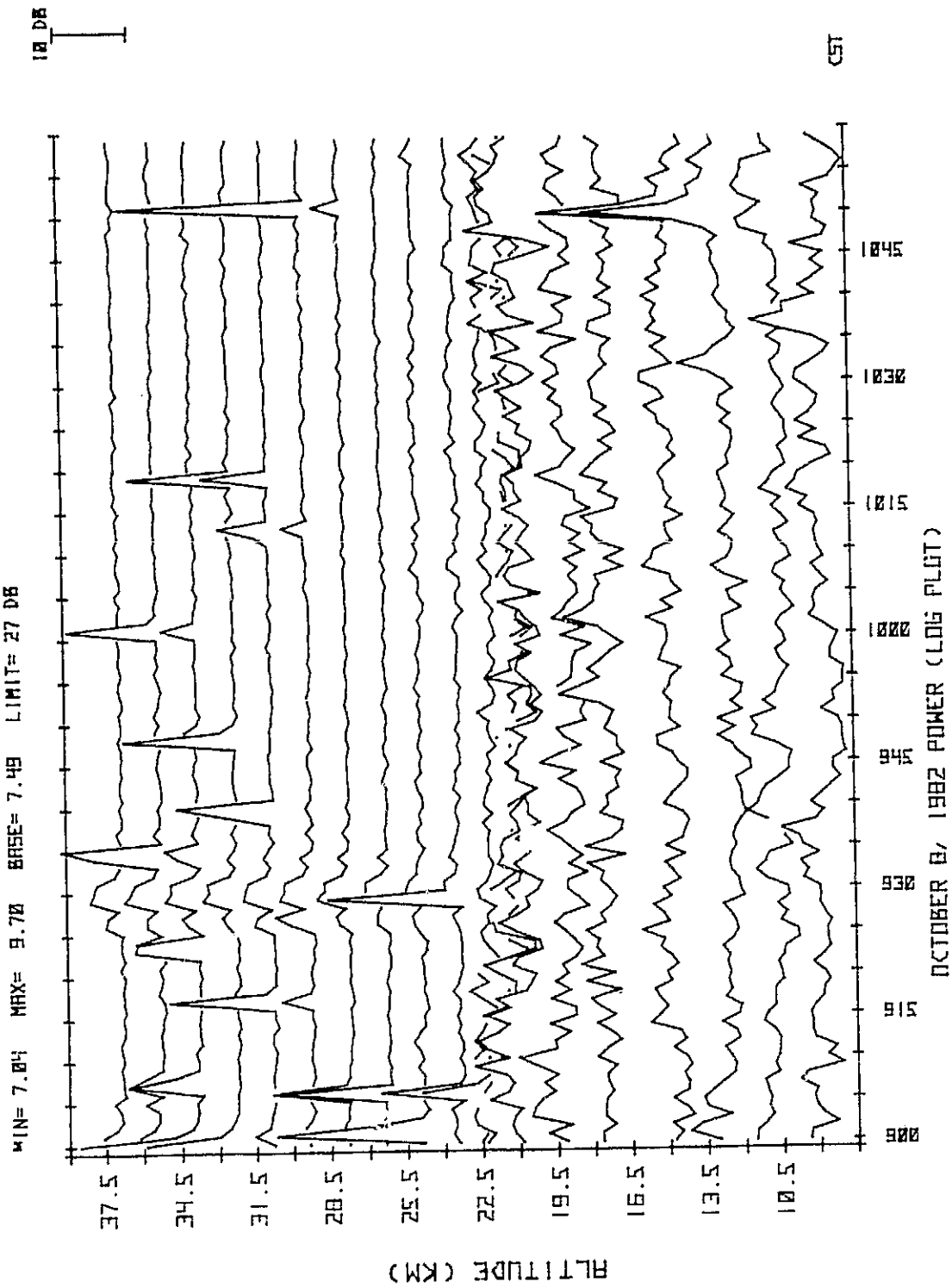

Figure 2.7 Scattered power at each sample altitude versus time beginning at 900 CST on October 8, 1982.

ORIGINAL PAGE IS
OF POOR QUALITY

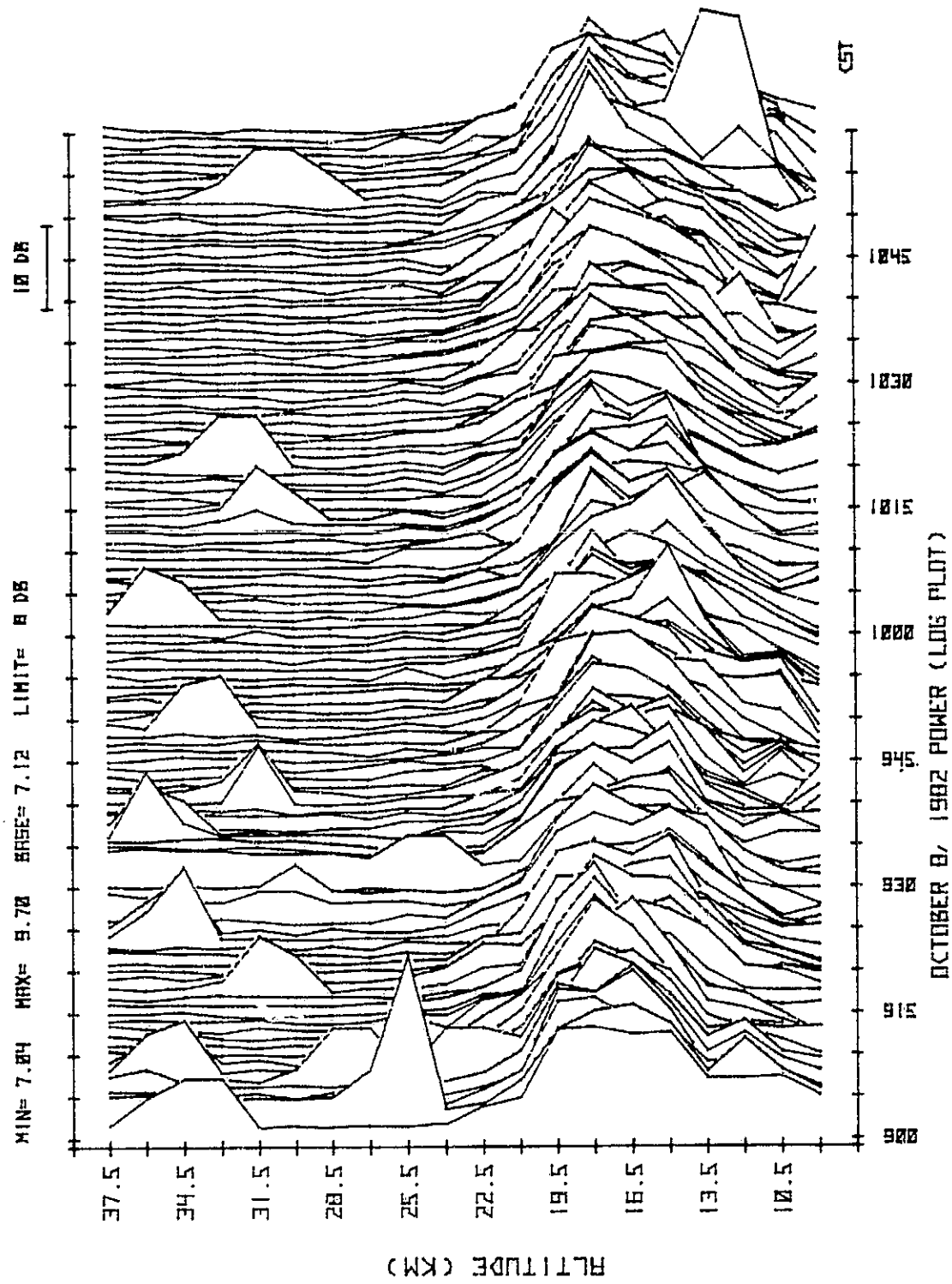

Figure 2.8 Scattered power at each minute versus altitude beginning at 900 CST on October 8, 1982.

1 meter/second (m/s), but it can easily be changed. An example is shown in Figure 2.9.

2.2.4 Correlation time. Values for the minute-by-minute correlation time at each altitude are found by taking one-half of the time necessary for the autocorrelation function to fall to zero. An example is shown in Figure 2.10. The scale at right is 1 second and the maximum value allowed is 1.5 seconds.

2.2.5 Derived horizontal winds. Since gravity waves have a strong vertical component and the antenna zenith angle is 1.5°, the line-of-sight velocities contain many short period oscillations. However, over periods longer than the Brunt-Vaisala period of 5--10 minutes it is known that vertical motions are negligible compared to horizontal motions [Hines, 1960]. Thus, an hourly-averaged horizontal wind can be calculated by assuming that the average line-of-sight velocity during the period is the component of the horizontal wind in the line-of-sight direction. The horizontal velocity is then found using simple trigonometry. Examples of hourly-averaged horizontal wind plots are given in Figure 2.11. Note that two profiles are shown for each hour, one each for one hourly-averaged standard deviation on either side of the mean. The horizontal wind profiles given in Chapter 3 represent the average of these two profiles.

The standard deviations themselves for each hour are shown below the wind profiles. They provide an indication of the amplitude of any short-period oscillations present during a one hour period at each sample height. Details concerning the calculation and plotting of hourly statistics are given in Gibbs and Bowhill [1983].

2.2.6 Hourly-averaged power levels. Minute-by-minute power returns at each sample height are averaged for 60 minutes and plotted. Examples are

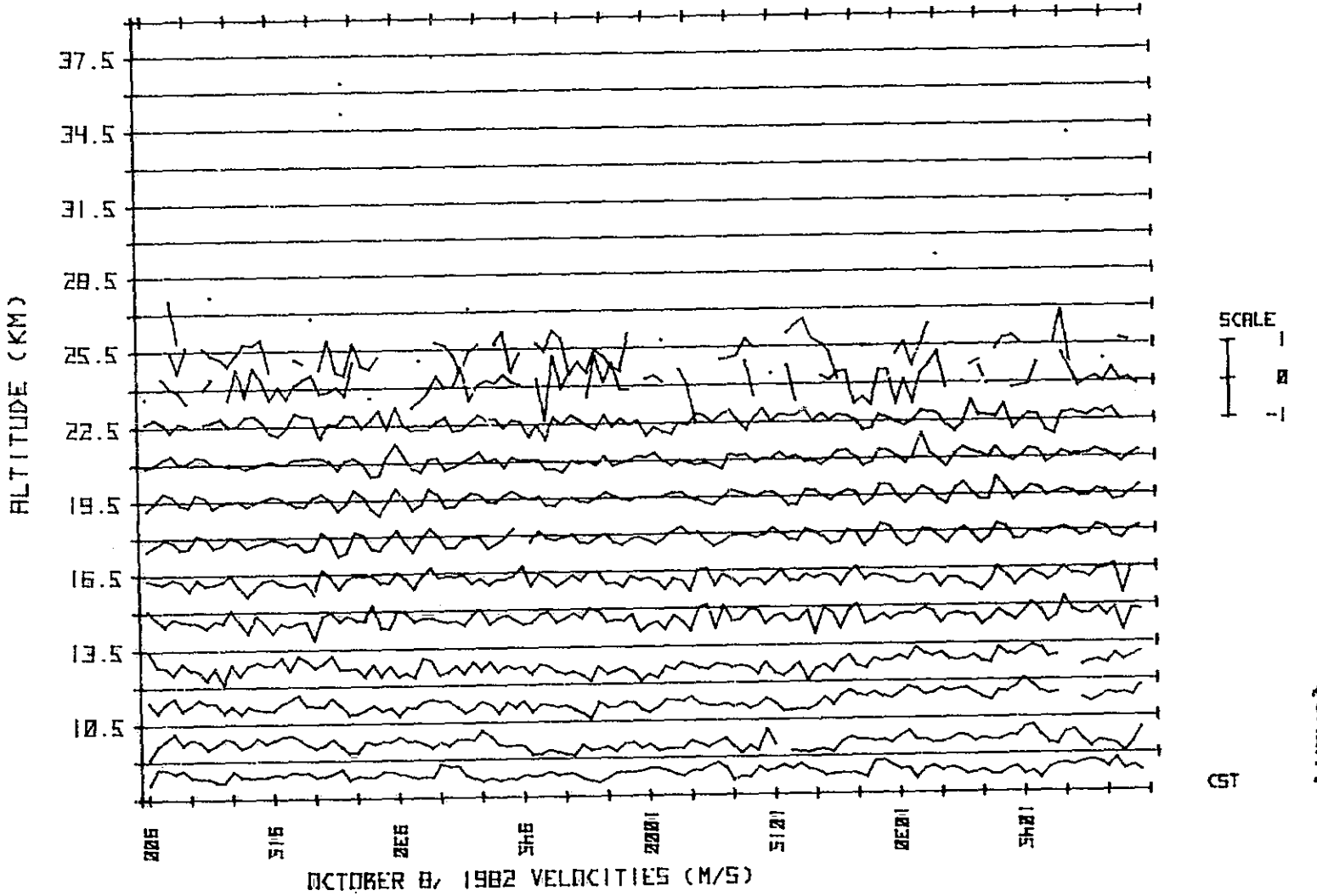

ORIGINAL PAGE IS
OF POOR QUALITY

Figure 2.9 Line-of-sight velocity at each sample altitude versus time beginning at 900 CST on October 8, 1982. Negative velocities correspond to motion away from the radar.

ORIGINAL PAGE IS
OF POOR QUALITY

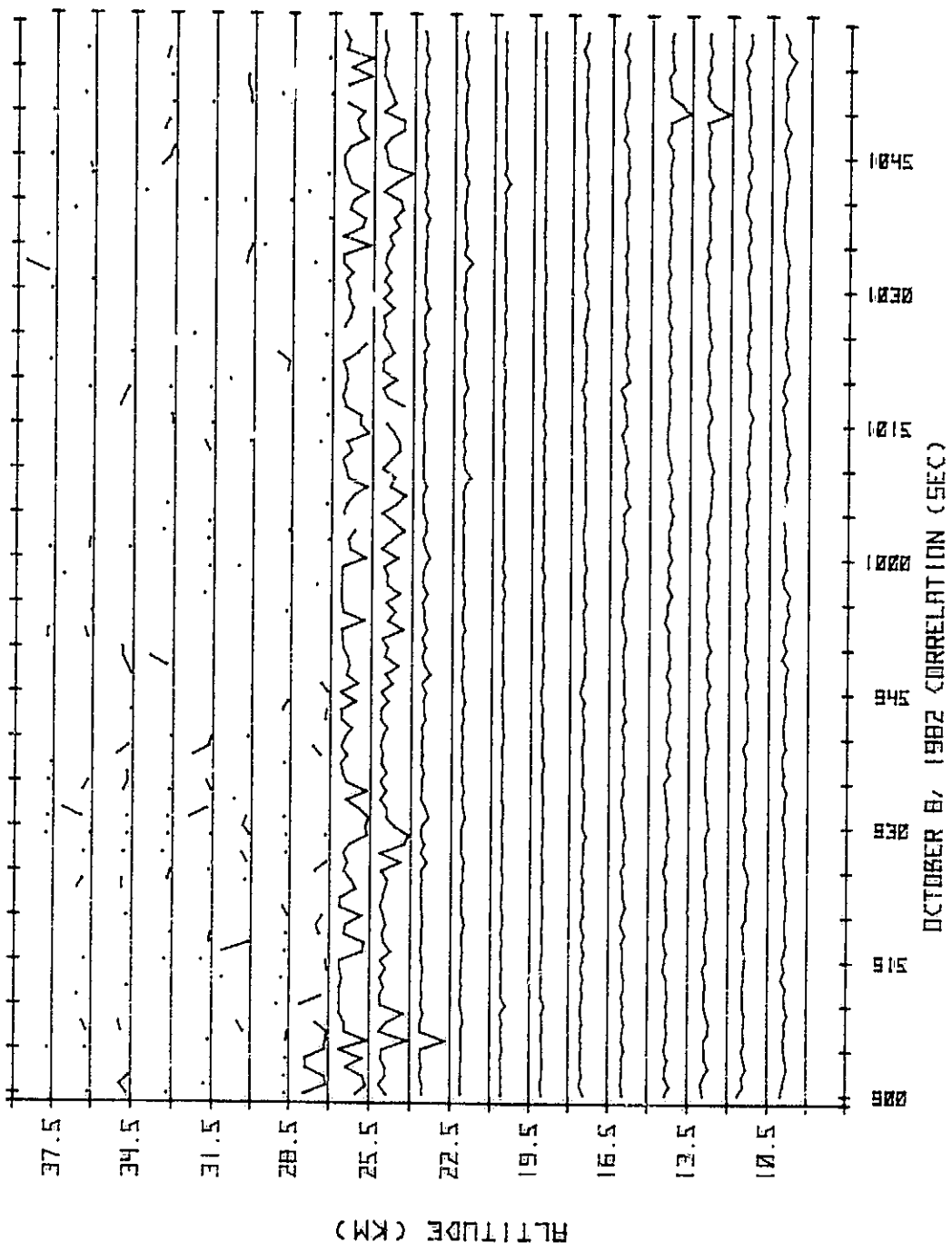

Figure 2.10 Correlation time at each sample altitude versus time beginning at 900 CST on October 8, 1982.

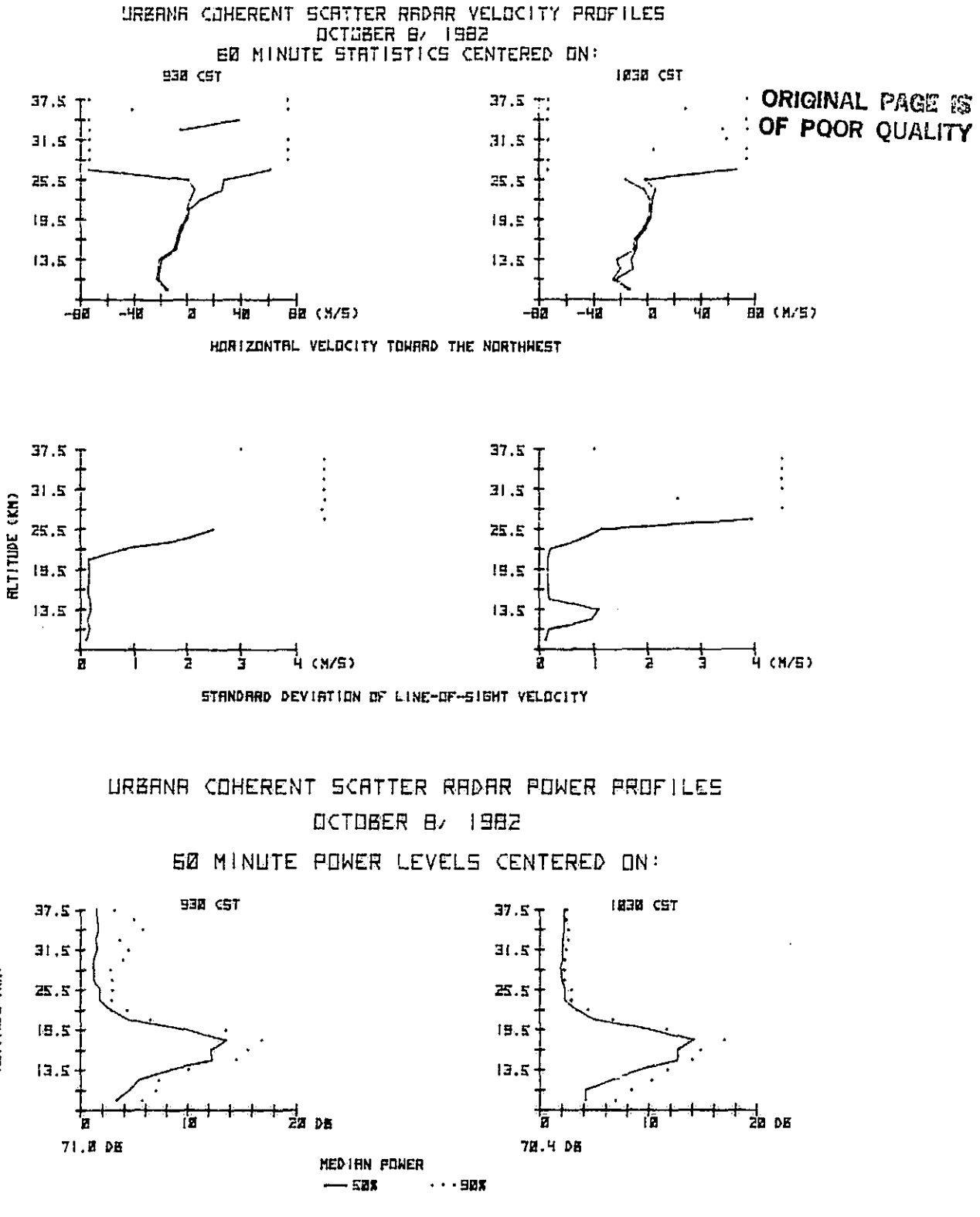

ORIGINAL PAGE IS
OF POOR QUALITY

Figure 2.11 Hourly averaged horizontal winds, standard deviations of line-of-sight velocities and power profiles for two consecutive hours.

also shown in Figure 2.11. For each hour, two profiles are plotted. The solid line represents that power level at each sample height which is exceeded 50% of the time during the hour. The dotted profile represents the power level exceeded 10% of the time. Thus the dotted profile tends to show where transient disturbances, or spikes, occur.

2.2.7 Power and velocity spectra of minute-by-minute data. Further analysis of the minute-by-minute power and velocity data is available through the use of a fast Fourier transform (FFT). Details of the calculations and plotting algorithms are given in Gibbs and Bowhill [1983]. Spectra of the velocity data are especially useful in the upper troposphere and lower stratosphere because of the opportunity to compare observed velocity fluctuation periods with the local Brunt-Vaisala period calculated from radiosonde data. An example velocity spectrum is shown in Figure 2.12. Spectra such as this are discussed in Section 4.5.

2.2.8 Power spectra of coherently integrated data. In addition to minute-by-minute data collection, it is also possible to collect the coherently integrated data directly, before it is formed into an autocorrelation function and averaged for one minute by the PDP-15 (data collection computer). In this case a data collection disk is filled in six minutes instead of the usual two hours. The data consist of 40 records, each having a length of 10 seconds.

A complete set of processing routines has been developed for these data [Gibbs and Bowhill, 1983]. For this work, the only procedure used is an FFT-generated power spectrum for the first 8 seconds of every 10 second record. An example is shown in Figure 2.13. All apectral plots shown herein are scaled so that the highest spectral peak corresponds to full scale on the plot. Spectra such as theseare discussed in Section 4.4.

ORIGINAL PAGE IS
OF POOR QUALITY

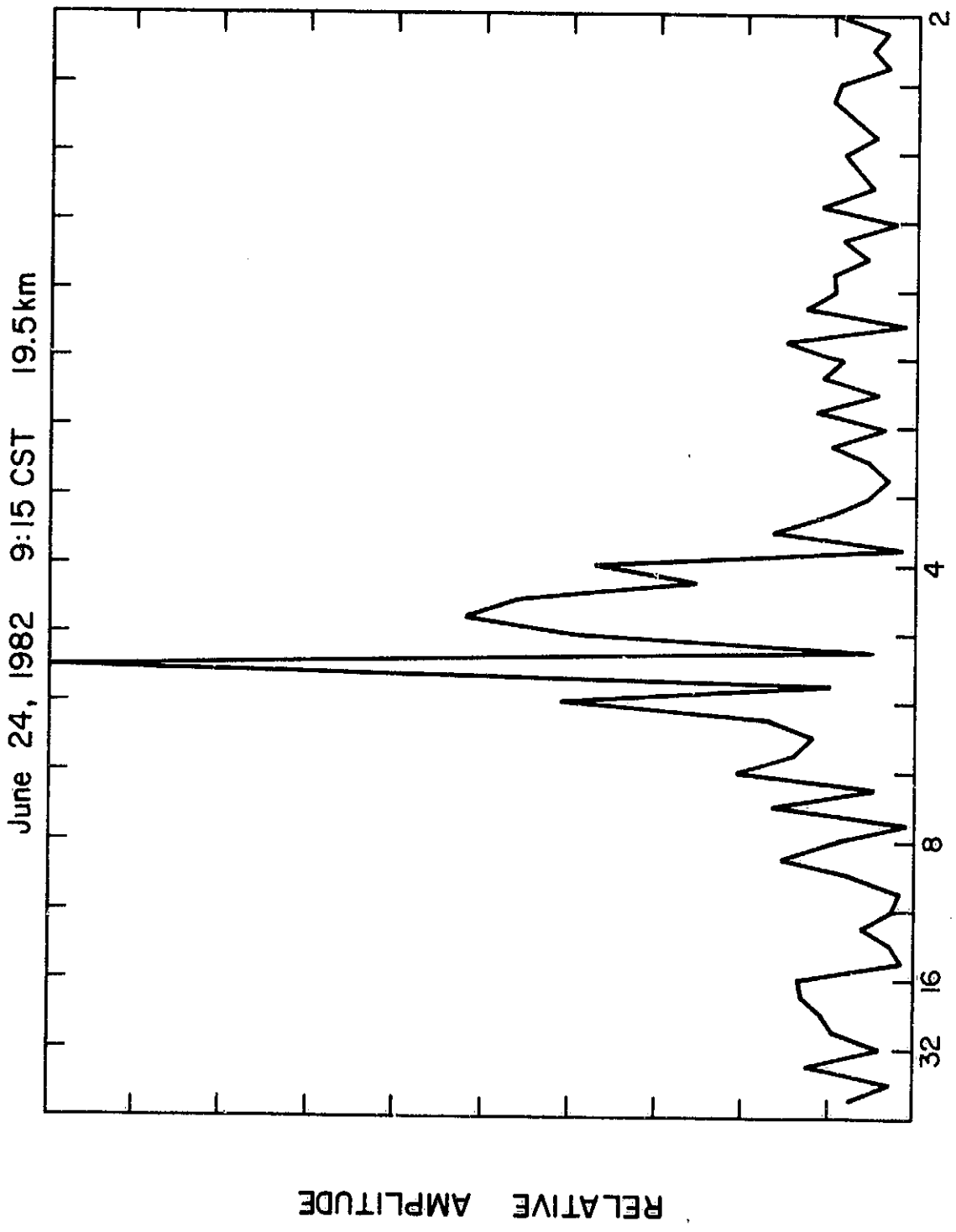

Figure 2.12 Power spectrum for the minute-by-minute velocity variations beginning at 915 CST on June 24, 1982.

ORIGINAL PAGE IS
OF POOR QUALITY

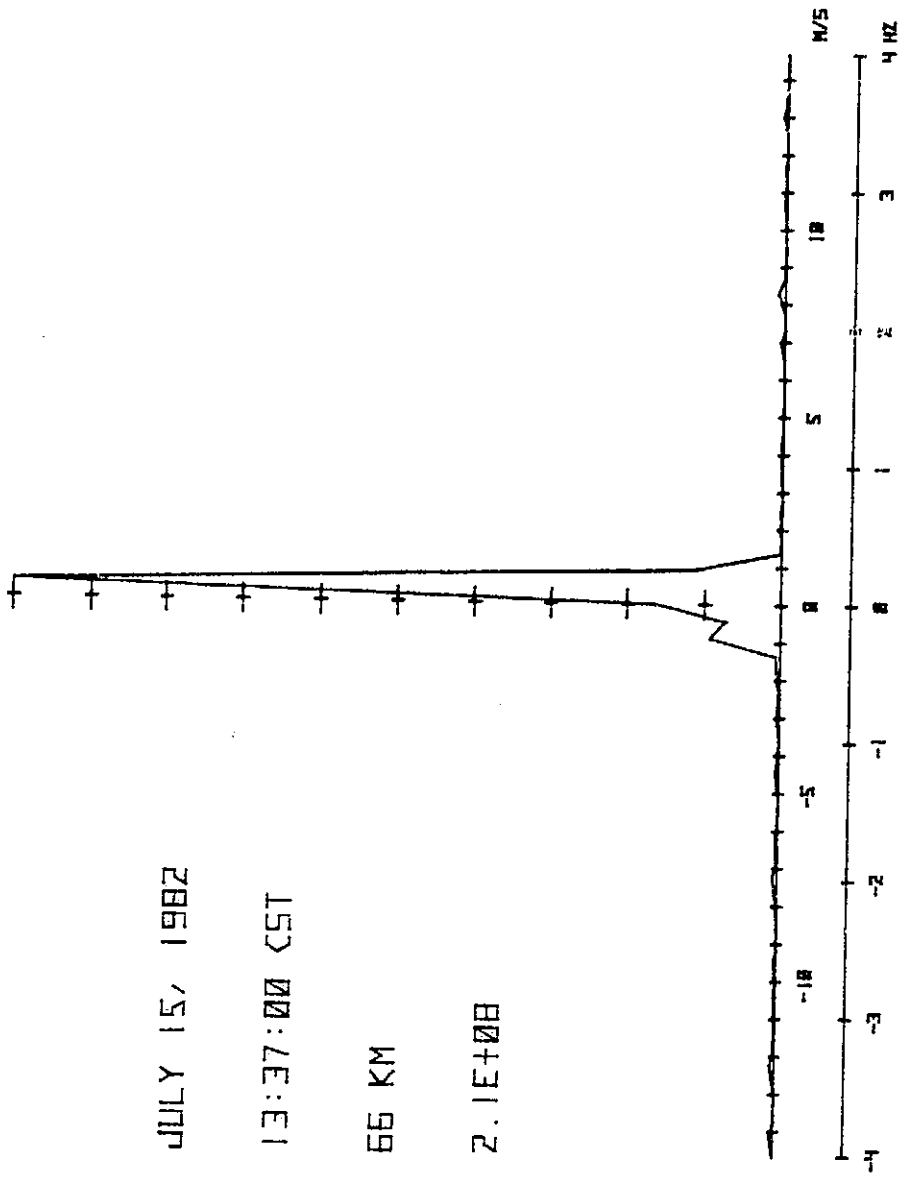

Figure 2.13 Power spectrum of 8 seconds of coherently integrated data beginning at 13:37:00 on July 15, 1982.

3. OBSERVATIONAL RESULTS

3.1 Scope and Extent of the Data

The Urbana radar was first used for lower atmospheric observation on April 22, 1982. At this time, as described previously, a small Yagi antenna was used for receiving, yielding backscatter above the noise floor up to an altitude of only 15 km. This system was used for seven days of observations. On June 9, 1982, the large antenna array was incorporated for both transmitting and receiving, in the same way that it is used during mesospheric observations [Gibbs and Bowhill, 1979]. Data were collected in this way until December 10, 1982 on 24 days. As of December 31, 1982, 134 hours of lower atmospheric data have been collected on 31 days.

The quality of the data shown in this section is typical of the quality obtained in all 134 hours of data. The figures have been chosen as an aid to explain and/or verify statements in the text. Wintertime measurements were hampered by ground backscatter interference, but this accounts for only a small fraction of the total data base.

3.2 Comparison with Radiosonde-Measured Winds

As explained in Section 2.2.5, an hourly-averaged horizontal wind component for each sample height toward the direction 36° south of east can be derived from the line-of-sight velocity data. These radar-derived wind profiles are compared to radiosonde wind profiles obtained from nearby National Weather Service balloon sites. The radiosonde wind speeds shown are found by computing the component of the true velocity toward the direction 36° south of east.

Several examples of radar wind profiles are given in this section. In particular, two types of plots are shown. The first type of plot compares

radar-derived wind profiles with profiles from the two nearest National Weather Service radiosonde sites, Peoria and Salem, Illinois. The second type of plot compares radar-derived wind profiles to each other. These plots demonstrate the radar's ability to detect changes in the wind field on an hourly basis.

In order to give a quantitative measure of agreement between the radar-derived and radiosonde wind profiles, one can define a variability index, I_v for each profile comparison. The variability index is found by calculating the absolute value of the difference in wind speed between the two profiles at each radar sample height, and then averaging these differences over all heights. The sample heights used extend to 16.5 km, above which radiosonde data are unavailable. The radiosonde wind speed at each radar sample height is approximated by using straight line interpolation between two adjacent data points.

A comparison of radiosonde and radar-derived wind profiles for July 22, 1982 is shown in Figure 3.1. The variability index of 4.8 m/s is probably caused by the nearly 5 1/2 hours time difference between the observations and the 168 km spatial separation between Urbana and Peoria. The agreement is better at altitudes above 13.5 km, where horizontal winds are generally more stable over time. Wind variability is discussed further in Section 4.3.

A nearly simultaneous comparison was made on the evening of September 16, 1982 during a 36-hour run. This comparison is shown in Figure 3.2. The profiles are nearly identical in shape, with an I_v of 4.8 m/s.

Data from September 24, 1982 are shown in Figure 3.3. Here, three hourly radar profiles taken in the morning are compared to the evening radiosonde profile. Once again, the lack of wind variability in the lower

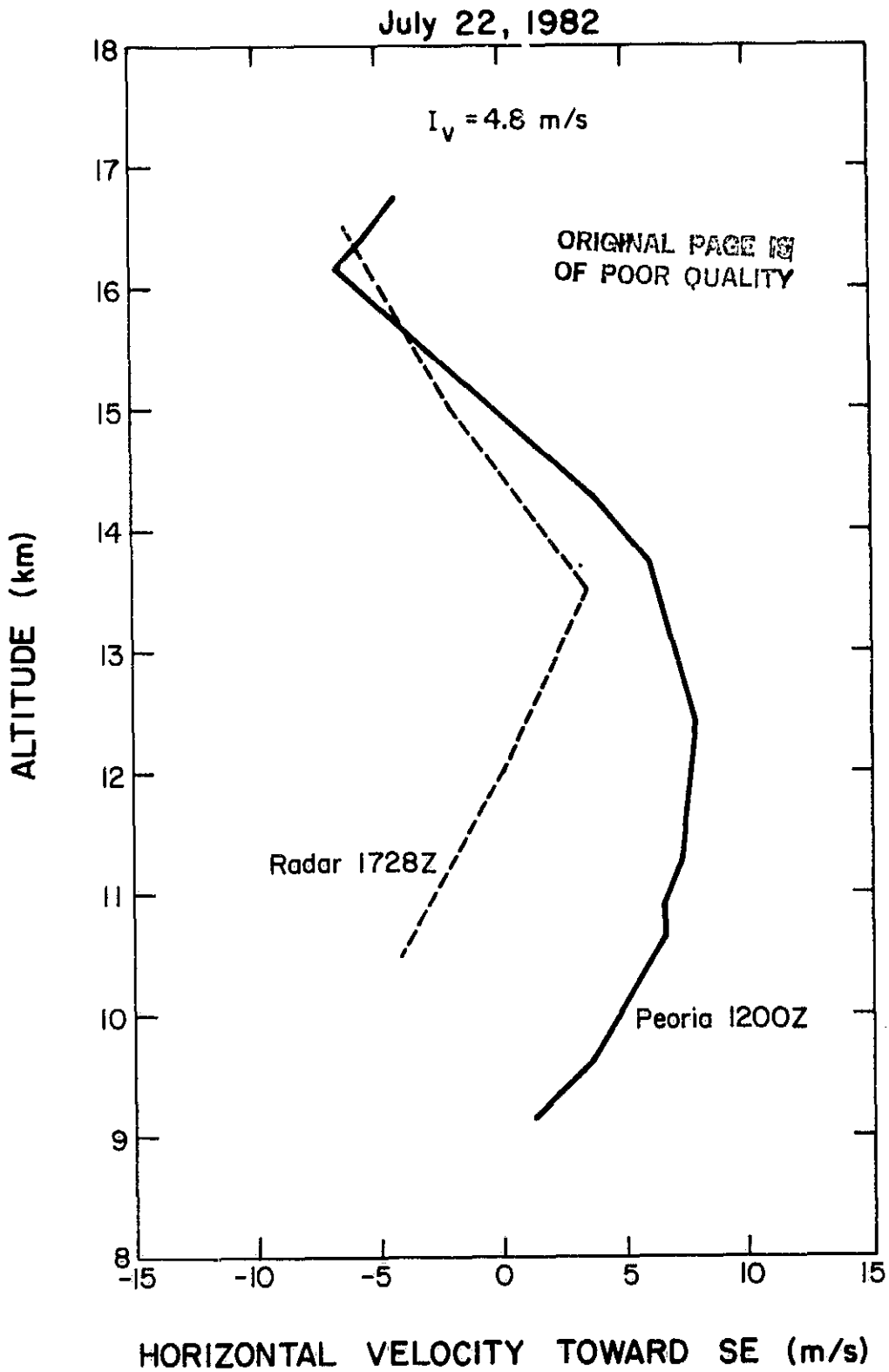

Figure 3.1 Comparison of horizontal wind profiles from NWS radiosonde and the Urbana radar.

ORIGINAL PAGE IS
OF POOR QUALITY

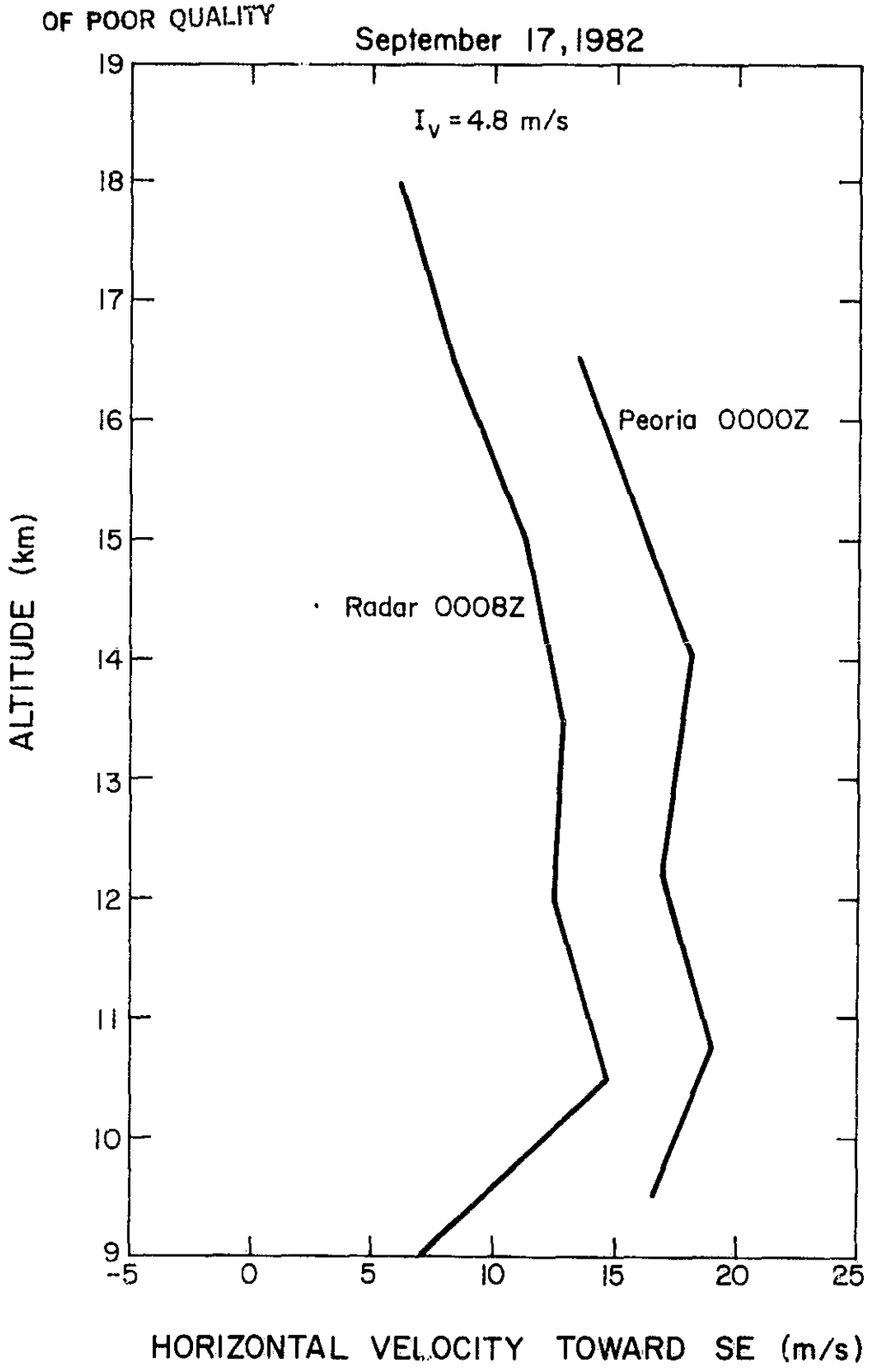

Figure 3.2 Simultaneous comparison of horizontal winds.

ORIGINAL PAGE IS
OF POOR QUALITY

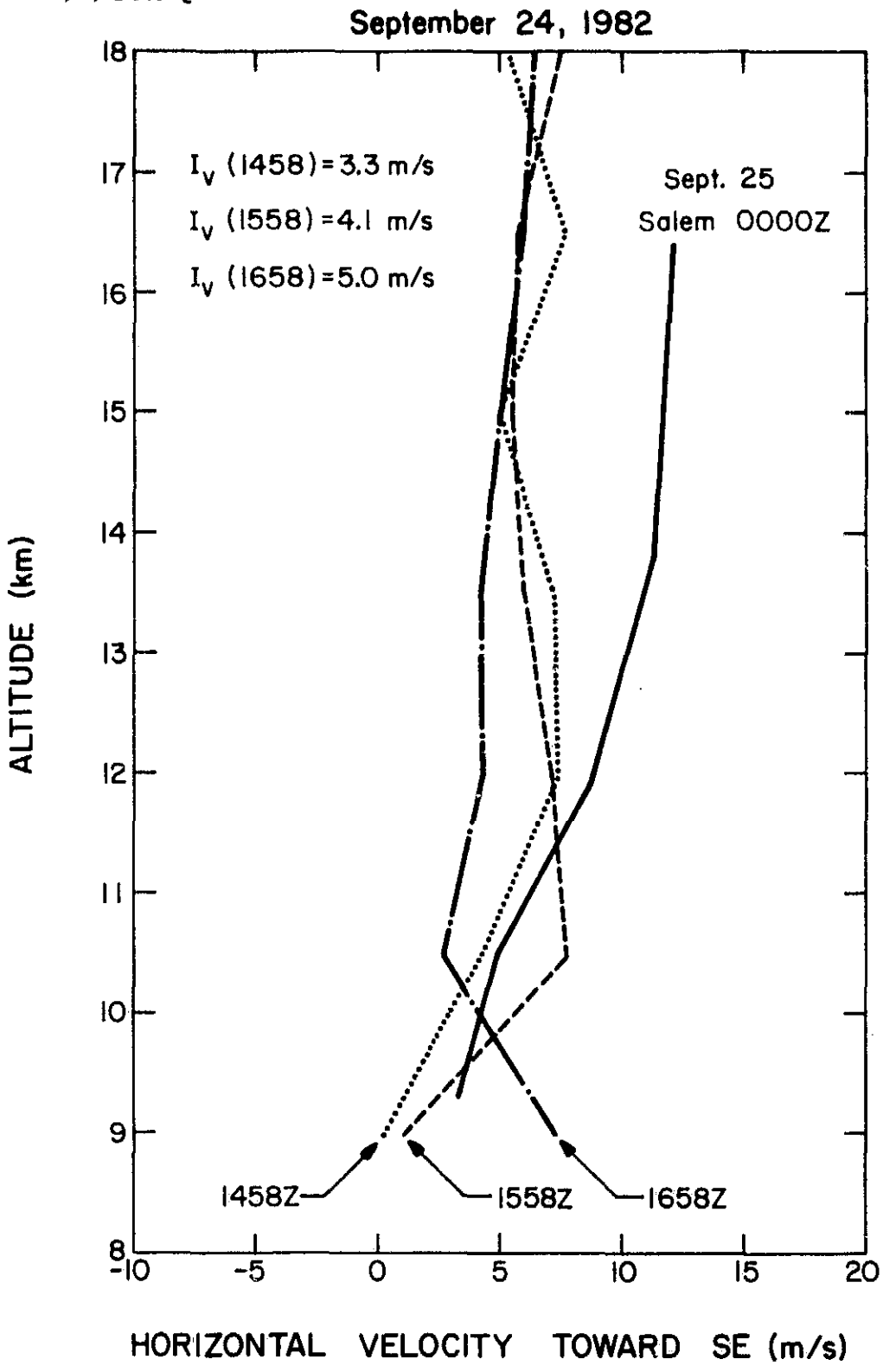

Figure 3.3 Three morning Urbana radar profiles compared to evening radiosonde.

stratosphere (above 15 km) is evident. The radiosonde profile, taken approximately 8 hours after the radar profiles, shows better agreement at the lower altitudes than in the stratosphere. This discrepancy is most likely caused by the large temporal separation of the two sets of observations. Scattered rain showers and thunderstorms were prevalent across the state throughout the day.

Comparisons for October 8 and October 15, 1982 are shown in Figure 3.4 and Figure 3.5, respectively. Again, considering the difference in time of over 3 hours in each case, I_V is still less than 4 m/s.

The data in Figure 3.6 were taken with the radar antenna pointing in a direction different than its normal operating position of 36° south of east, 1.5° off-vertical. The Urbana coherent-scatter antenna can also be phased to point in both the south and east positions with a small feed system change. The antenna consists of three modules, each fed by an open-wire transmission line [Allman and Bowhill, 1976]. By inserting extra lengths of open-wire transmission line into two of the three open-wire feeders, the main lobe of the antenna can be tipped in the E-plane, which is perpendicular to 36° south of east. S. W. Henson (personal communication, 1983) calculated the extra lengths necessary to tip the main lobe toward both the east and south. These extra lengths are inserted in the feeds to the NE and SW modules of the antenna, with the middle module feed left untouched. Zenith angles for the east and south pointing directions are also calculated. Knowledge of these zenith angles is necessary to derive the hourly-averaged horizontal winds in either of these two directions. These zenith angles as well as necessary phase shifts and line lengths needed to implement the various pointing directions are given in Table 3.1.

ORIGINAL PAGE IS
OF POOR QUALITY

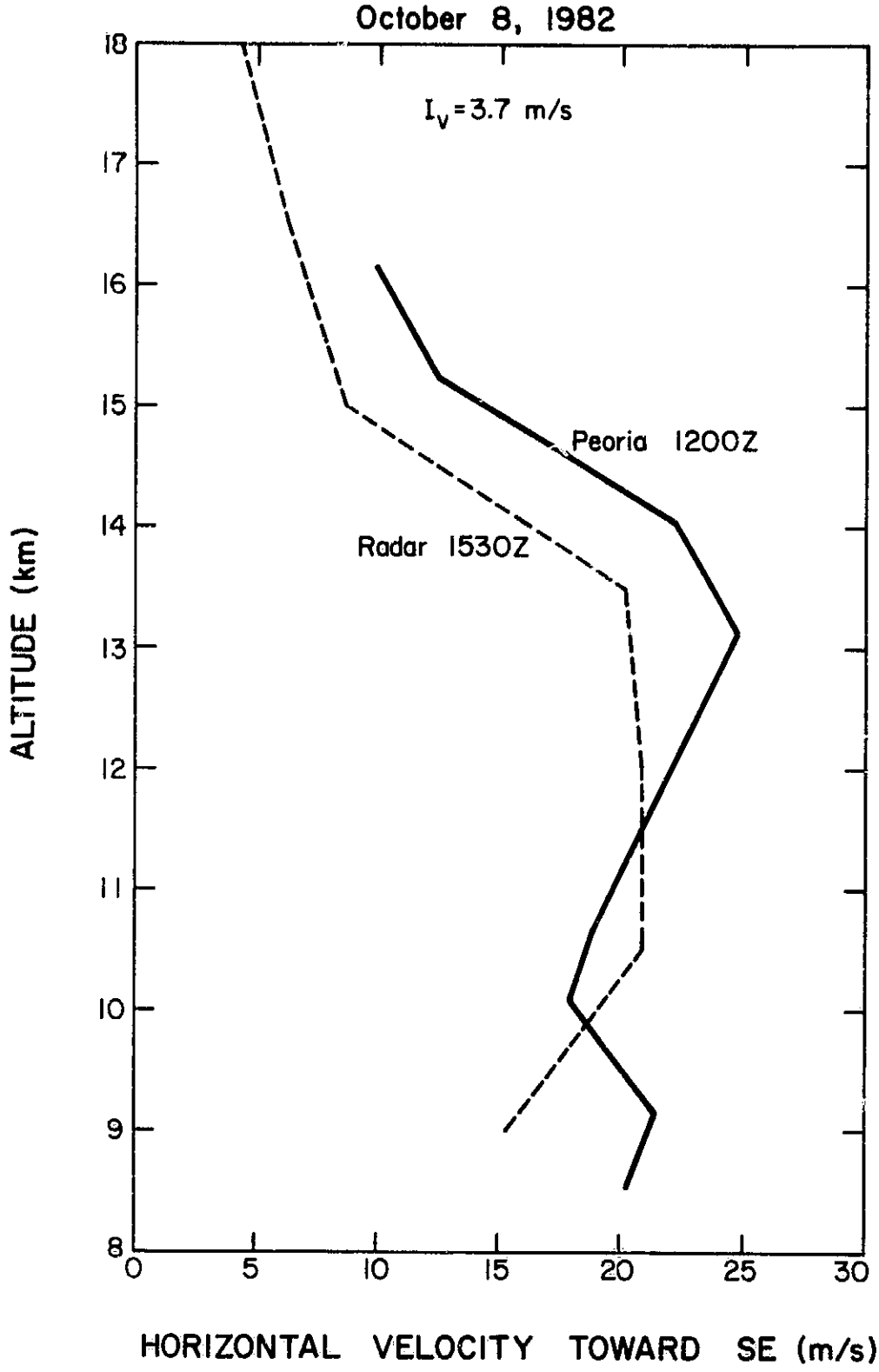

Figure 3.4 Comparison of horizontal wind profiles from Peoria radiosonde and Urbana radar.

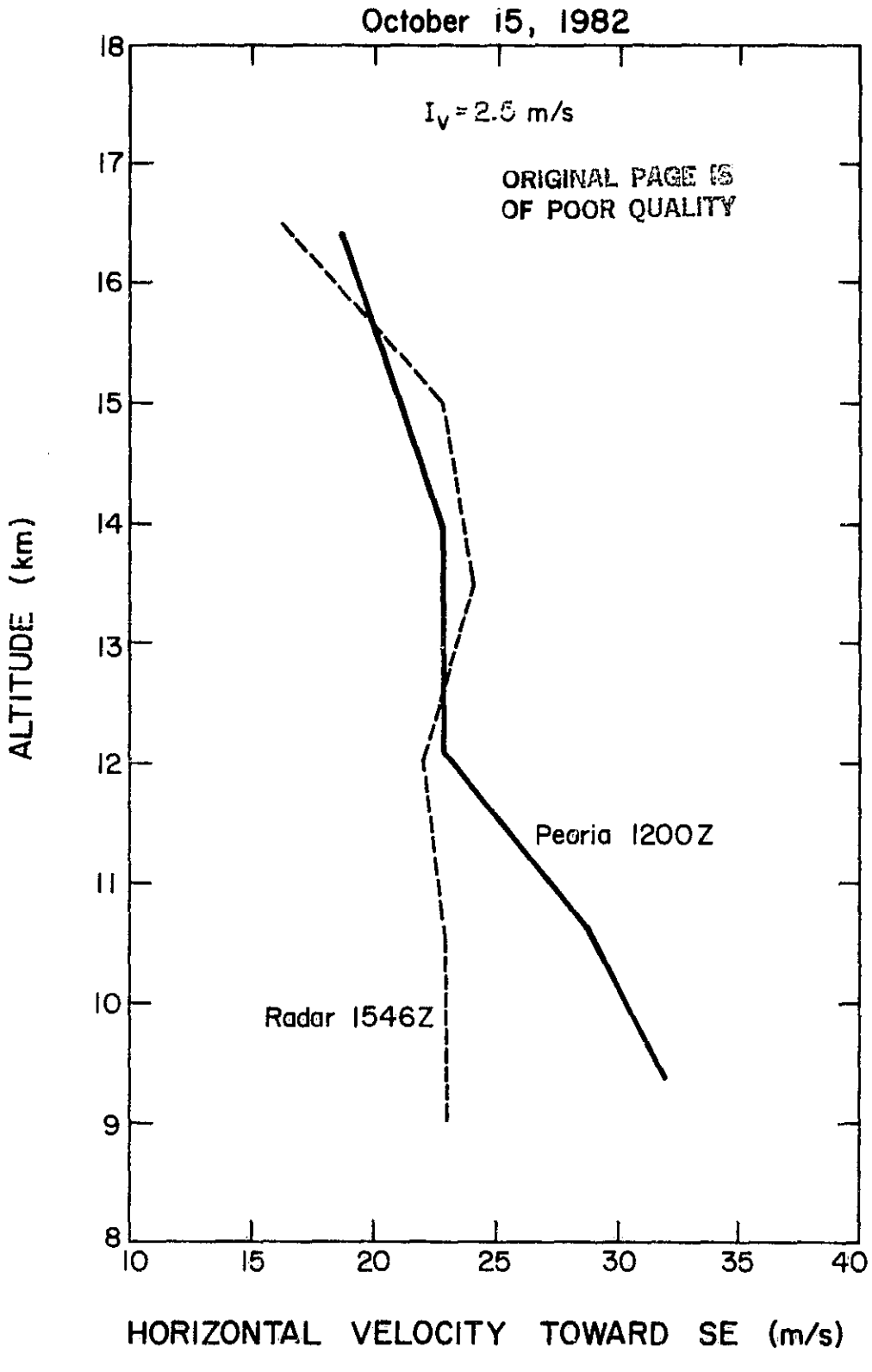

Figure 3.5 Comparison of horizontal wind profiles from Peoria, Illinois radiosonde and Urbana radar.

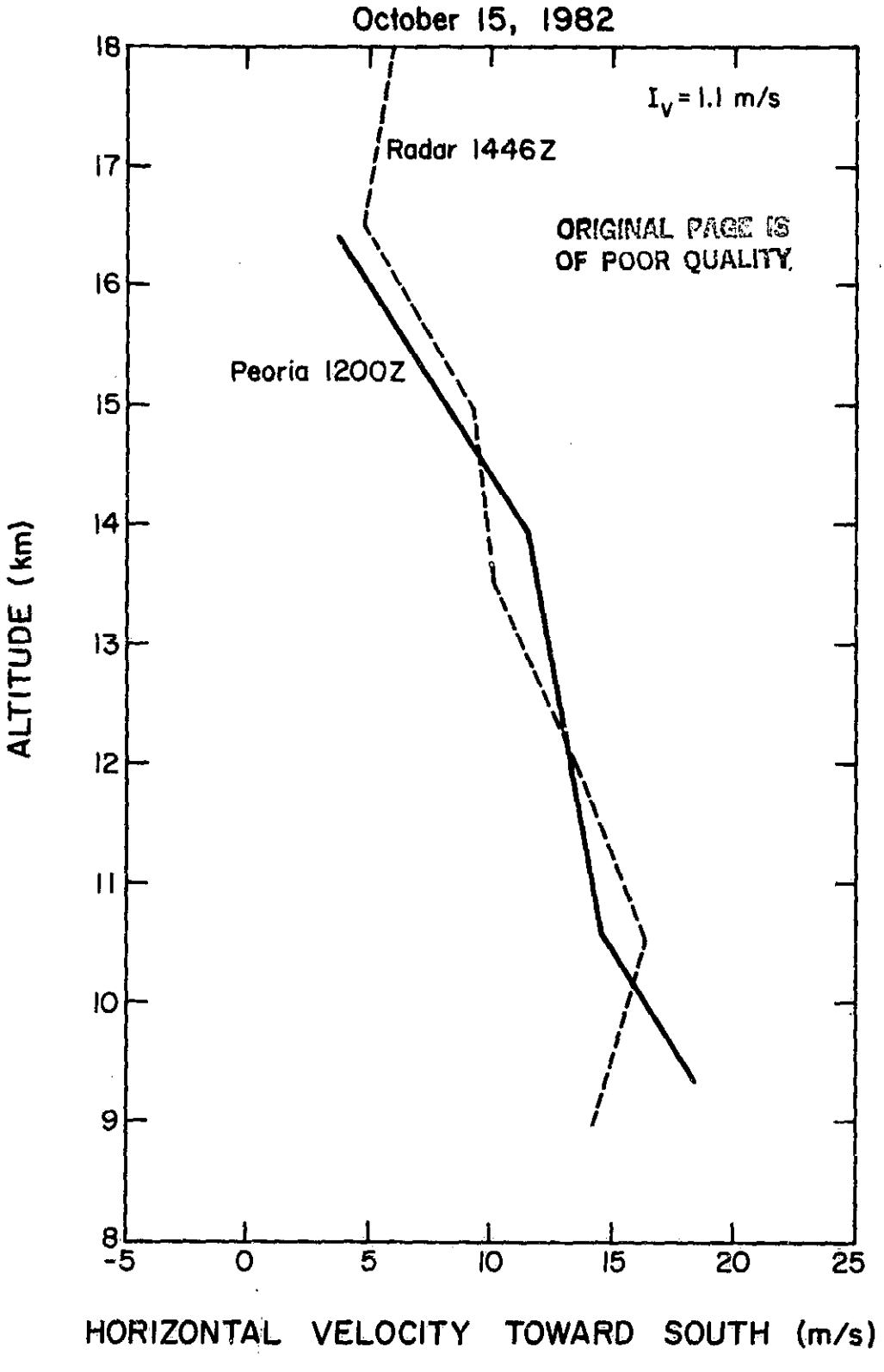

Figure 3.6 Comparison of horizontal velocity toward the south. Radar data were collected with antenna pointed toward the south.

TABLE 3.1 COHERENT SCATTER ANTENNA POINTING DIRECTIONS.

POINTING DIRECTION	ZENITH ANGLE	NE MODULE		SW MODULE	
		Phase Shift	Additional Feedline	Phase Shift	Additional Feedline
SE (normal)	1.50°	0°	0 m	0°	0 m
EAST	1.85°	-37.7°	.75 m	+37.7°= -322.3°	2.83 m (note 1)
SOUTH	2.55°	+71.1°= -288.9°	2.17 m (note 1)	-71.1°	1.41 m

Note 1: this feed line is connected with its two wires inverted, producing a 180° phase shift.

ORIGINAL PAGE IS
OF POOR QUALITY

The most desirable arrangement would involve fast mechanical switching of the antenna pointing direction while the transmitter was in operation. However, as an interim measure, a manually switched system was constructed. Only two of the three antenna modules need be phase shifted to attain the desired pointing directions. The two outboard modules were chosen for symmetry purposes.

Each antenna module has one feed line attached at any one time. The two outboard groups each have two additional feed lines available for use. Alternate pointing positions are selected by manually disconnecting the normal feed line and installing one of the other two, depending upon which direction is desired. Of course, the transmitter must be off while this change takes place. However, this change can be accomplished in as little as five minutes, so that only a small amount of data is lost in the process.

For the data shown in Figure 3.6, the antenna was phased to point toward the south. The zenith angle for this pointing position is therefore 2.55°. For this plot, the southward component of velocity was computed from the radiosonde data for comparison. These data were taken on October 15, 1982, approximately one hour previous to the data shown in Figure 3.5. I_v in this case is only 1.1 m/s.

Another nearly simultaneous set of observations is shown in Figure 3.7. In this case, a jet stream was over the northern portion of Illinois, centered at about 11 km. This shows up clearly on the Peoria radiosonde profile. Also shown in this figure is the radiosonde profile from Salem, Illinois, 177 km to the south-southwest of Urbana. Very little evidence of the jet can be seen in this profile. Since Urbana is somewhat between Peoria and Salem, one would expect a combination of these two profiles to be present. That is exactly what appears in the figure. Notice again that the

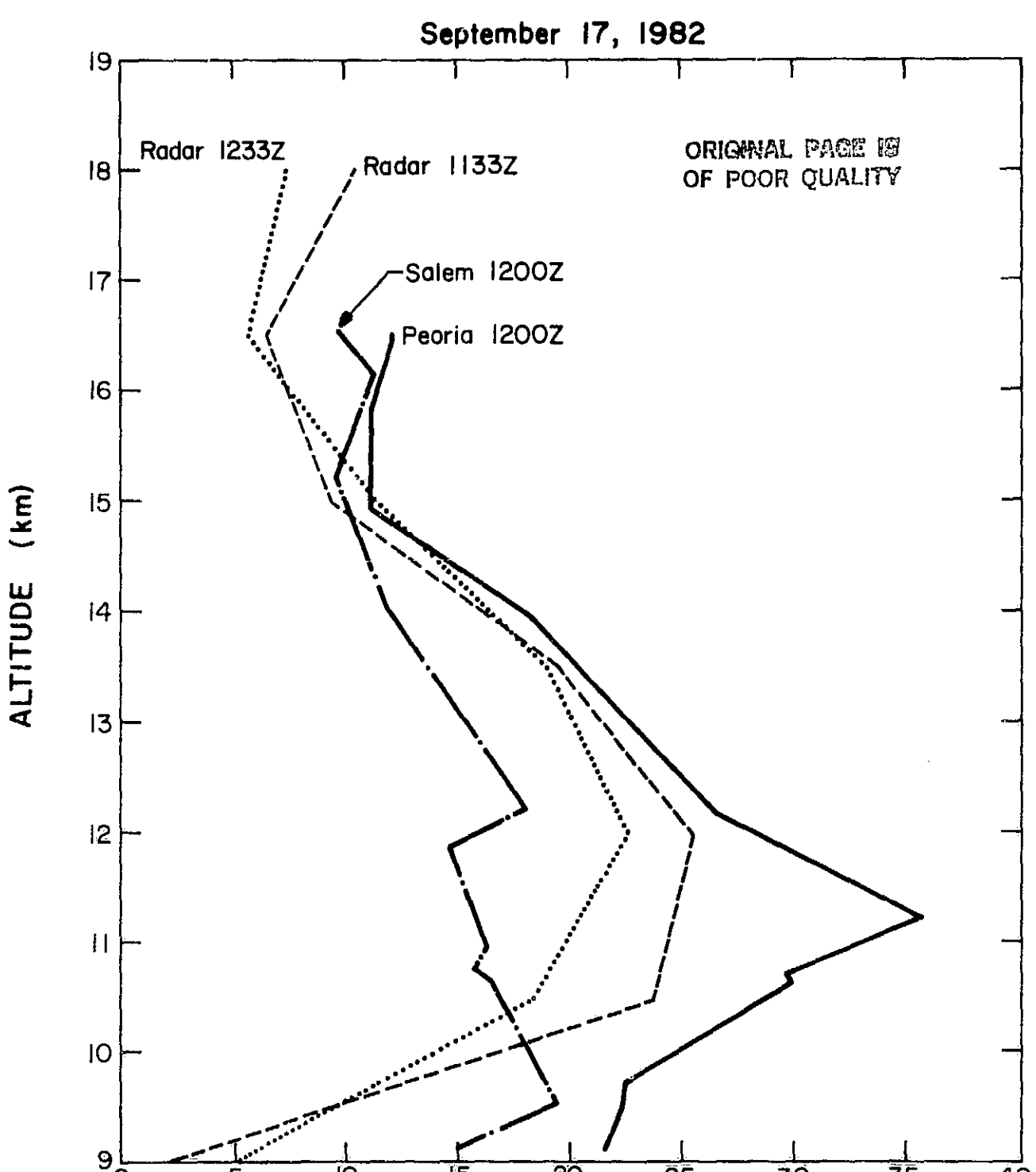

Figure 3.7 Comparison of two radar profiles with morning radiosonde profiles from Peoria and Salem, Illinois. Data were collected during jet stream passage.

tropospheric winds vary greatly between locations while the stratospheric winds remain generally constant.

One case in which there is large variability in the stratospheric wind over time is shown in Figure 3.8. During the morning hours of September 1, 1982, thunderstorms were present in the Urbana area. The profile at 1452Z was taken during one of these storms. Notice that the winds in the lower stratosphere are much stronger than those in any previous figure. A profile taken at 1844Z, after the storms had subsided, compares much more favorably to the morning balloon sounding with I_v = 2.6 m/s as opposed to 9.2 m/s for the 1452Z profile. Thus, in this case, the large winds in the stratosphere were probably associated with the passage of scattered thunderstorms. A similar situation probably caused the stratospheric wind variation shown in Figure 3.3.

Four consecutive radar wind profiles are shown in Figure 3.9. This figure represents an excellent example of the unique ability of the radar to follow a constantly changing wind profile. On July 15, 1982, the passage of a warm front caused a significant wind shift in the 12-14 km region during the morning hours. This change can be easily followed on an hourly basis in Figure 3.9. Shown in Figure 3.10 are the morning and evening radiosonde wind profiles from the same day. A comparison of Figure 3.9 and 3.10 reveals many similarities. The earliest radar profile, 1541Z, resembles the morning balloon sounding. By the time of the latest radar profile, 1845Z, the wind structure resembles the evening radiosonde profile, especially below 15 km. Also, both plots show an area of general stability at 15 km, while the major changes take place at 16.5 km and in the 12-14 km range.

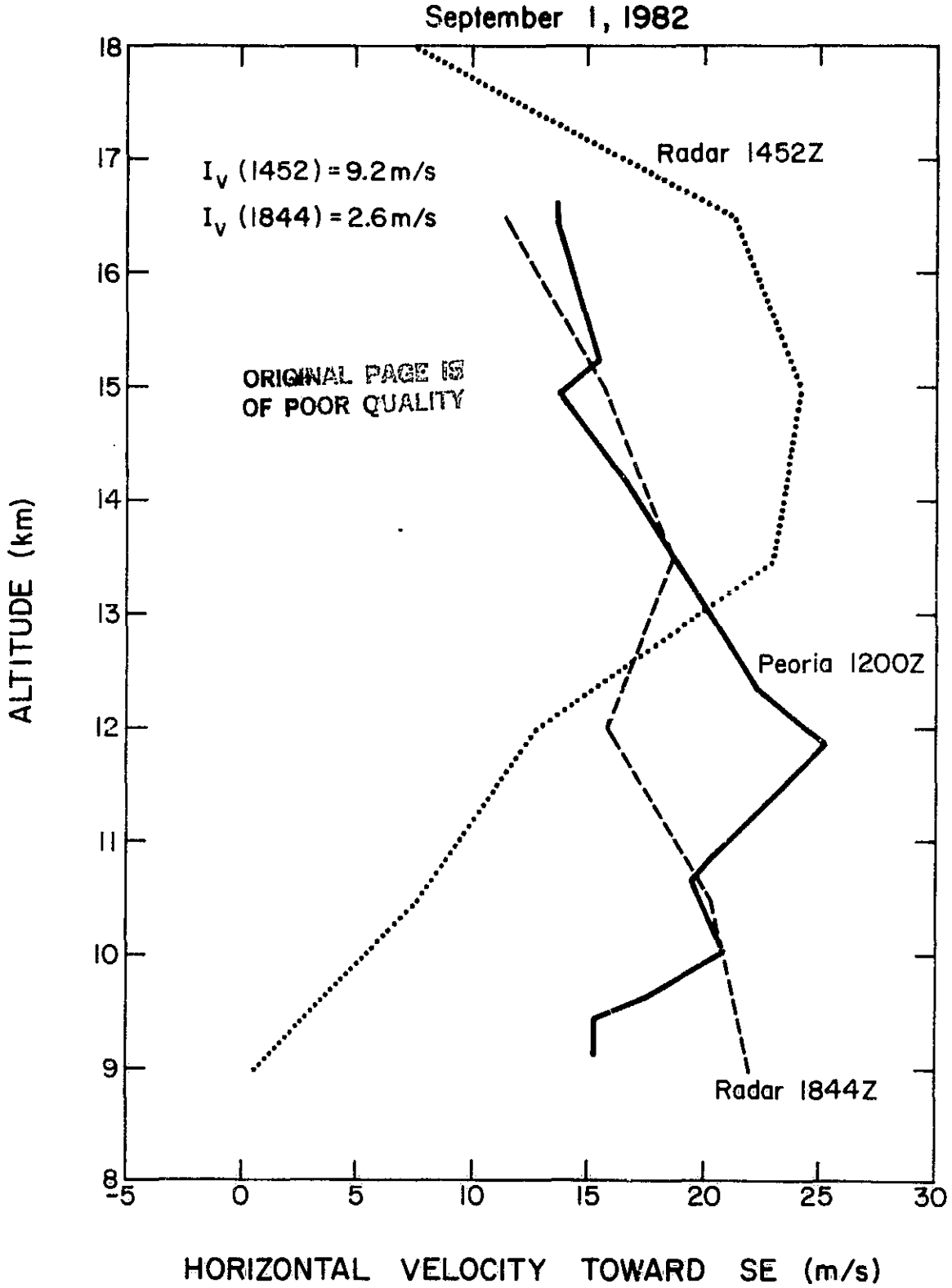

Figure 3.8 Comparison of two radar profiles to the morning radiosonde profile. The earlier radar profile is affected by thunderstorms in the neighborhood of the radar.

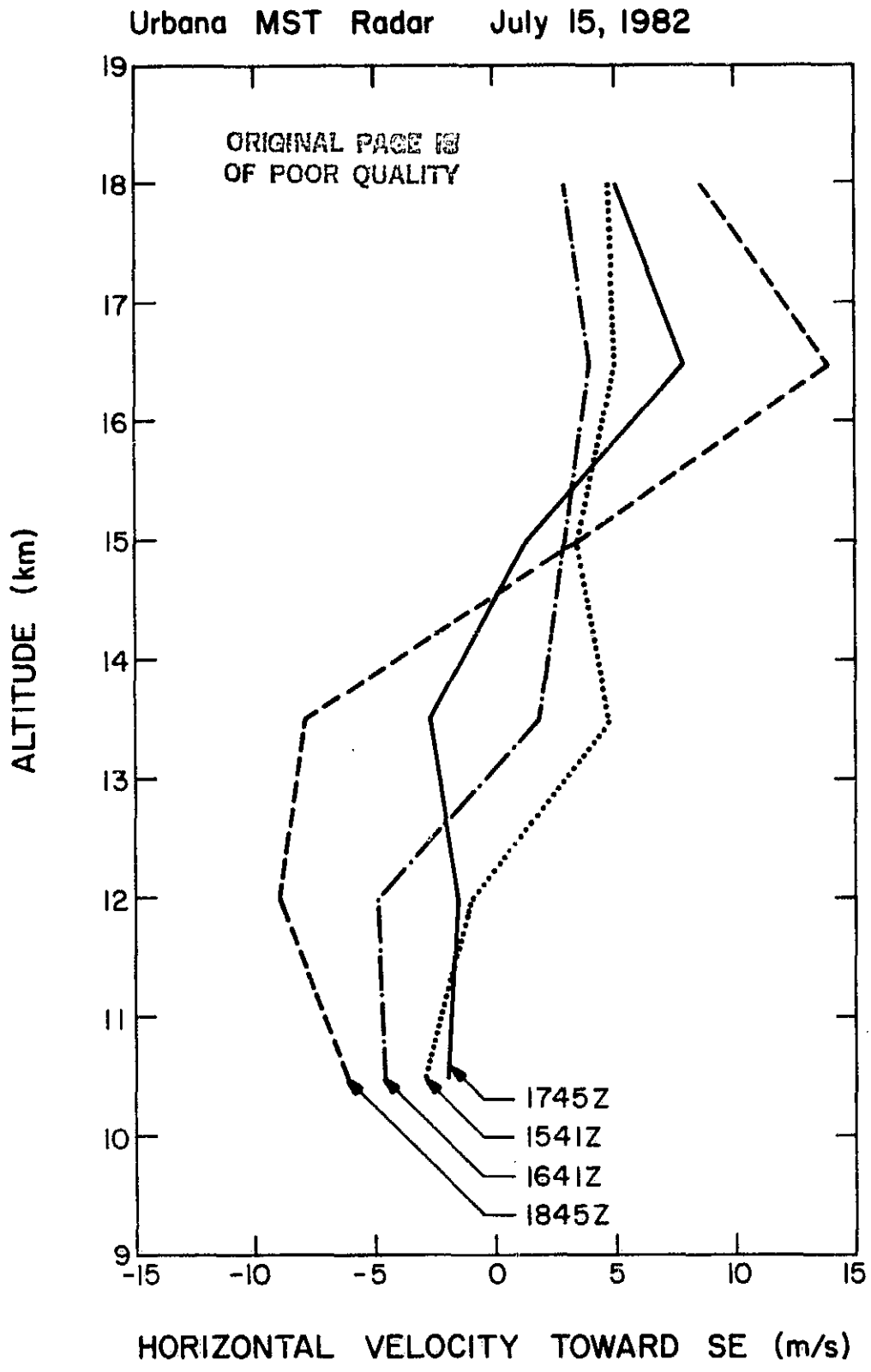

Figure 3.9 Four consecutive radar profiles showing significant change in a short time period.

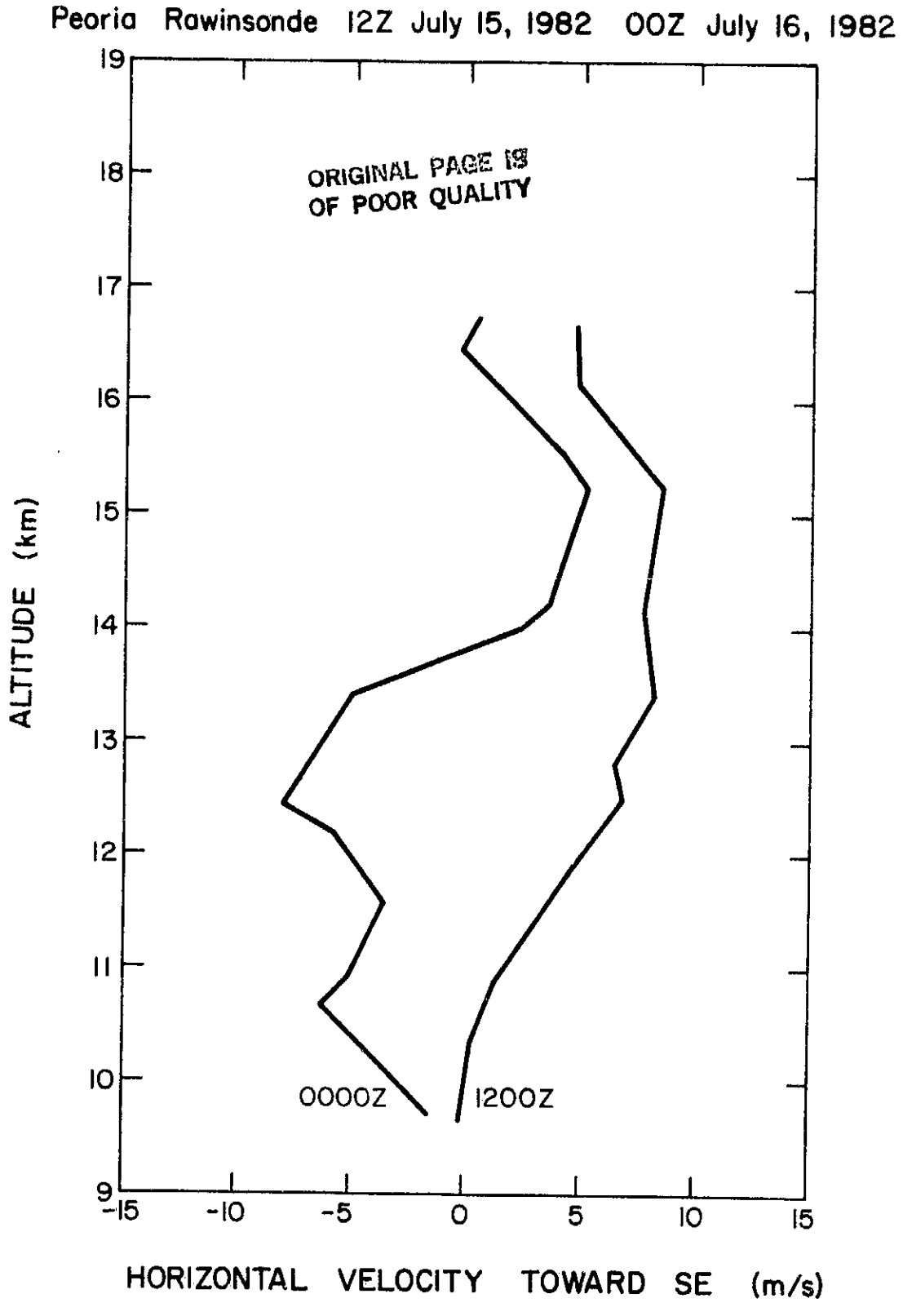

Figure 3.10 Morning and evening radiosonde profiles for comparison to Figure 3.9.

In general, the Urbana radar wind profiles are in good agreement with those of the radiosonde. Exactly specifying this accuracy is difficult because of both the spatial separation of the two observing stations and the limited range resolution of the radar. In addition, balloon measurements give an instantaneous sample of the wind velocity while the radar profiles are averaged over a one hour period.

3.3 Observations in the Vicinity of Thunderstorms

In addition to observing winds and turbulence in the clear atmosphere, the VHF radar can also be used to study atmospheric dynamics during periods of strong convective activity in the troposphere. The Urbana radar was operated under these conditions on several occasions during the summer and fall of 1982.

One such occasion was on September 14, 1982. Severe thunderstorms were forecast for the area in the afternoon. The radar was turned on at 1218 CST, more than three hours before it began raining at the Field Station. Figure 3.11 shows the line-of-sight velocity for each altitude for the first two hours of the run. Gravity waves occur throughout the region. The period of the oscillations is 4-5 minutes in the stratosphere (above 16.5 km), which corresponds to the Brunt-Vaisala period for this region (see Section 4.5). Longer period oscillations are present in the troposphere, corresponding to the longer Brunt-Vaisala period in this region. A moderate horizontal wind component is present at 13.5 km from 1320 CST until 1410 CST.

Figure 3.12 is a continuation of the line-of-sight velocity for an additional hour and 24 minutes. Note the scale of this figure is 1/3 that of Figure 3.11. Thus, by approximately 1500 CST, about 1/2 hour before rain begins on the ground, the amplitudes of the gravity waves in the lower

ORIGINAL PAGE IS
OF POOR QUALITY

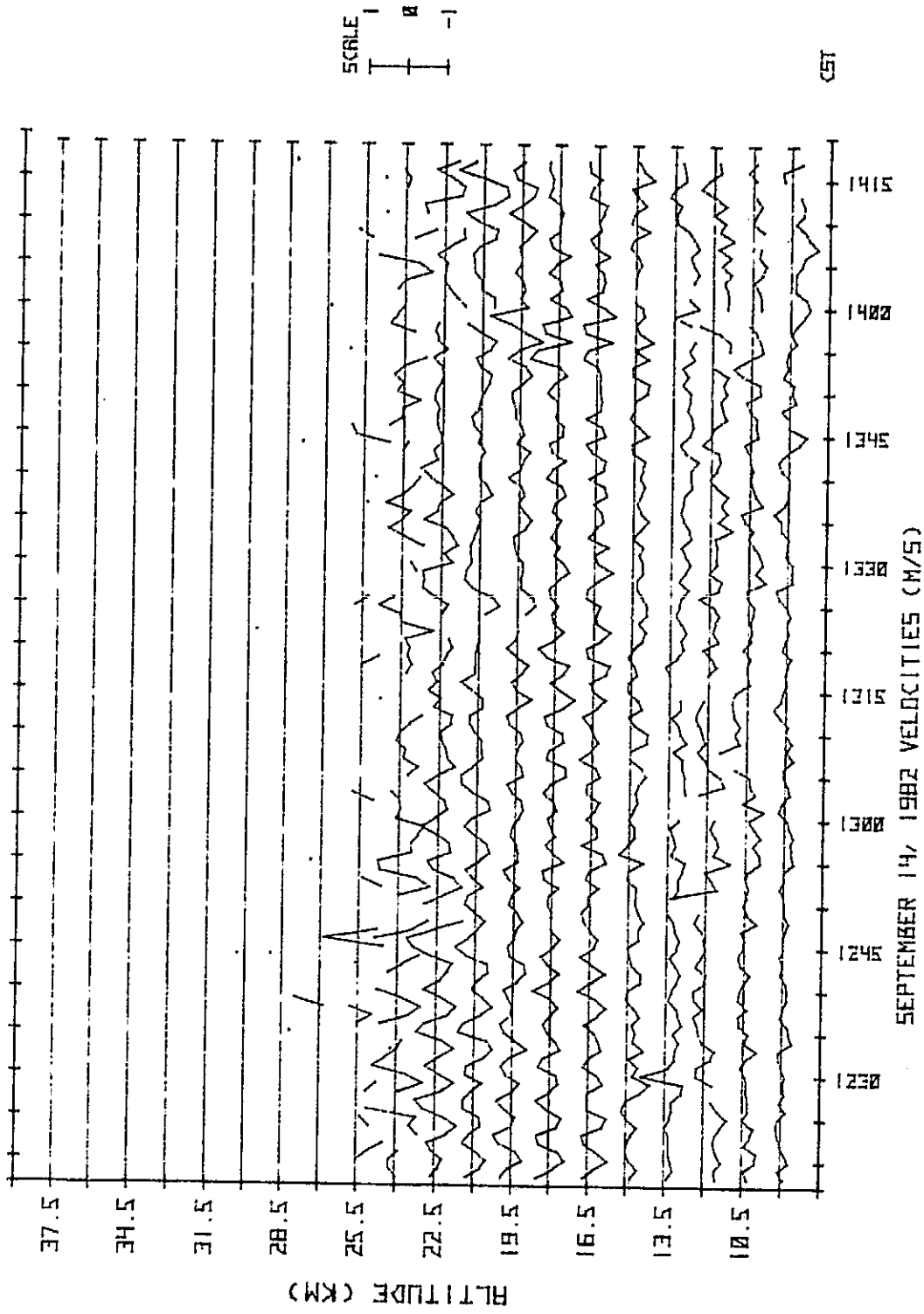

Figure 3.11 Line-of-sight velocity beginning at 1218 CST on September 14, 1982.

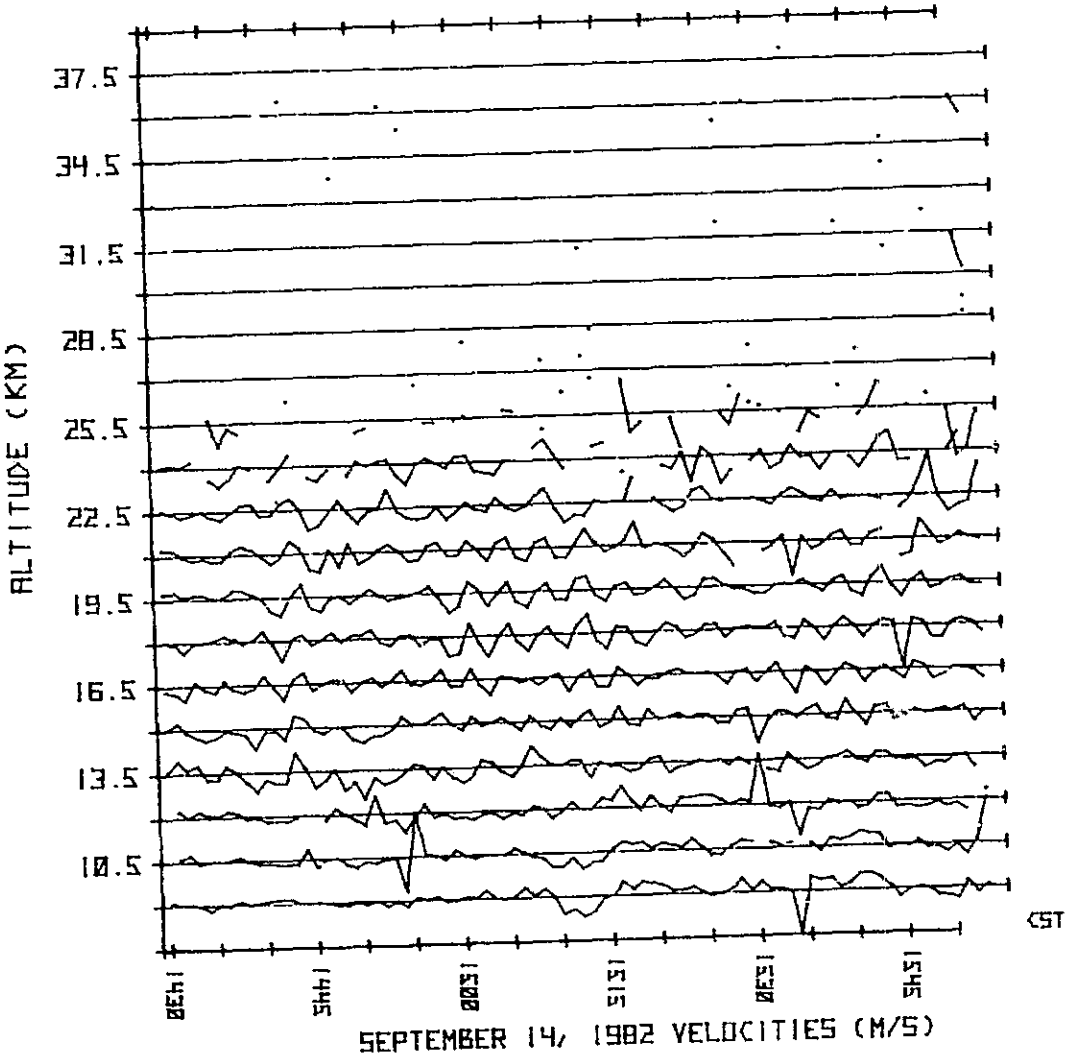

ORIGINAL PAGE IS
OF POOR QUALITY

Figure 3.12 Line-of-sight velocity beginning at 1430 CST on September 14, 1982, during a thunderstorm. Negative velocities correspond to motion away from the radar. Note scale of 3 m/s.

stratosphere have increased by about a factor of 3. This substantial increase in gravity wave amplitude during thunderstorms is typical of all thunderstorm observations at Urbana, as discussed in Section 4.2.

Another interesting feature of note in Figure 3.12 is found at the lower altitudes. At 1508 CST, an updraft of 7 minutes duration occurs at both 9 and 10.5 km. This is followed immediately by a downdraft lasting almost 30 minutes at these same two altitudes, and about 15 minutes at 12 km. (Recall that on the line-of-sight velocity plots, a negative velocity corresponds to a velocity away from the radar while a positive velocity corresponds to a velocity toward the radar.) Rain began falling on the ground at the radar site at approximately 1530 CST, which is in the middle of this downdraft period.

A plot of scattered power at a fixed altitude versus time for the same time frame as Figure 3.12 is given in Figure 3.13. Power levels increase dramatically at 9 km and moderately at 10.5 km during the time at which the updrafts and downdrafts are present. A reasonable explanation of this increase in scattered power is that the vertical motion generates turbulence in the region of interest. The turbulence in turn induces changes in the radio index of refraction, causing the increase in scattered power. This explanation is supported by a plot of correlation time at a fixed altitude versus time, Figure 3.14, which shows a substantially shorter correlation time between 1510 CST and 1540 CST at 9.0 and 10.5 km. This shorter correlation time suggests that a turbulent mechanism is responsible for the increase in scattered power rather than some sort of horizontally stratified structure.

The next set of observations were taken on September 1, 1982. Thunderstorms were located about 50 km south of the radar site. The initial 2

ORIGINAL PAGE IS
OF POOR QUALITY

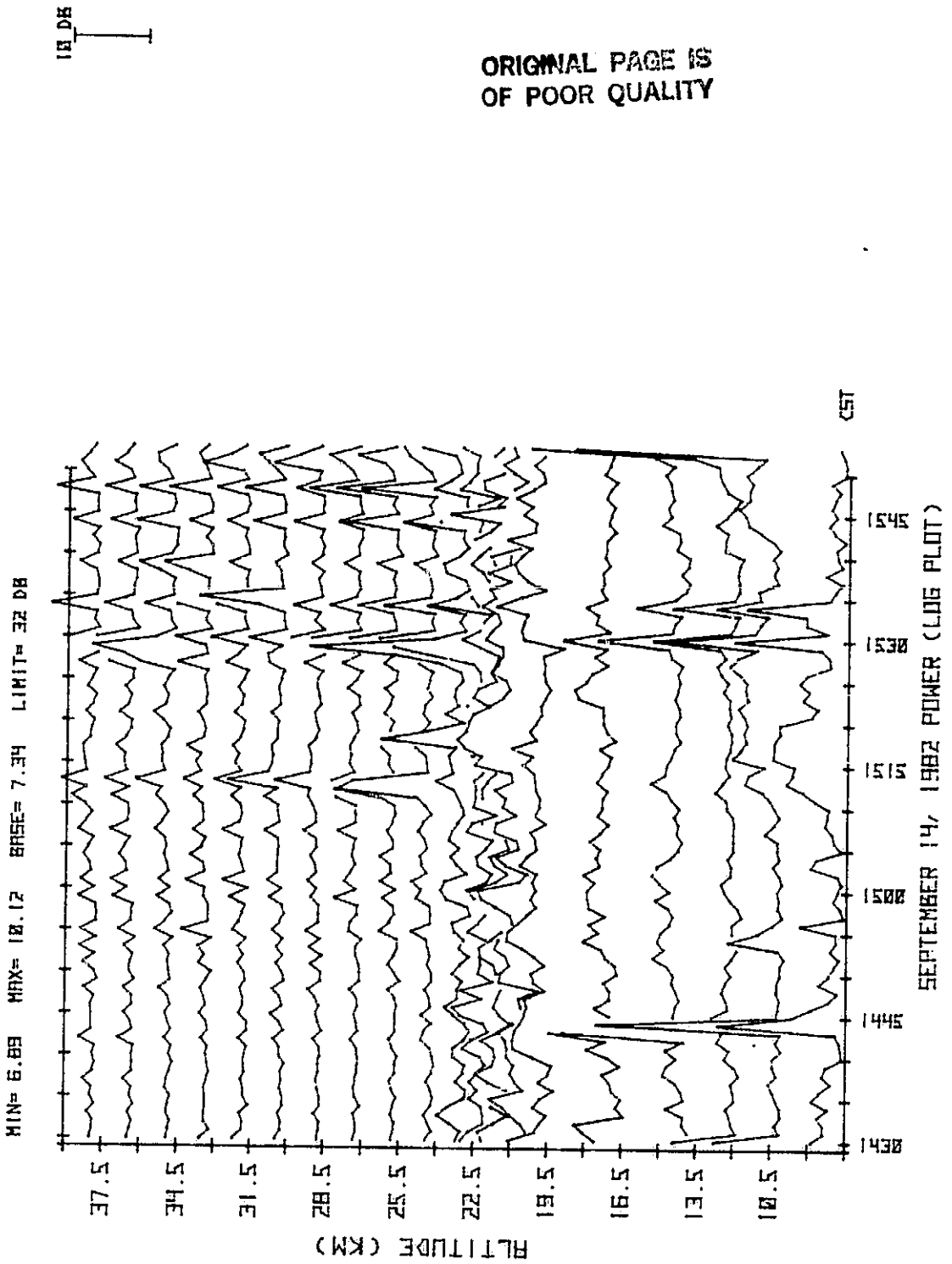

Figure 3.13 Scattered power at each sample altitude versus time beginning at 1430 CST on September 14, 1982.

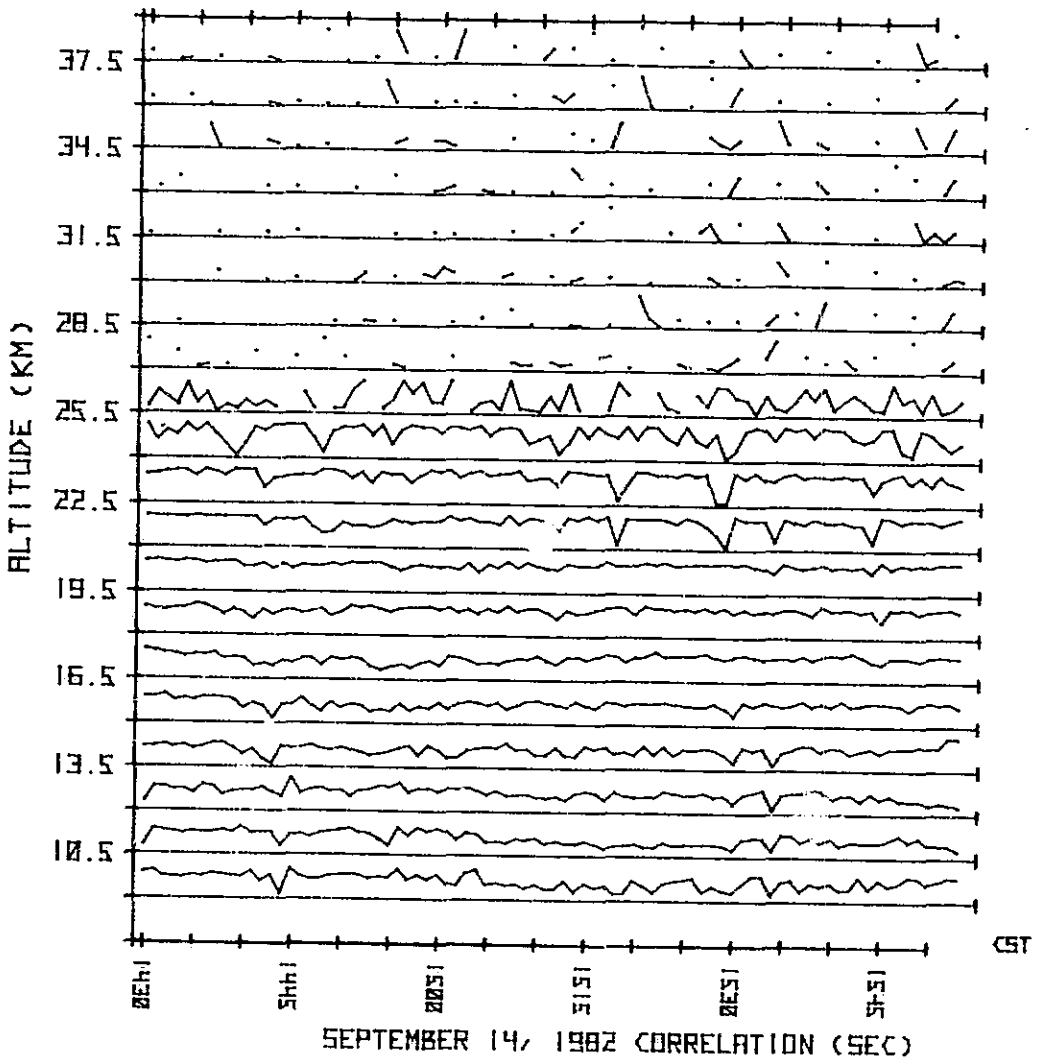

SCALE
I —

ORIGINAL PAGE IS
OF POOR QUALITY

Figure 3.14 Correlation time at each sample altitude versus time beginning at 1430 CST on September 14, 1982.

hours of data taken were hampered by transmitter difficulty. However, good data were still obtained at altitudes above 15 km. The line-of-sight velocities for 822 CST to 1022 CST are given in Figure 3.15. Note the velocity scale of 2 m/s. Figure 3.16 shows velocities during the period 1114 CST to 1314 CST. By this time, the weather had turned sunny and warm. However, this figure continues to show moderate gravity wave activity. These waves are at times in phase over as much as a 10.5 km vertical region. An example of this can be found at 1225 CST. Also, the line-of-sight velocities of two adjacent altitudes sometimes correlate highly with one another. This is apparent for 16.5 km and 18 km between 1140 CST and 1210 CST, although it is more common above 18 km. Given the radar height resolution of 1.5 km, this correlation is generally not expected.

A very strong thunderstorm occurred in the neighborhood of the radar on the evening of September 17, 1982. Before reaching Urbana, the storm produced golf-ball size hail in Decatur, Illinois, 76 km to the southwest. A lightning strike on the power line caused the radar transmitter to fail at 1736 CST, shortly before it began raining at Urbana. However, some useful data were collected before this time. Figure 3.17 shows the velocities, with a 5 m/s vertical scale. Worth noting in this figure are the significant updrafts on two separate occasions, 1703 CST and 1727 CST. Note that a negative line-of-sight velocity corresponds to motion away from the radar. The larger of the two extends to 12 km, a higher altitude than those of previous figures, and reaches a velocity of 2.5 m/s, larger than those previously. The fact that the storm was more intense than the previous two supports these observations.

The strongest thunderstorm to be in the Urbana area while the radar was in operation occurred on June 29, 1982. This storm produced both high winds

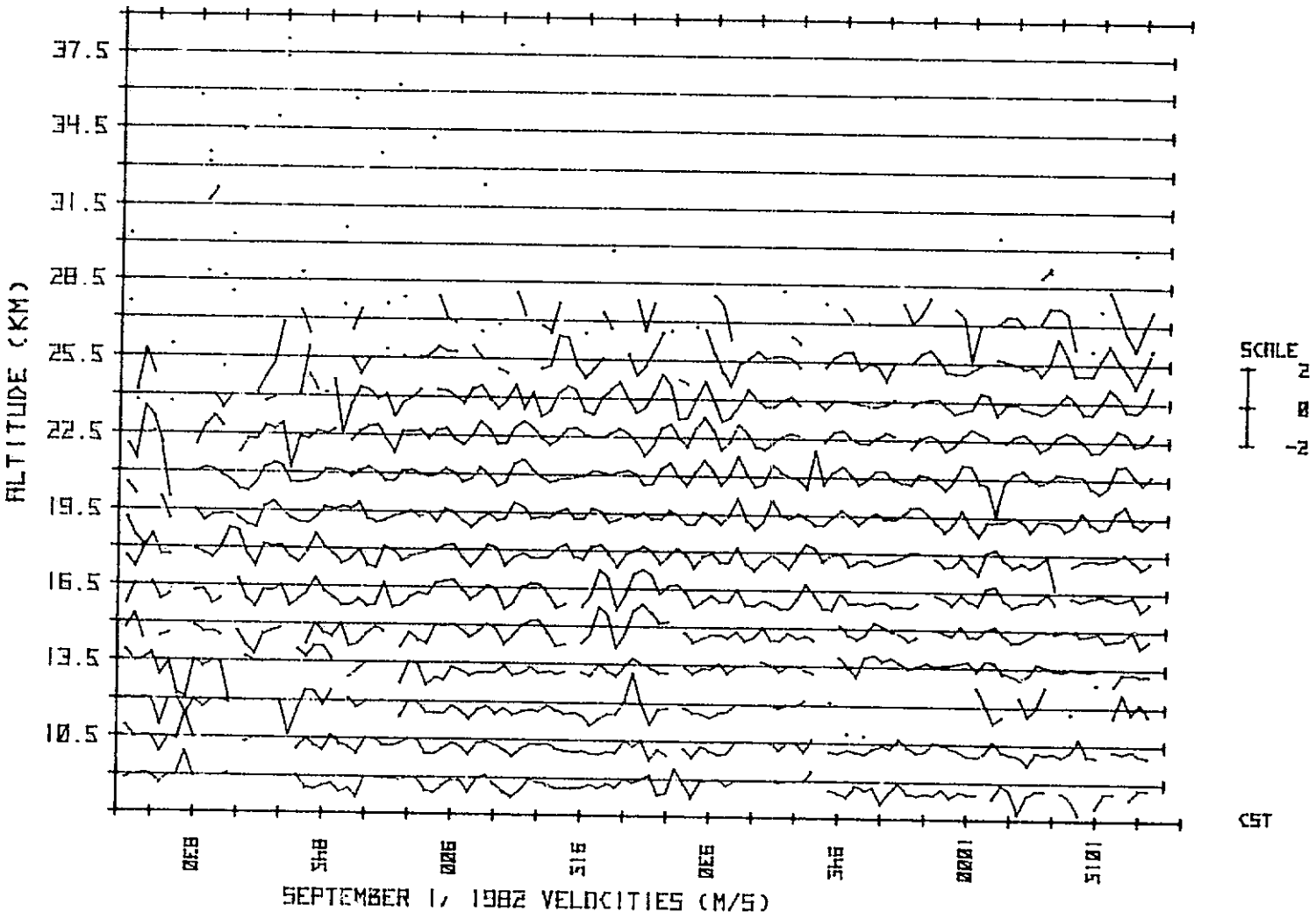

Figure 3.15 Line-of-sight velocity beginning at 822 CST on September 1, 1982. Note scale of 2 m/s.

ORIGINAL PAGE IS
OF POOR QUALITY

ORIGINAL PAGE IS
OF POOR QUALITY

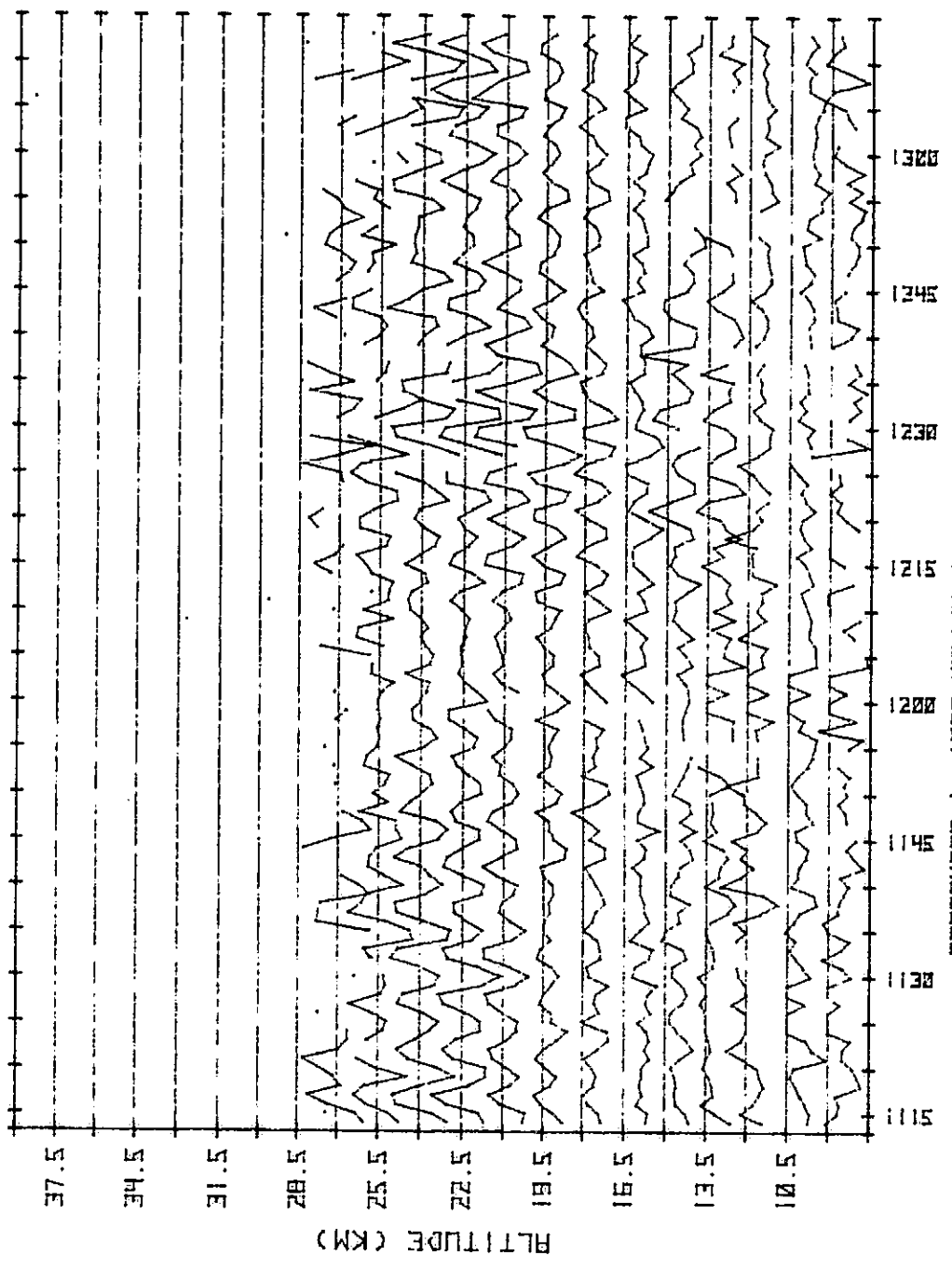

Figure 3.16 Line-of-sight velocity beginning at 1114 CST on September 1, 1982.

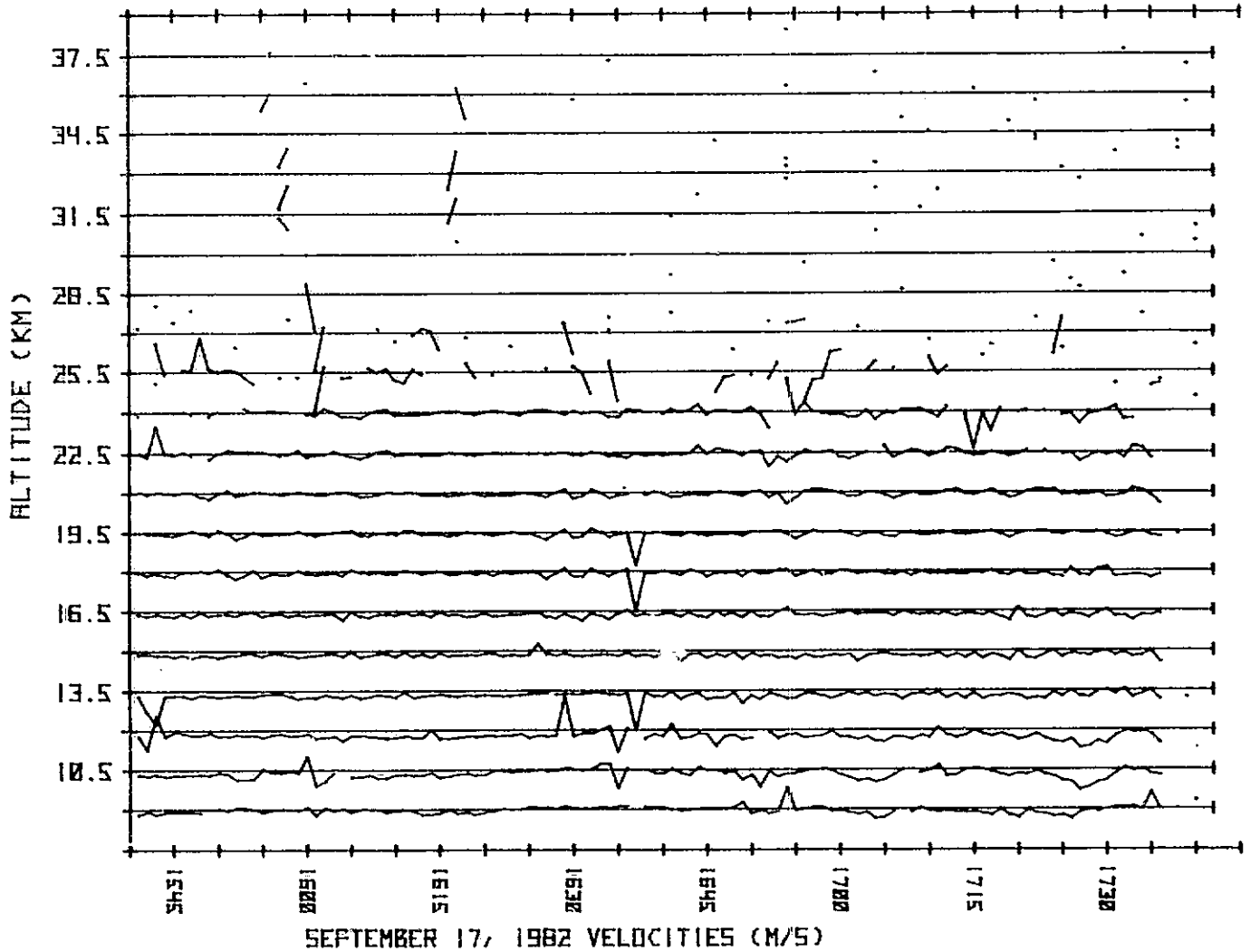

Figure 3.17 Line-of-sight velocity beginning at 1541 CST on September 17, 1982, showing updrafts. Note scale of 5 m/s.

ORIGINAL PAGE IS
OF POOR QUALITY

and heavy rains. The radar was turned on after the main storm had passed. Figure 3.18 shows the velocity data taken during a two hour period immediately after the storm had passed. Again, the scale is 5 m/s. There is strong gravity wave activity as in the other observations. However, the most interesting feature of these data is the strong updraft (corresponding to negative line-of-sight velocity) located from 12 km to 15 km at the beginning of the observation period. This updraft lasted for at least 20 minutes at 12 km and reached a velocity of almost 5 m/s at 13.5 km. At one point the updraft extended as far up as 15 km, which clearly suggests that this storm was stronger relative to the others. This deduction is supported by the National Weather Service radar summary at 1735 CST, approximately 1 hour before data collection began. The summary shows cloud top heights of 55,000 feet, or 16.7 km, in an area just west of Urbana. Thus, the observation of an updraft at 15 km is entirely possible for this storm. Ironically, of the four occasions during which thunderstorms were in the neighborhood of the operating Urbana radar, this was the only time that central Illinois was not under a severe weather watch or warning.

3.4 Continuous 36-Hour Observations

Hourly-averaged power levels and horizontal velocities can be used to study the dynamics of the atmosphere over long time periods. Observations of power and velocity in the upper troposphere and lower stratosphere over a 36-hour period are given below.

The Urbana radar was operated continuously from 601 CST on September 16, 1982 until 1736 CST on September 17, 1982, a period of nearly 36 hours. Data were collected on a continuous basis for two hours at a time, with a short break between each two-hour period required to dump the data from disk to DECtape. Hourly averaged power levels and horizontal winds for each

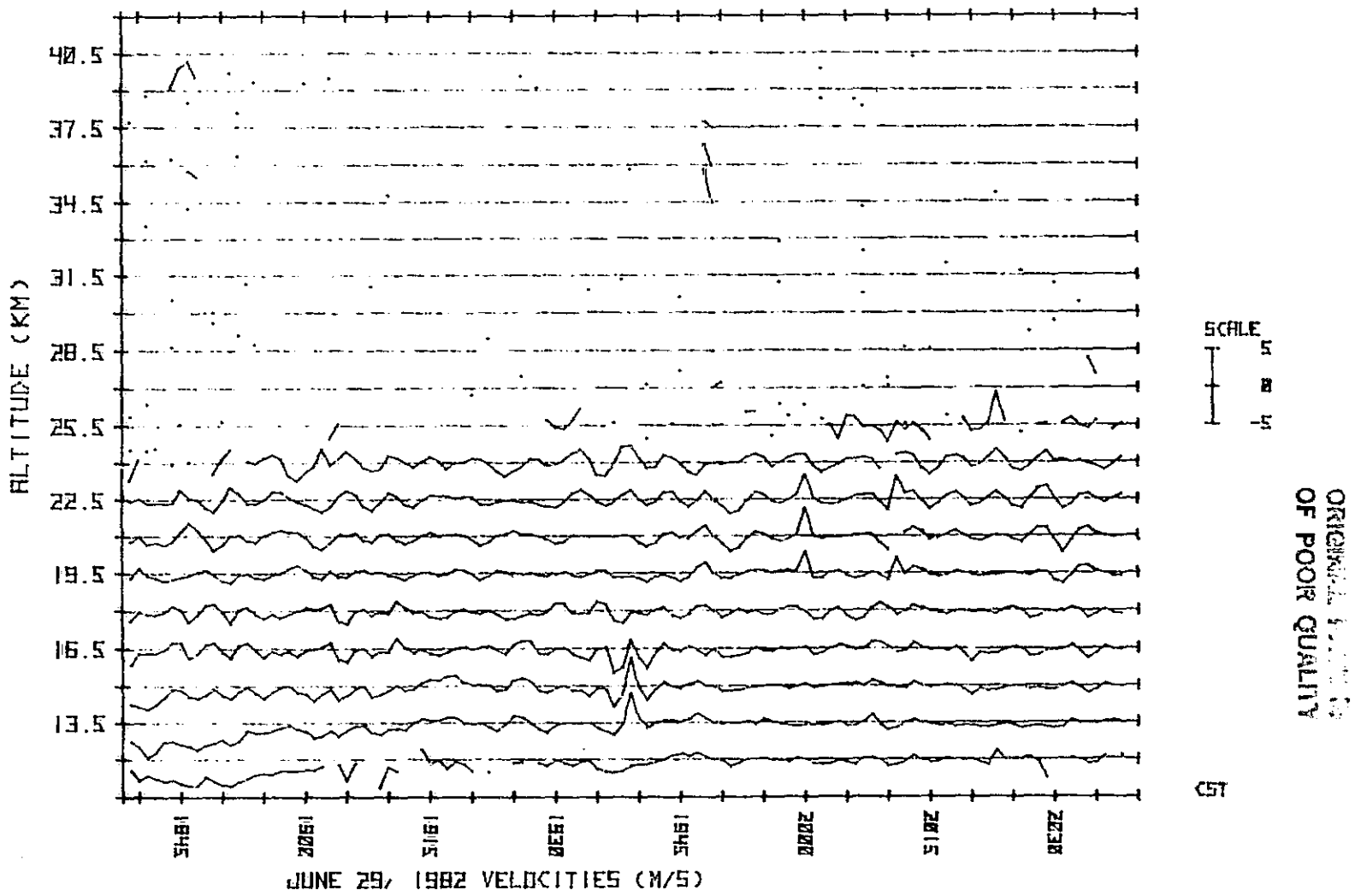

Figure 3.18 Line-of-sight velocity beginning at 1839 CST on June 29, 1982, showing large updraft. Note scale of 5 m/s.

ORIGINAL PAGE IS
OF POOR QUALITY

height gate between 10.5 and 24.0 km are given in Figures 3.19-3.28. Data from 2013 CST until 2217 CST on September 16 should be ignored as they were contaminated by the passing of celestial radio source Cygnus-A through the antenna beam. Sharp changes in power levels at all altitudes during this time period are caused by increased attenuation being switched into the receiving system.

The most interesting feature of the data occurs between 0329 CST and 1711 CST on September 17, 1982 at 10.5 and 12 km (Figures 3.19 and 3.20). Horizontal velocities oscillate with a period of approximately four hours. Velocities at 10.5 km lead those at 12 km by one hour. This wave motion is superimposed upon a gradual increase in velocity caused by a jet stream passage (Figure 3.7). A 6 dB decrease in scattered power occurs at 12 km at 737 CST. From Figure 3.7, 12 km lies near the core of the jet. High wind velocities at this altitude are a possible cause for this power decrease. In contrast, power levels at 13.5 km (Figure 3.21) increase slightly during this time. Shear-induced turbulence above the jet could be the cause of this increase.

Little power or wind variability exists at 15 km (Figure 3.22), although it appears that this altitude has become more stable after approximately 2321 CST on September 16. Some evidence of the jet can be seen in the velocity plot at 1155 CST on September 17.

The high power levels at 16.5 km suggest that we are in the vicinity of the tropopause height. Most power levels at this height are in excess of 90 dB, more than 20 dB above the noise floor. In the velocity plot, some evidence of long-period wave motion can be found after 737 CST on September 17.

ORIGINAL PAGE IS
OF POOR QUALITY

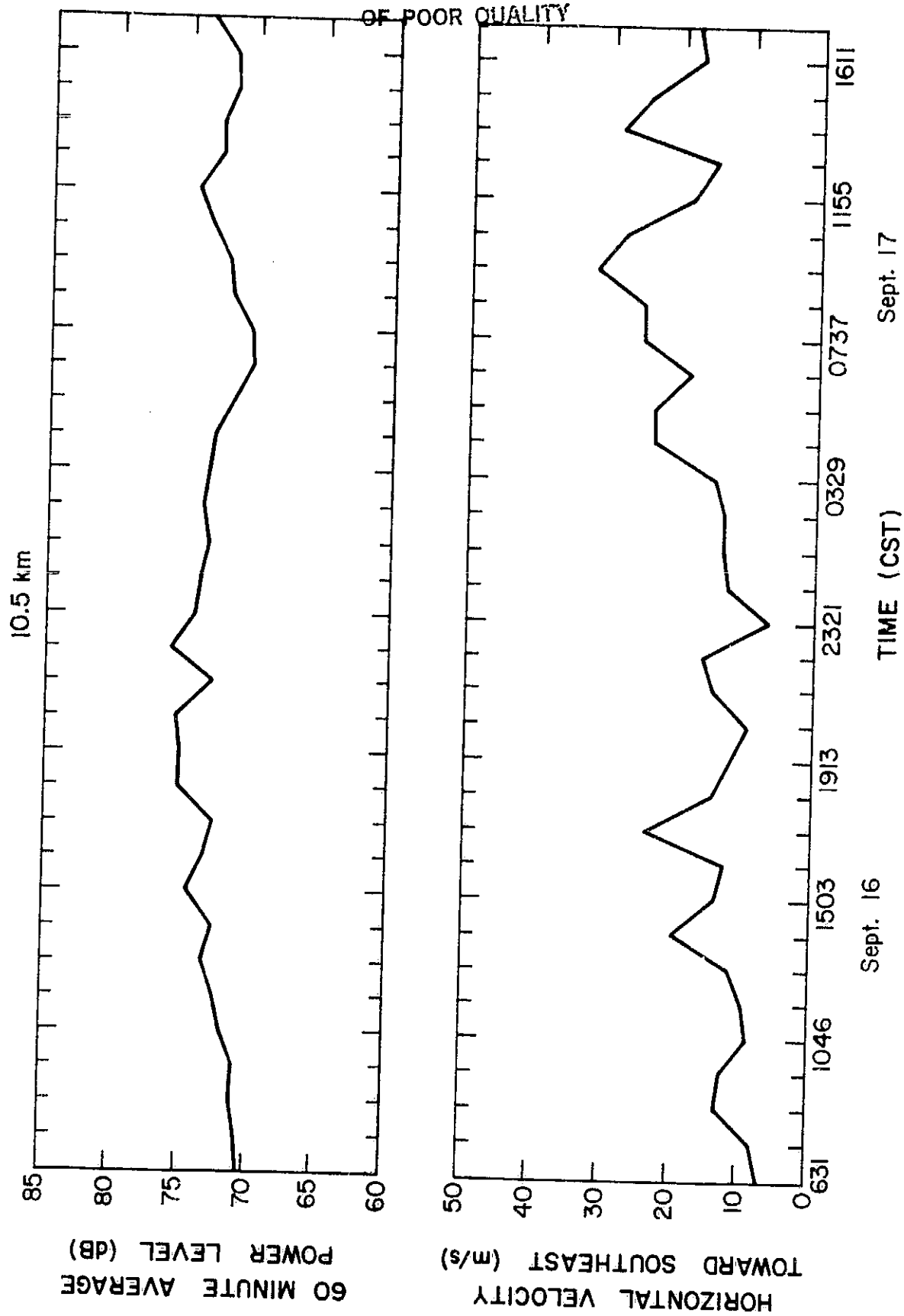

Figure 3.19 Hourly averaged power and velocity at 10.5 km for a 36-hour period on September 16-17, 1982.

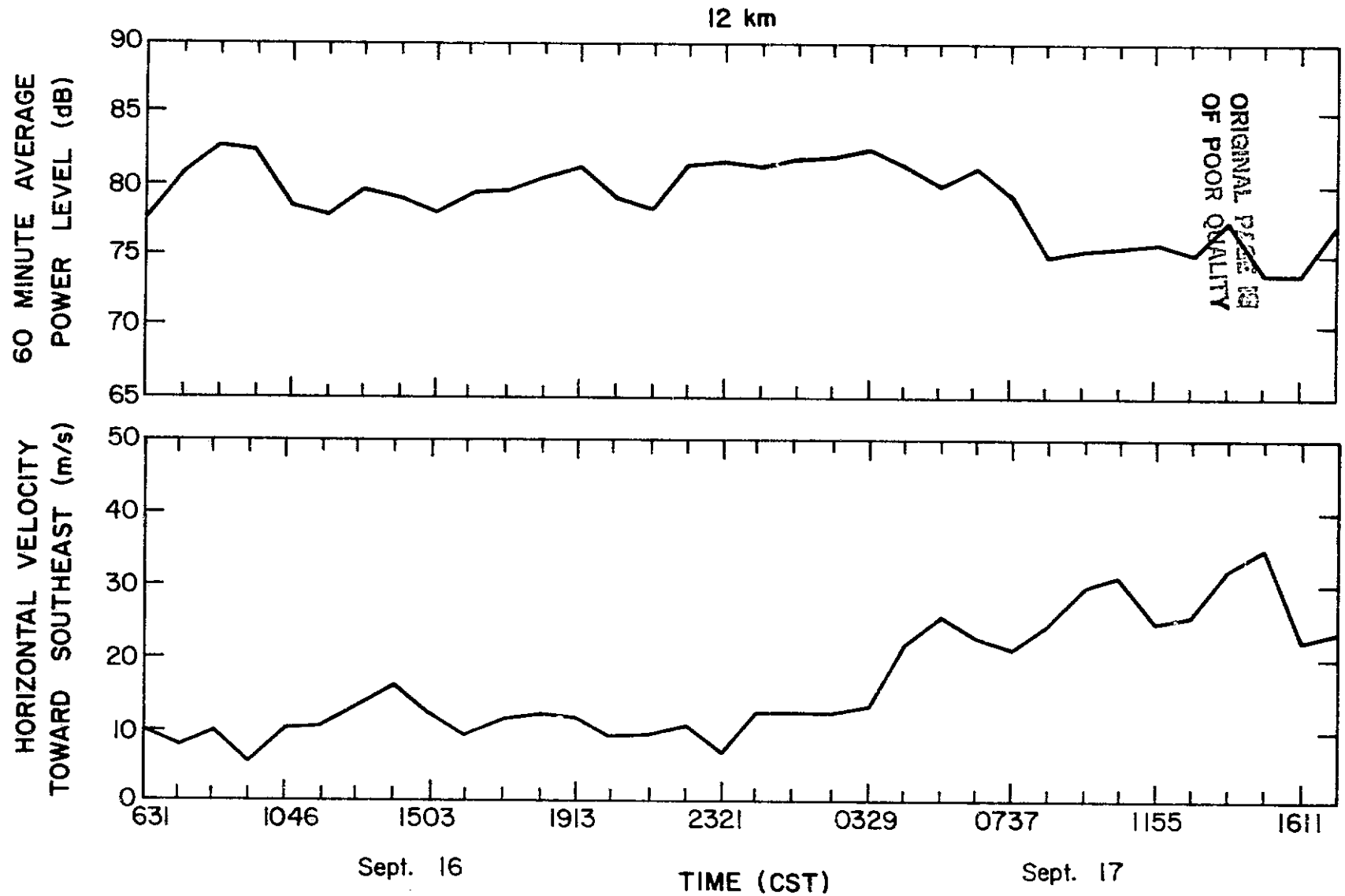

Figure 3.20 Hourly averaged power and velocity at 12 km for a 36-hour period on September 16-17, 1982.

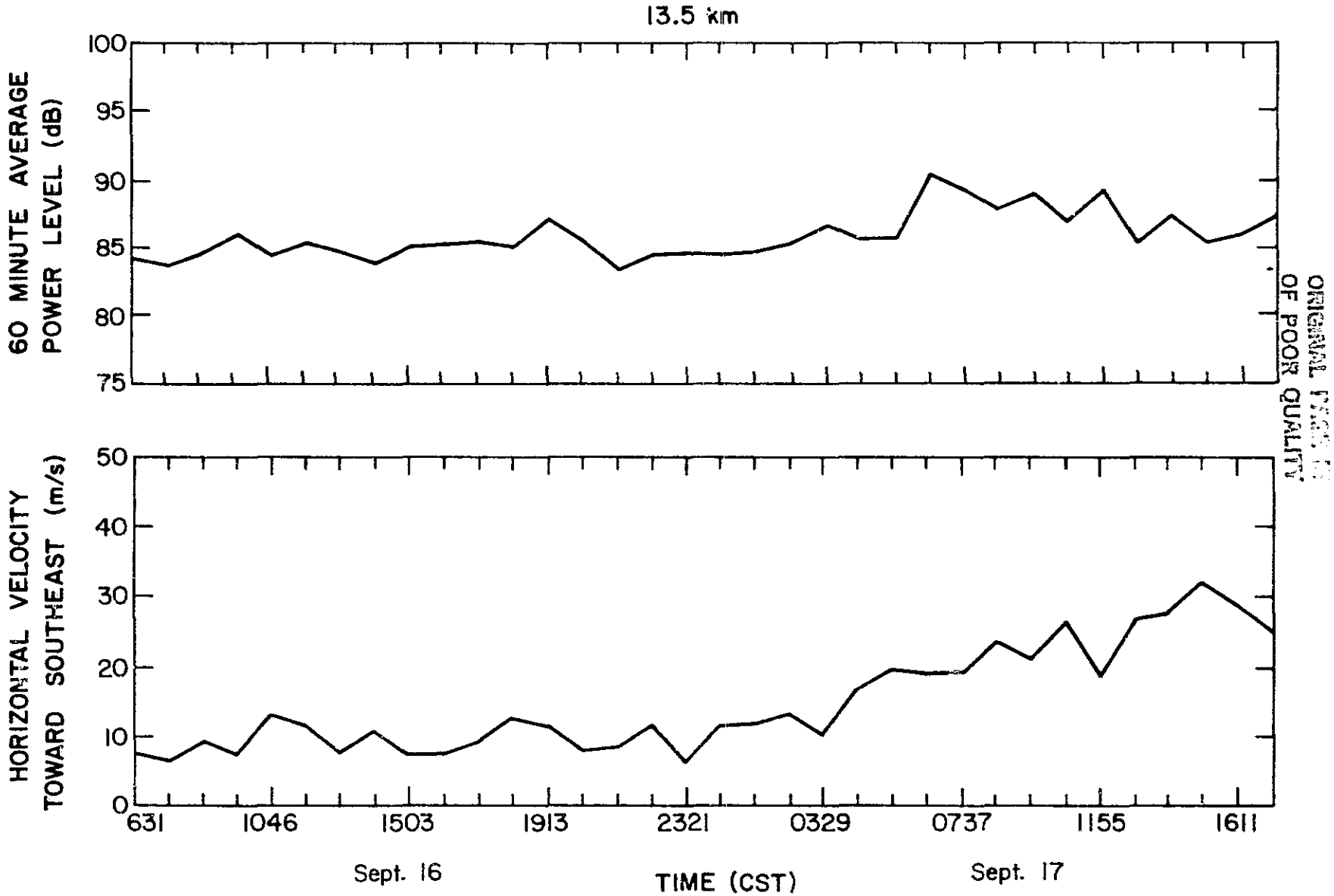

ORIGINAL PAGE IS OF POOR QUALITY

Figure 3.21 Hourly averaged power and velocity at 13.5km for a 36-hour period on September 16-17, 1982.

ORIGINAL PAGE IS
OF POOR QUALITY

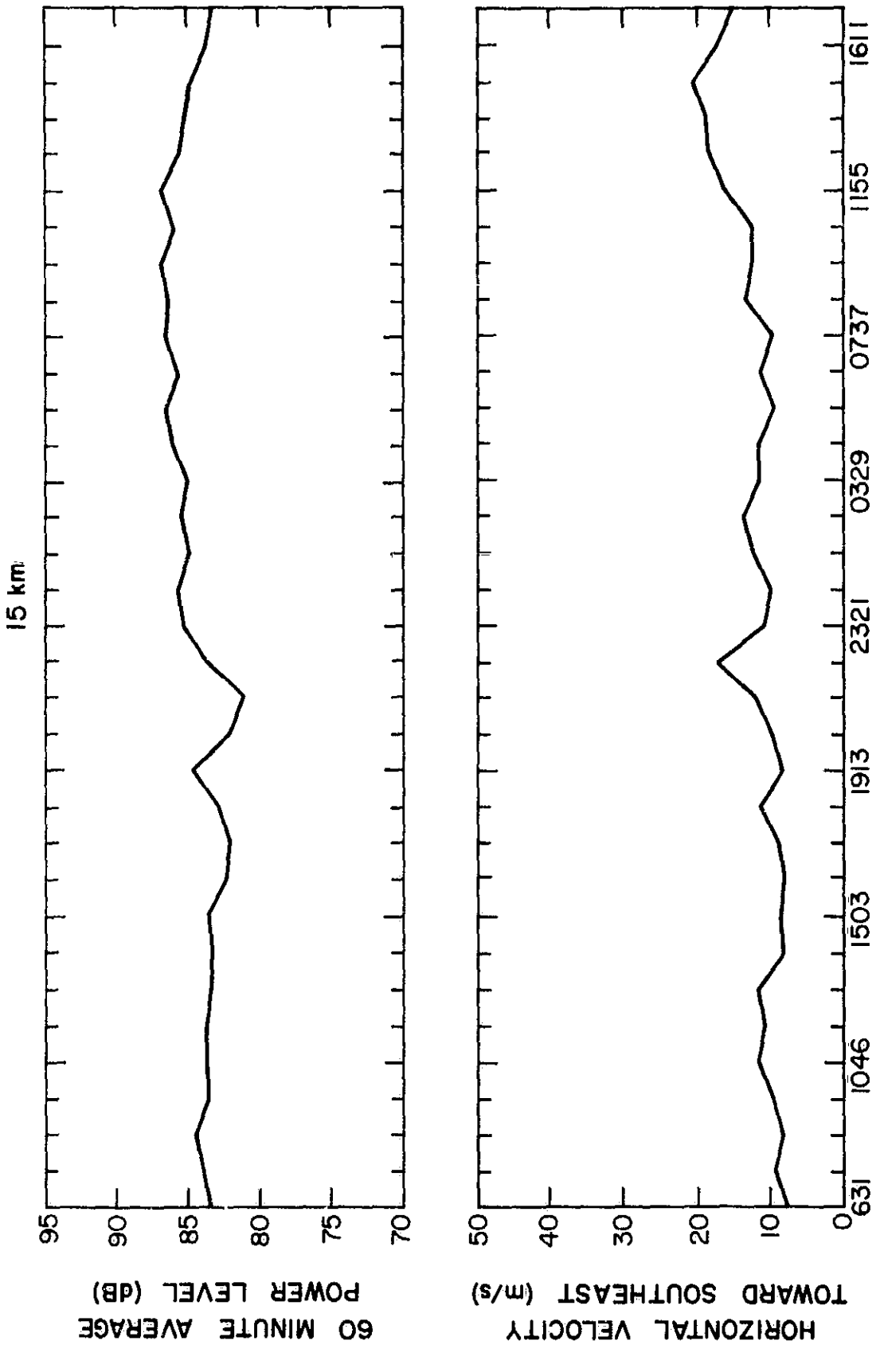

Figure 3.22 Hourly averaged power and velocity at 15 km for a 36-hour period on September 16-17, 1982.

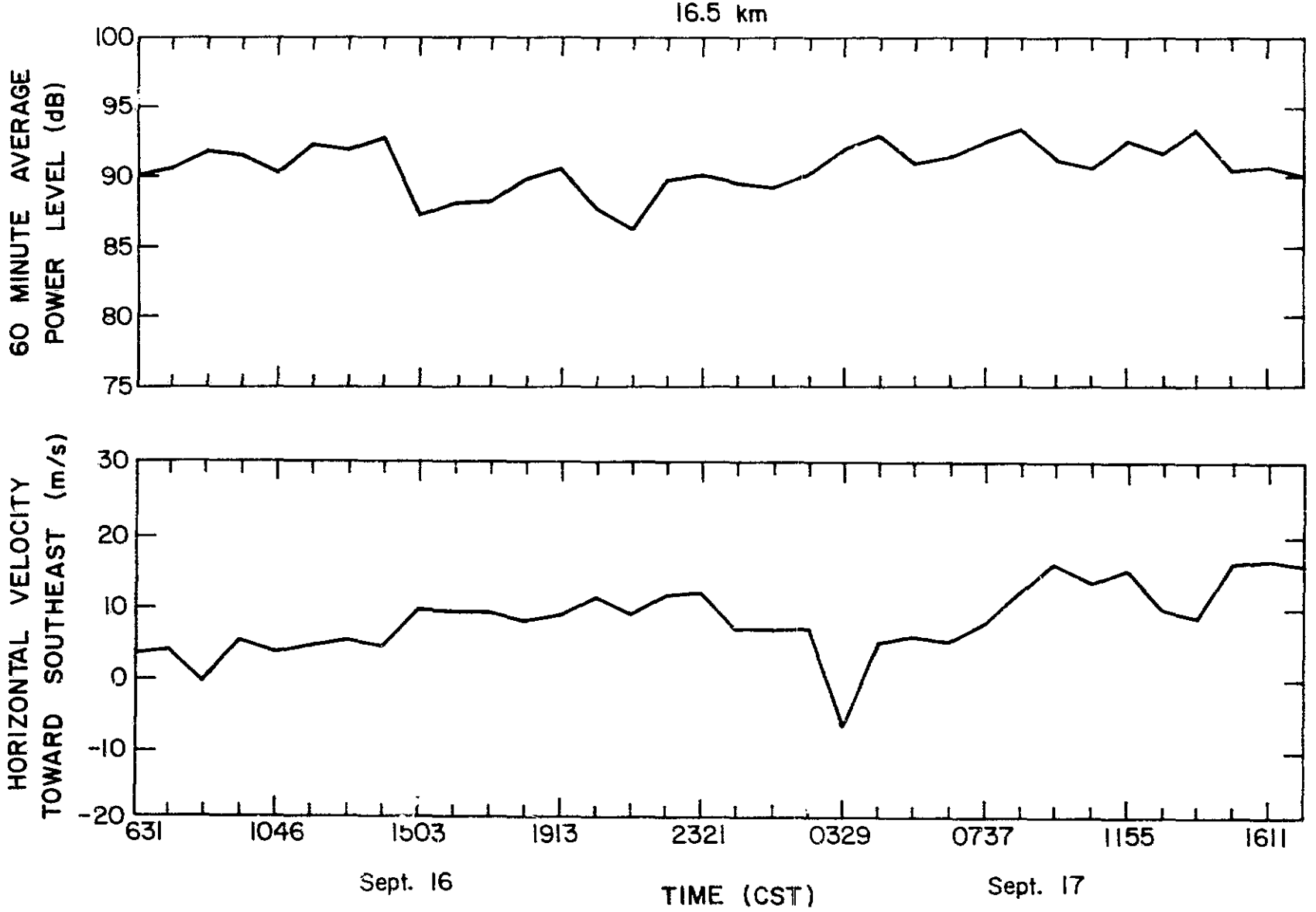

Figure 3.23 Hourly averaged power and velocity at 16.5 km for a 36-hour period on September 16-17, 1982.

ORIGINAL PAGE IS
OF POOR QUALITY

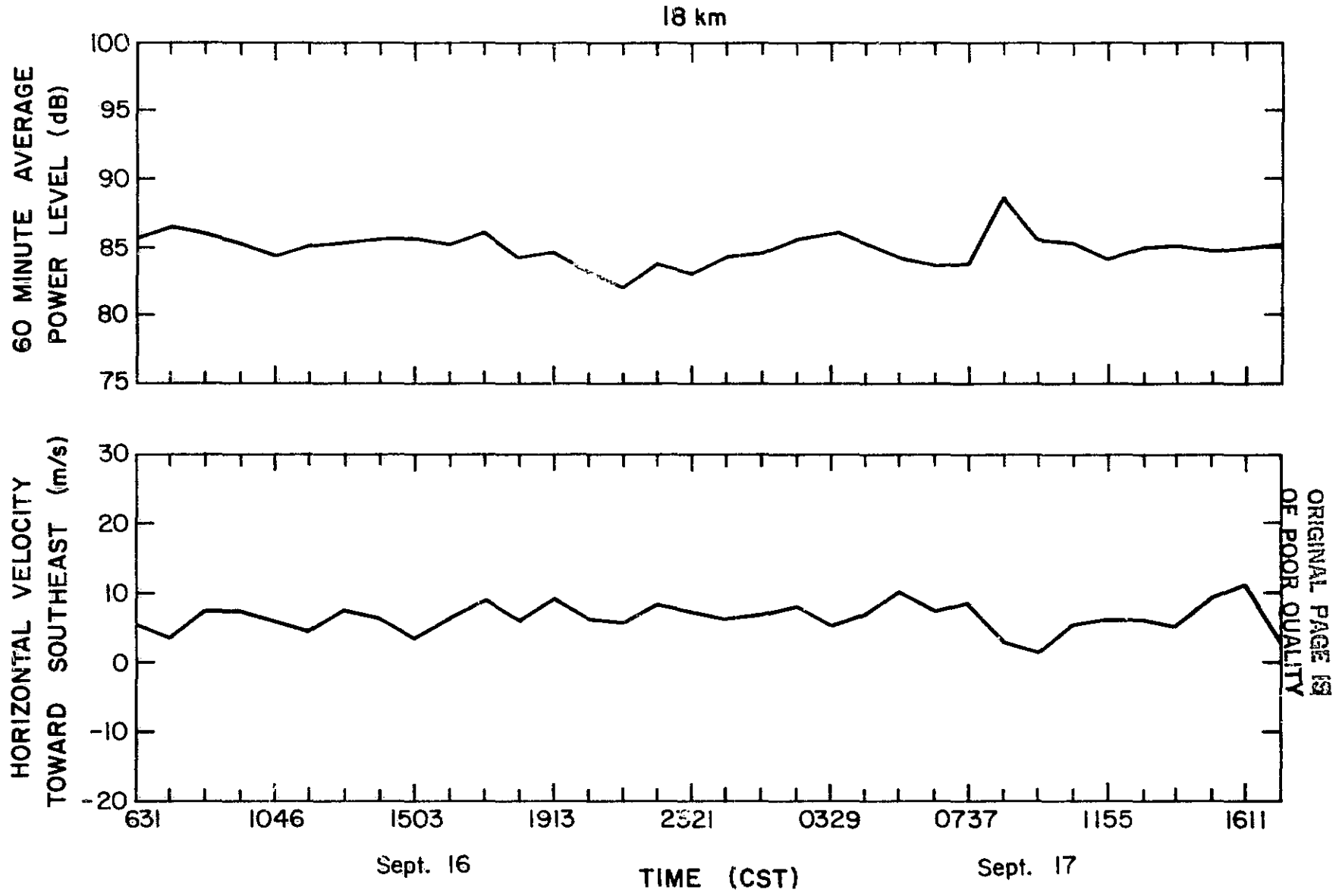

Figure 3.24 Hourly averaged power and velocity at 18 km for a 36-hour period on September 16-17, 1982.

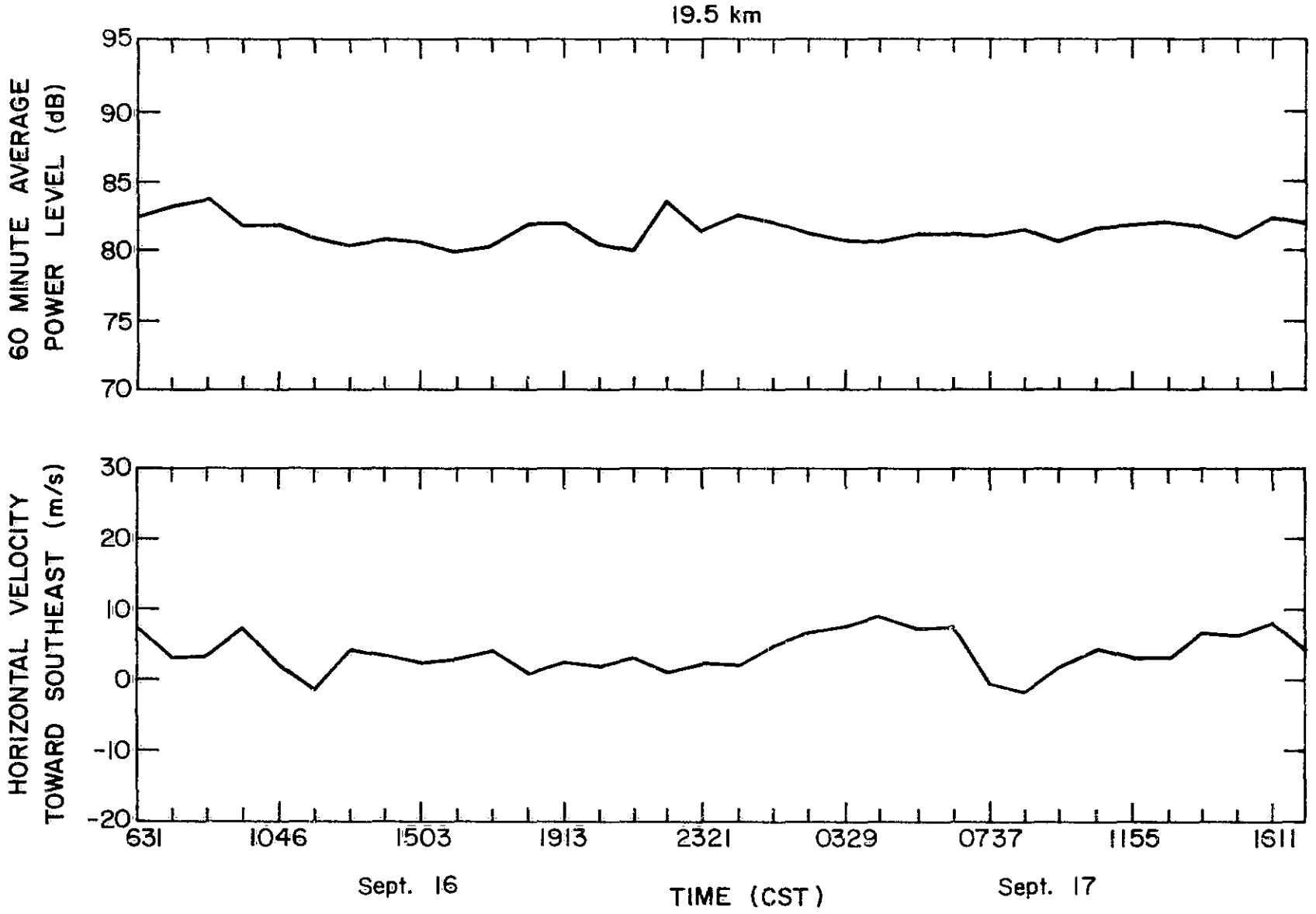

ORIGINAL PAGE IS
OF POOR QUALITY

Figure 3.25 Hourly averaged power and velocity at 19.5 km for a 36-hour period on September 16-17, 1982.

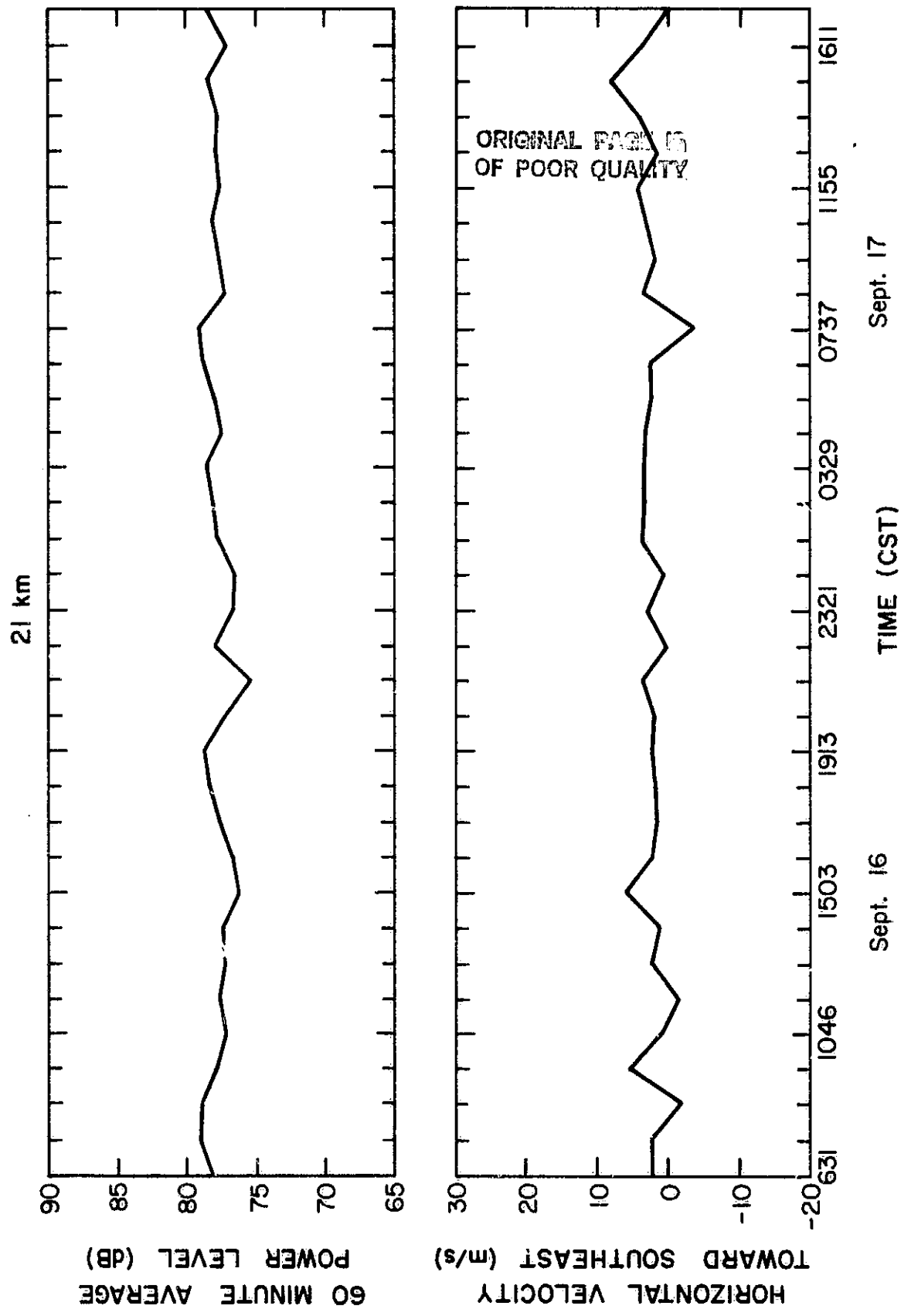

Figure 3.25 Hourly averaged power and velocity at 21 km for a 36-hour period on September 16-17, 1982.

ORIGINAL PAGE IS
OF POOR QUALITY

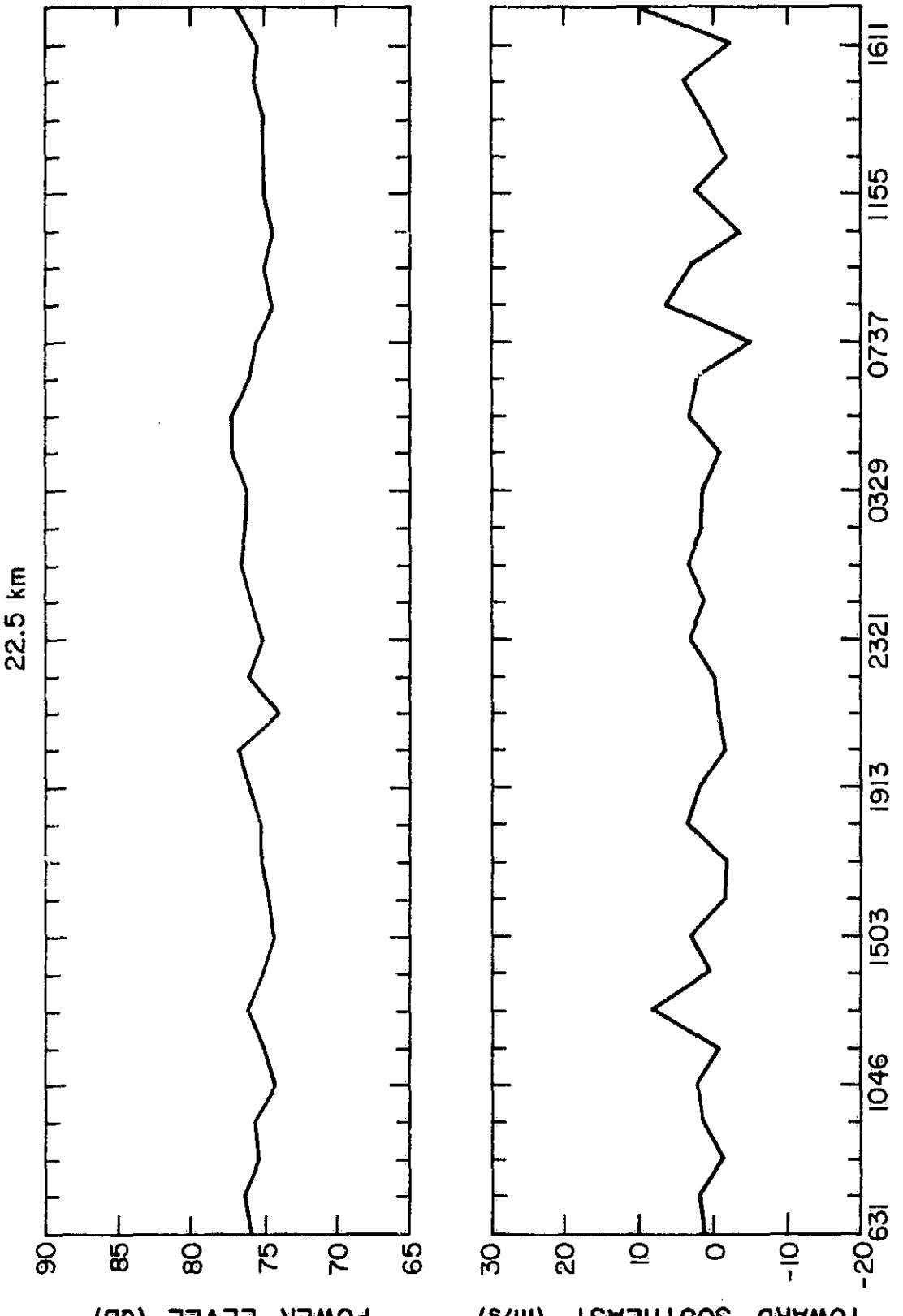

Figure 3.27 Hourly averaged power and velocity at 22.5 km for a 36-hour period on September 16-17, 1982.

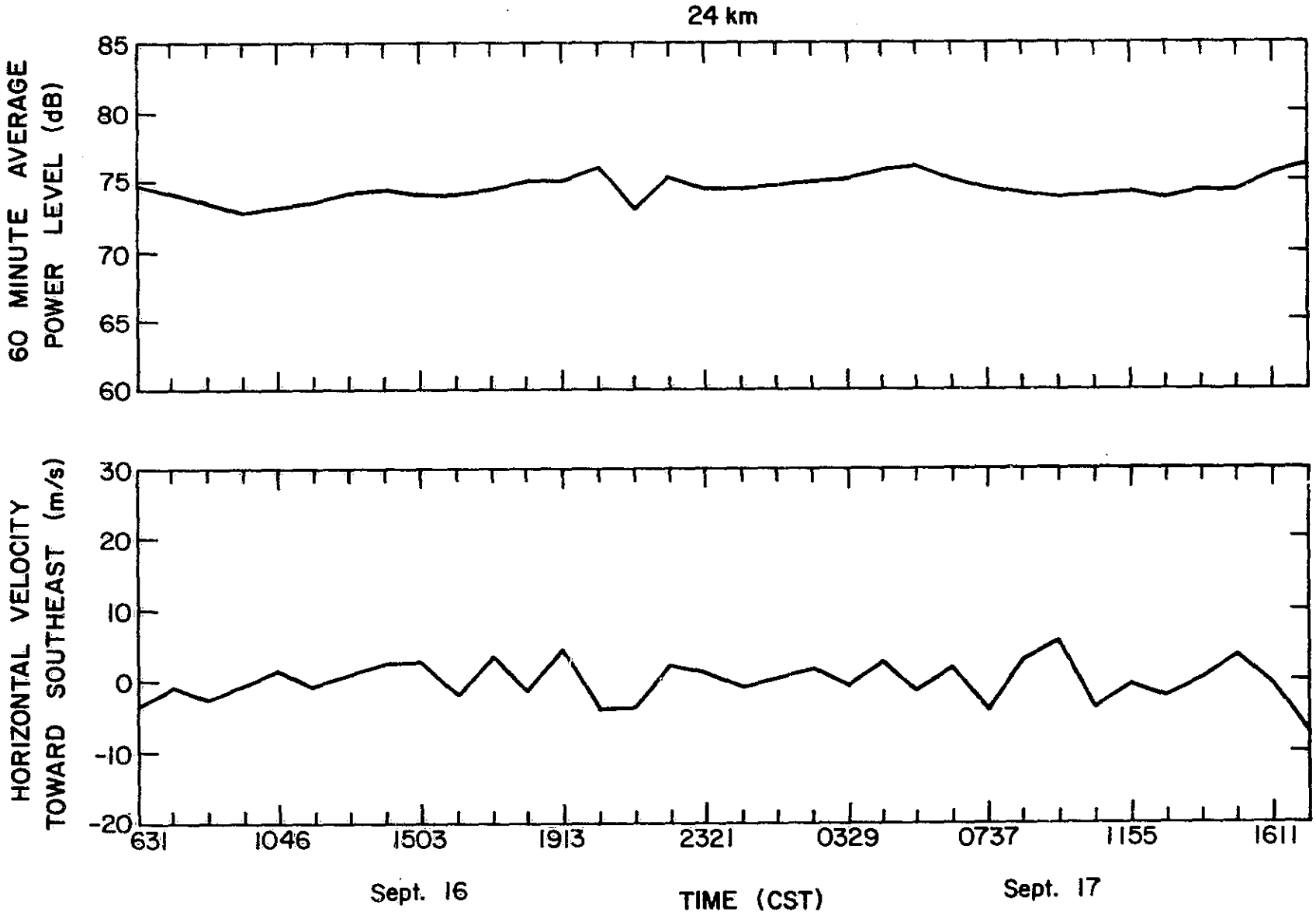

Figure 3.28 Hourly averaged power and velocity at 24 km for a 36-hour period on September 16-17, 1982.

ORIGINAL PAGE IS OF POOR QUALITY

Wave motion is also present during this time period in velocities at 18 and 19.5 km. These waves have periods which are approximately twice those at 16.5 km. As we go up in the stratosphere, power levels are observed to decrease 3-4 dB per 1.5 km, as explained earlier. Also, velocities are less variable on an hour-to-hour basis than they were in the upper troposphere. Estimates of hourly averaged velocities at 22.5 and 24 km become worse because low signal levels at these altitudes prevent the calculation of all sixty minute-by-minute velocities needed for the average.

4. INTERPRETATION AND DISCUSSION

4.1 Scattered Power Level and Atmospheric Stability

Many groups using VHF radars have reported enhanced returns at vertical incidence. These returns are thought to be caused by specular reflections from horizontally stratified layers in the lower stratosphere as opposed to scattering from isotropic turbulence, which is not aspect sensitive [Gage and Green, 1978]. Scattering at VHF wavelengths is caused by changes in the radio index of refraction [Rottger, 1980b]. In the upper troposphere and lower stratosphere, electron concentration and humidity are negligible contributors to this index so that $(n-1) = 77.6 \times 10^{-6} P/T$, where n is the radio index of refraction, P is the pressure in millibars (mb), and T is absolute temperature. Thus, sharp gradients of temperature with altitude cause a large change in n.

The most common and easily detectable sharp temperature gradient is the tropopause. The tropopause height is easily recognized on Urbana power plots as an altitude which exhibits constantly strong power returns over time. An important characteristic of inversions is that they are hydrostatically stable. That is, very little vertical mixing is present. Gage and Green [1980] have shown evidence of a relation between the magnitude of the enhanced vertical returns and the level of hydrostatic atmospheric stability present at the time.

In this section, similar comparisons made with the Urbana radar are shown. Hourly-averaged power levels of the radar sample heights are compared to profiles of the change in potential temperature with altitude, $\partial\theta/\partial z$ The potential temperature is defined as $\theta = T(1000/P)^{2/7}$, where T is the absolute temperature and P is the pressure in mb. The potential temperature

is calculated from data available from nearby National Weather Service balloon soundings at five points common to the range probed by the radar. The change in θ between successive heights is then calculated and plotted as an average value throughout each layer. These values are directly proportional to the amplitude of the inversion.

Several of these comparisons are shown in Figures 4.1-4.9. As with the horizontal wind comparisons, the temporal and spatial differences between the observations most likely cause some discrepancies. However, many figures have excellent agreement. For instance, Figure 4.3 shows a very stable layer present between 14.2 and 16.7 km. As a result, the power level at 15 km shows an 11 dB increase over that at 13.5 km.

More convincing evidence is found in Figures 4.4 and 4.5. Here, a stable layer can be seen forming at 1200Z at an altitude of 10 km. By 0000Z on July 23, the layer has moved up to between 11 km and 12 km in altitude, and has increased in stability. The power levels observed at 1828Z, also shown in Figure 4.4, indicate that this upward movement actually occurred before midday. Power levels at 2133Z in Figure 4.5 also show this layer at 12 km. Thus, indications are that this stable layer persisted at 11-12 km for at least a six-hour period.

Figure 4.7 shows a stable layer detected in the middle of the observation range at 12.5 km. Again, the power return follows the temperature gradient closely. Figure 4.9 shows a bifurcation similar to those of Figure 4.4 and 4.5. Multiple layers of stability are a fairly common occurrence at Urbana. The power levels here also show excellent agreement.

4.2 Vertical Velocity Variations

In Section 3.3 it is observed that, in general, gravity wave amplitude is larger during periods of convective activity. More data are shown here

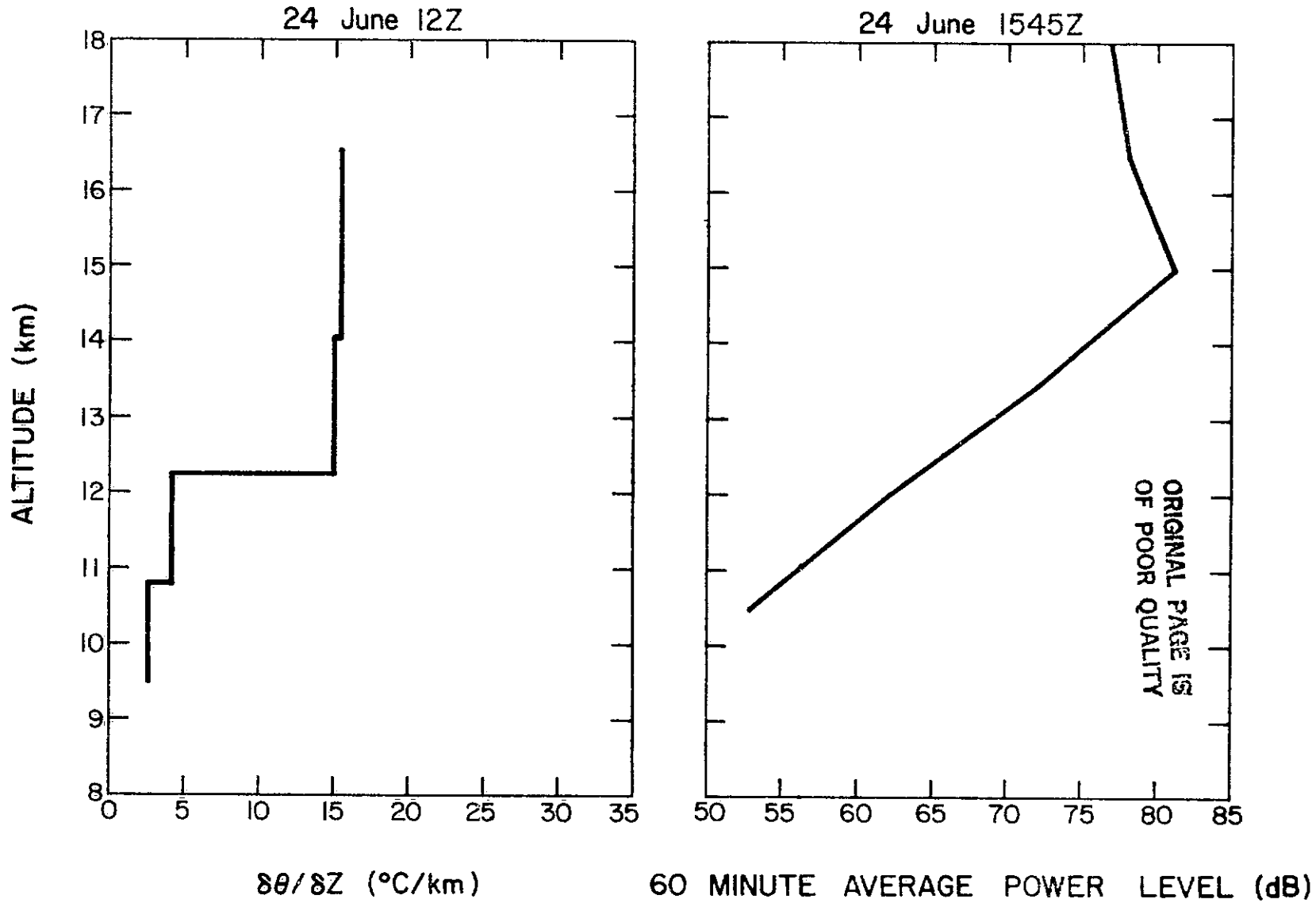

Figure 4.1 Comparison of potential temperature gradient and hourly averaged power profiles on morning of June 24, 1982.

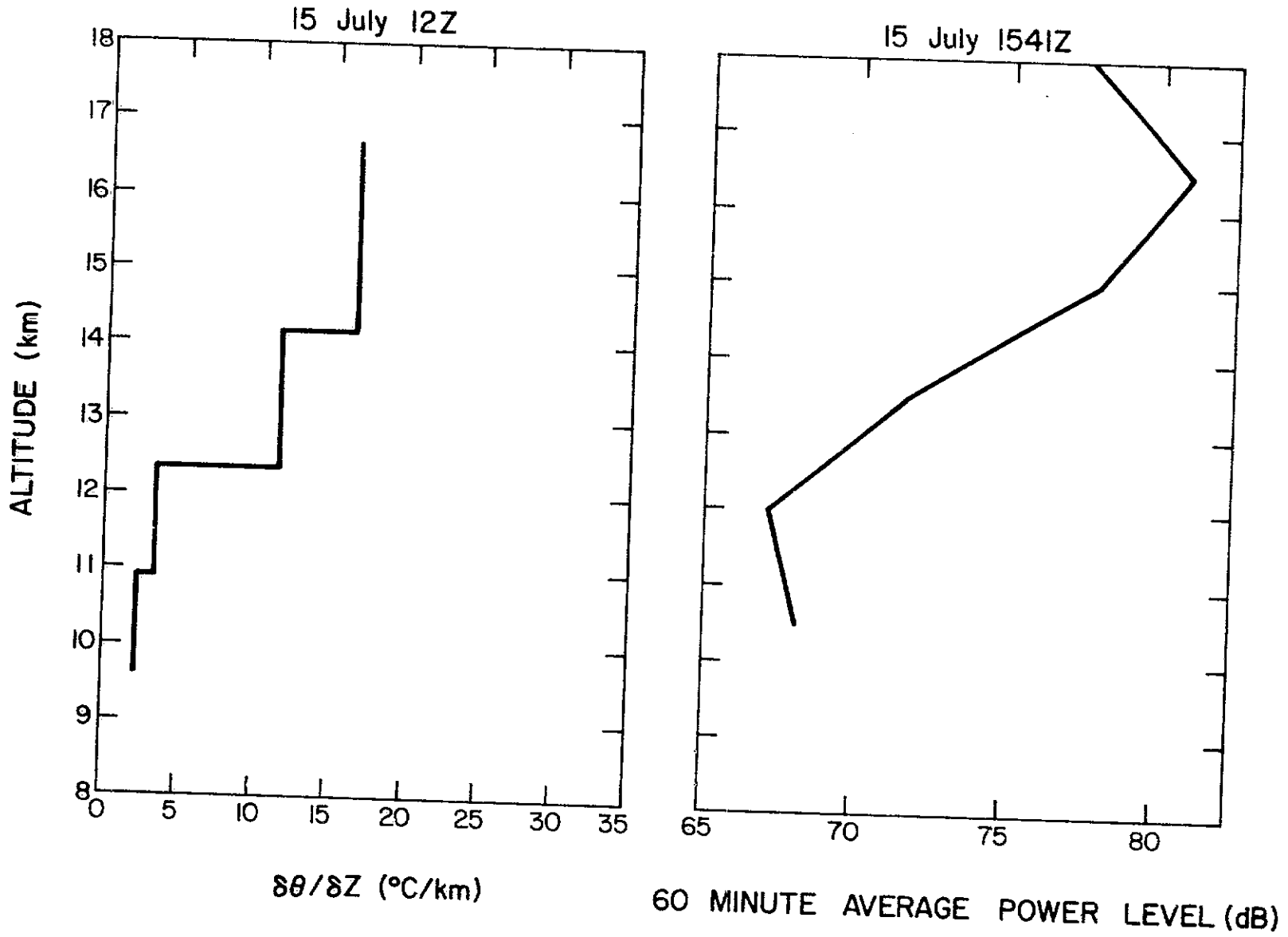

Figure 4.2 Comparison of potential temperature gradient and hourly averaged power profiles on morning of July 15, 1982.

ORIGINAL PAGE IS
OF POOR QUALITY

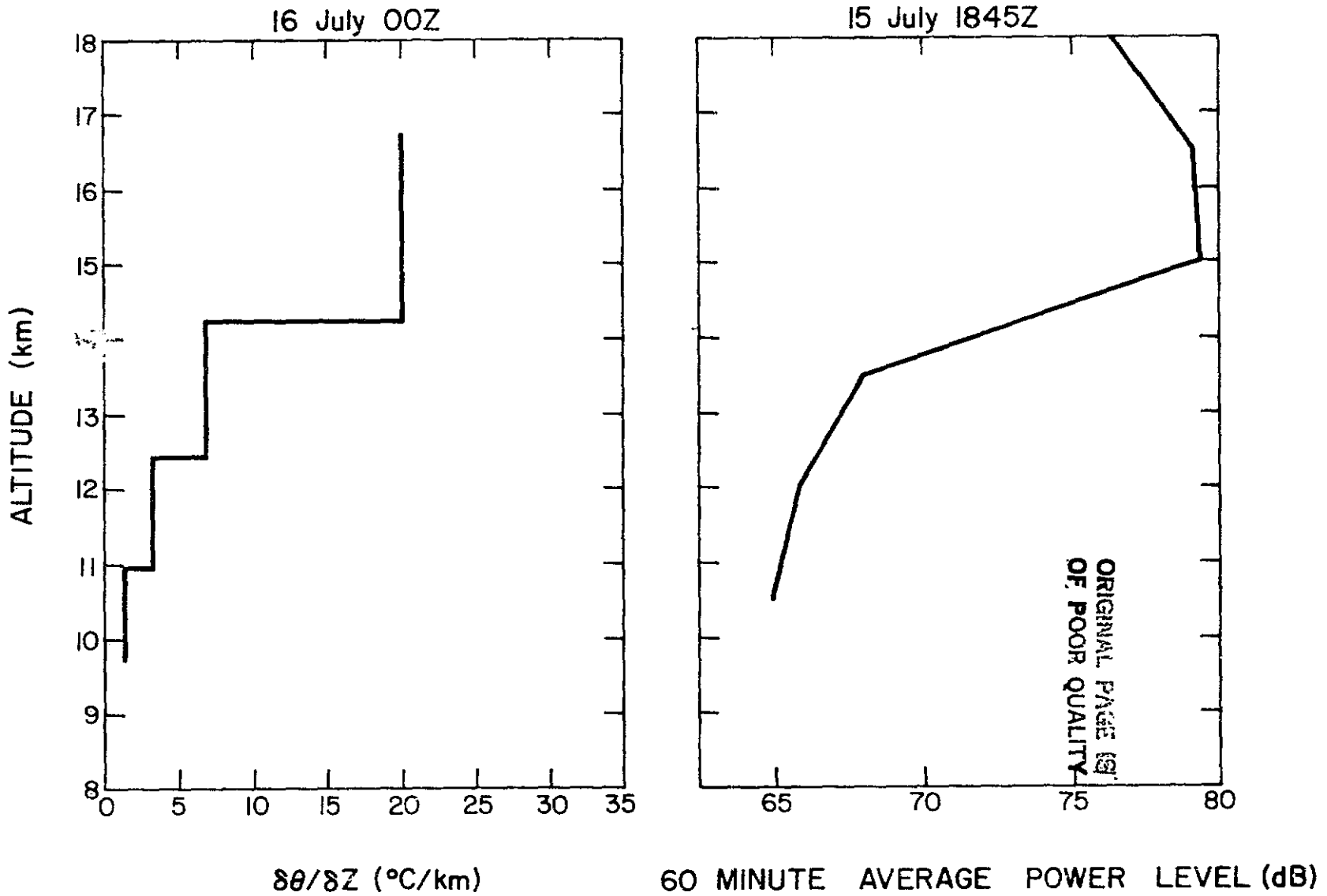

Figure 4.3 Comparison of potential temperature gradient and hourly averaged power profiles on afternoon of July 15, 1982.

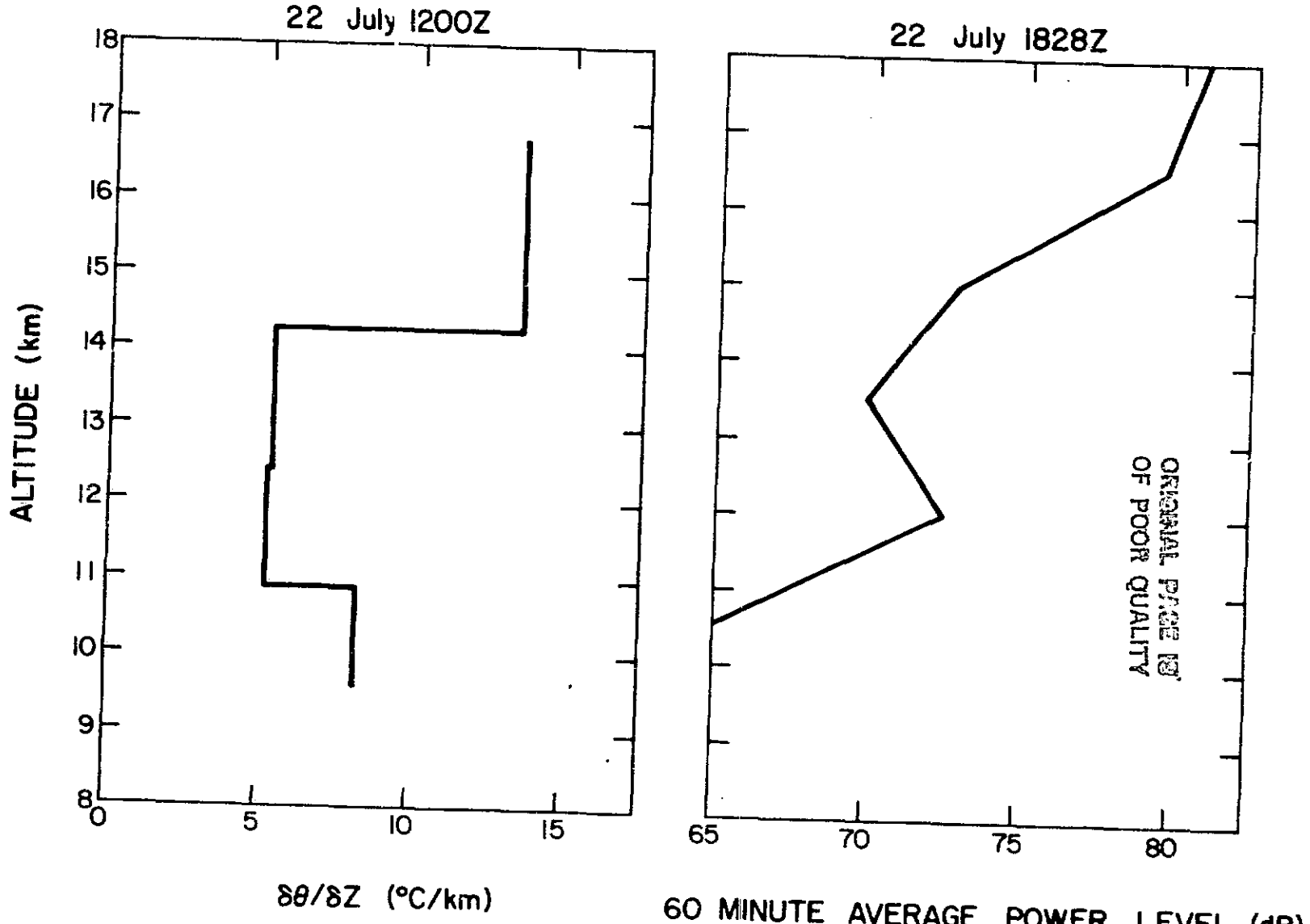

Figure 4.4 Comparison of potential temperature gradient and hourly averaged power profiles on morning of July 22, 1982.

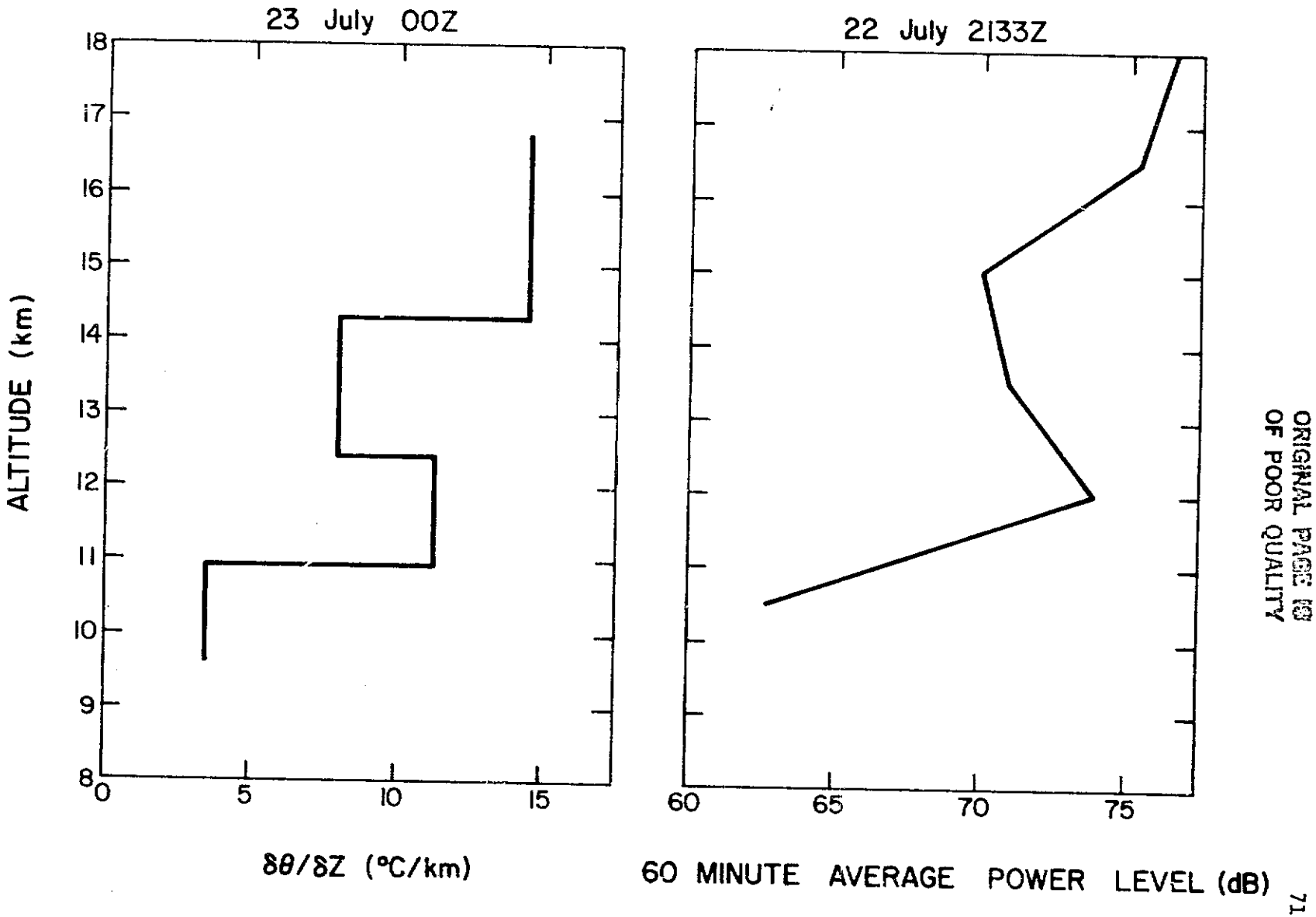

ORIGINAL PAGE IS
OF POOR QUALITY

Figure 4.5 Comparison of potential temperature gradient and hourly averaged power profiler on afternoon of July 22, 1982.

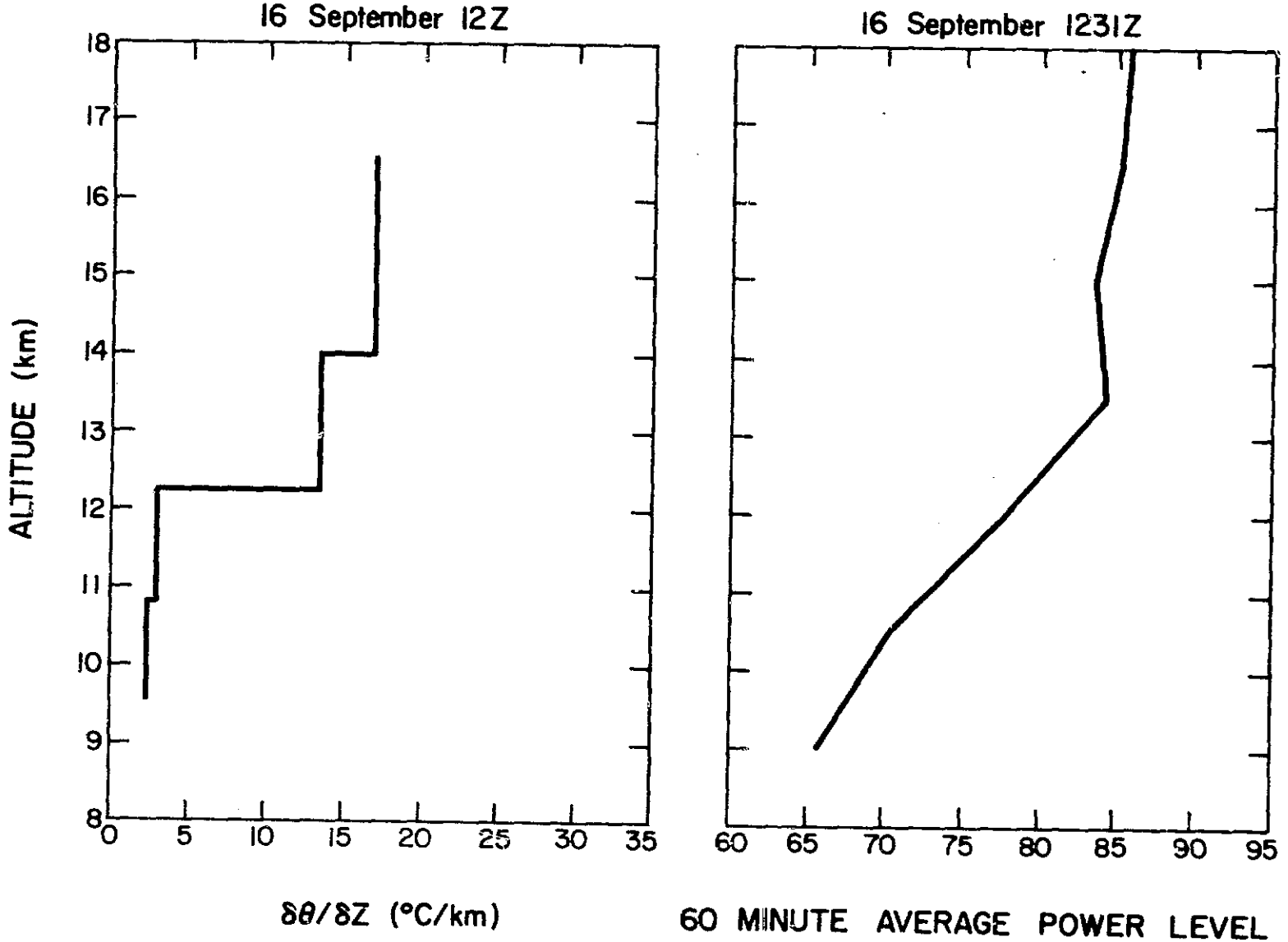

ORIGINAL PAGE IS
OF POOR QUALITY

Figure 4.6 Comparison of potential temperature gradient and hourly averaged power profiles on morning of September 16, 1982.

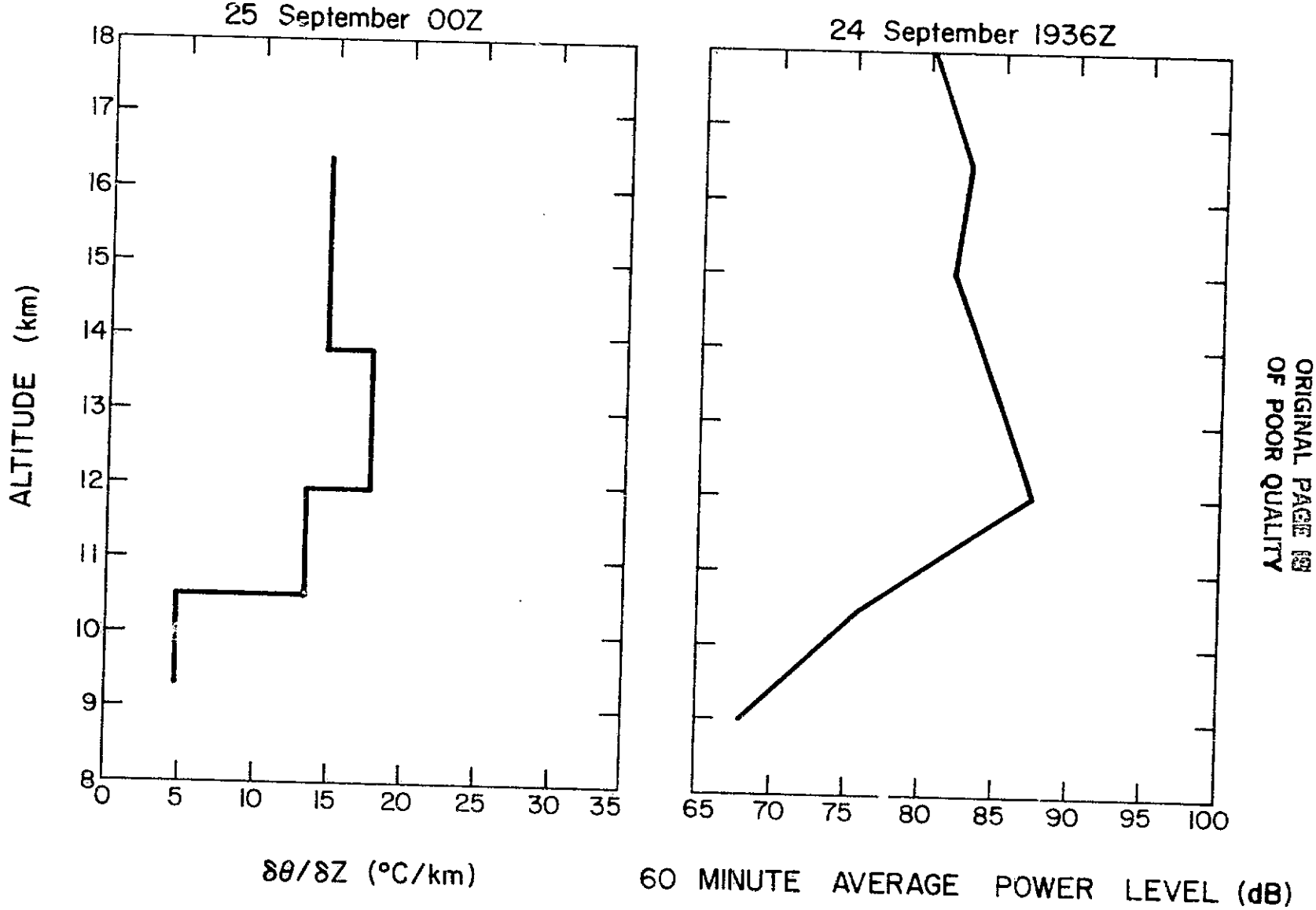

Figure 4.7 Comparison of potential temperature gradient and hourly averaged power profiles on afternoon of September 24, 1982.

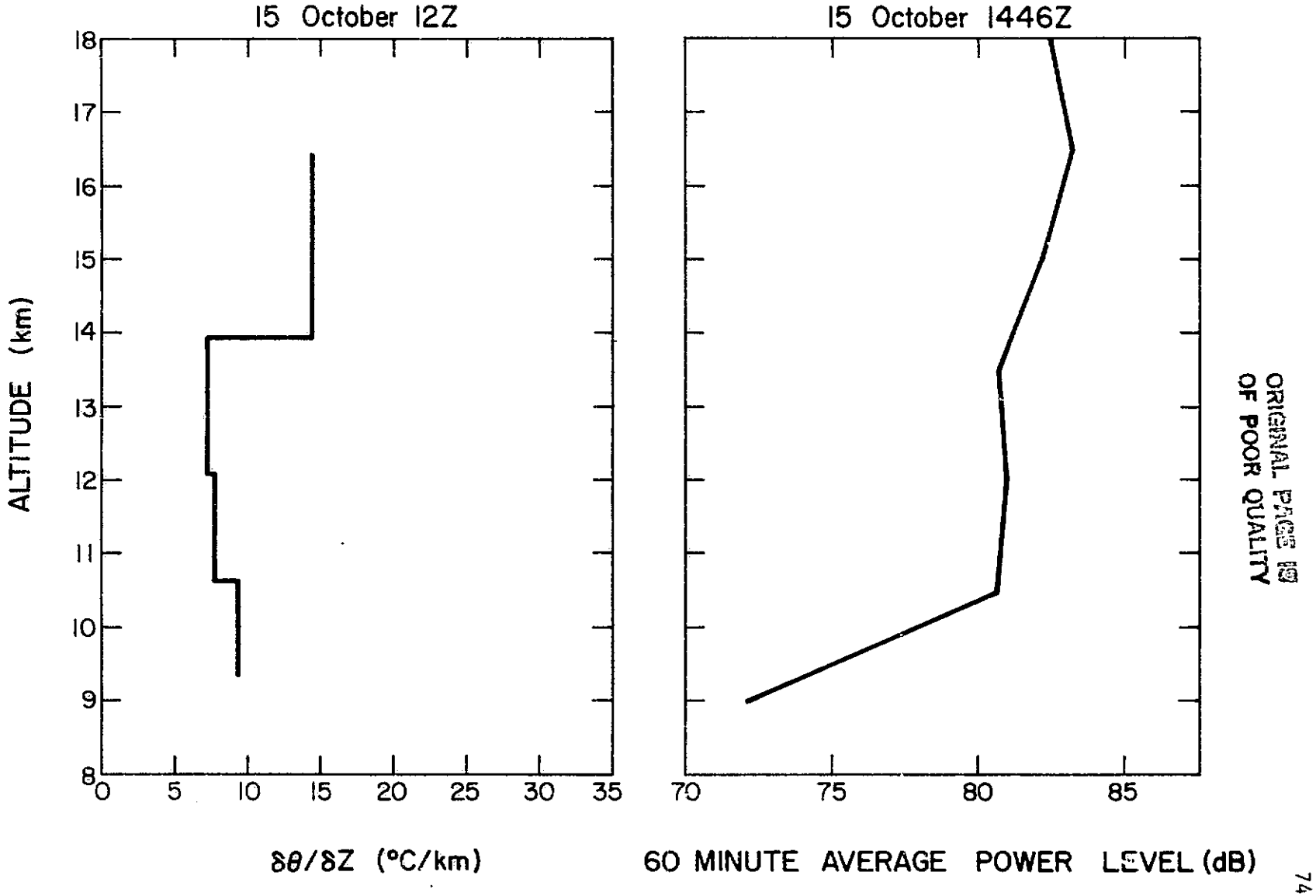

ORIGINAL PAGE IS
OF POOR QUALITY

Figure 4.8 Comparison of potential temperature gradient and hourly averaged power profiles on morning of October 15, 1982.

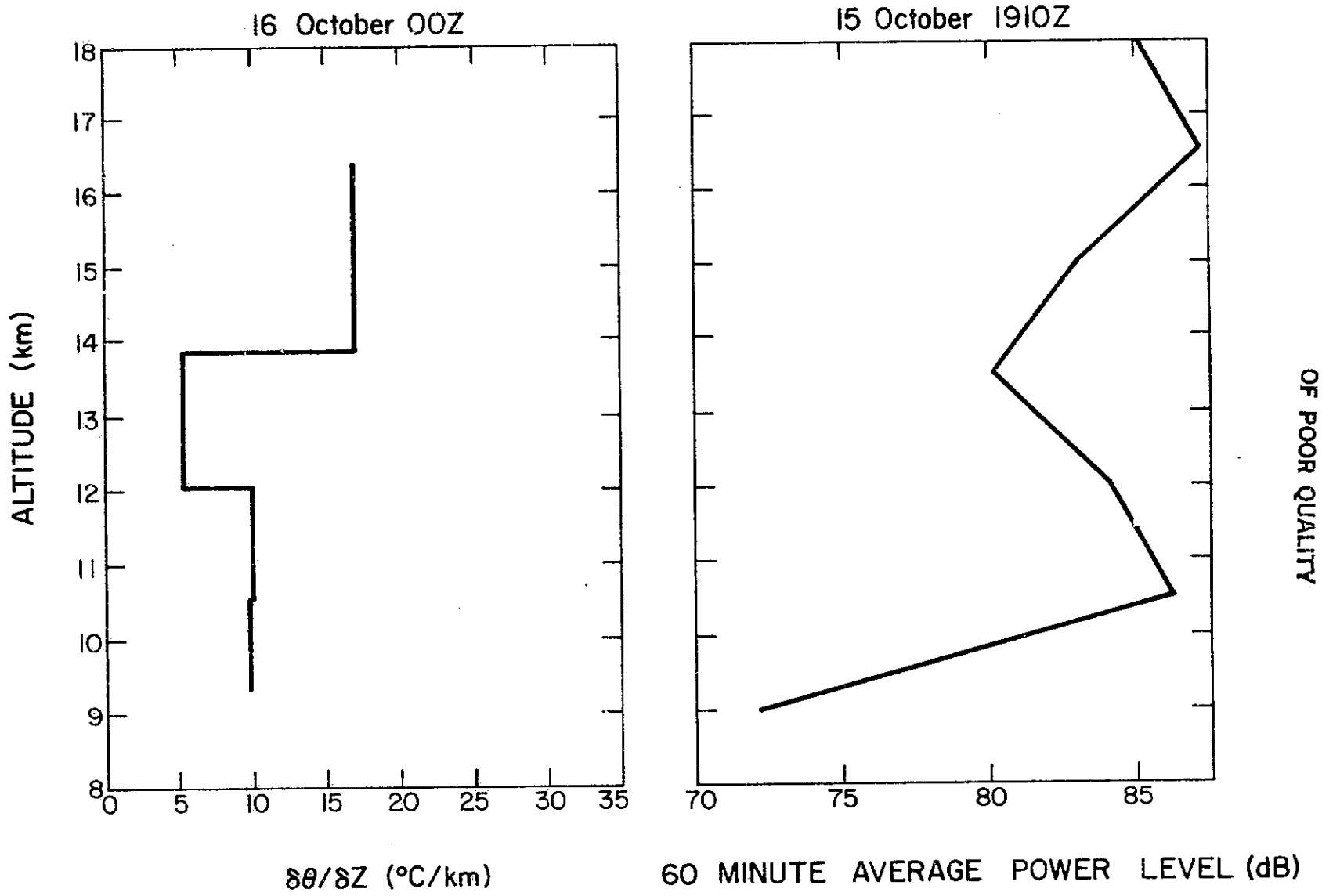

ORIGINAL PAGE IS
OF POOR QUALITY

Figure 4.9 Comparison of potential temperature gradient and hourly averaged power profiles on afternoon of October 15, 1982.

to support this observation.

The hourly-averaged standard deviation of line-of-sight velocity is a convenient measure of wave amplitude during the hour. A compilation of standard deviations of line-of-sight velocities at 19.5 km during both "storm" and "non-storm" conditions is shown in Figure 4.10. The altitude of 19.5 km is chosen because significant gravity wave activity can be found there on a near daily basis. Non-storm data consists of 36 hourly-averaged standard deviations collected on 12 separate days. Storm data consists of 8 hourly-averaged standard deviations collected on 4 days when a thunderstorm was at or near the radar site. The number of standard deviations which occur in each 0.10 m/s range are then plotted, with the storm occurrences shaded.

It is easily seen that the standard deviations of velocities collected during thunderstorms dominate the right-hand portion of the chart. The average of all non-storm standard deviations is 0.15, whereas for storm standard deviations it is 0.36. This indicates that, on the average, gravity wave amplitudes at 19.5 km are larger during convective activity by a factor of approximately 2.4.

4.3 Hourly Variability of Horizontal Winds

Observations shown in Chapter 3 indicate that horizontal winds in the lower stratosphere vary less over time than winds in the upper troposphere. In particular, comparisons of horizontal winds measured by balloon versus those measured by the Urbana radar generally show good agreement in the lower stratosphere, even though the respective observations are considerably separated in both time and distance.

Horizontal wind data collected over a 36-hour period are used to test the hypothesis that the better agreement in the lower stratosphere is caused

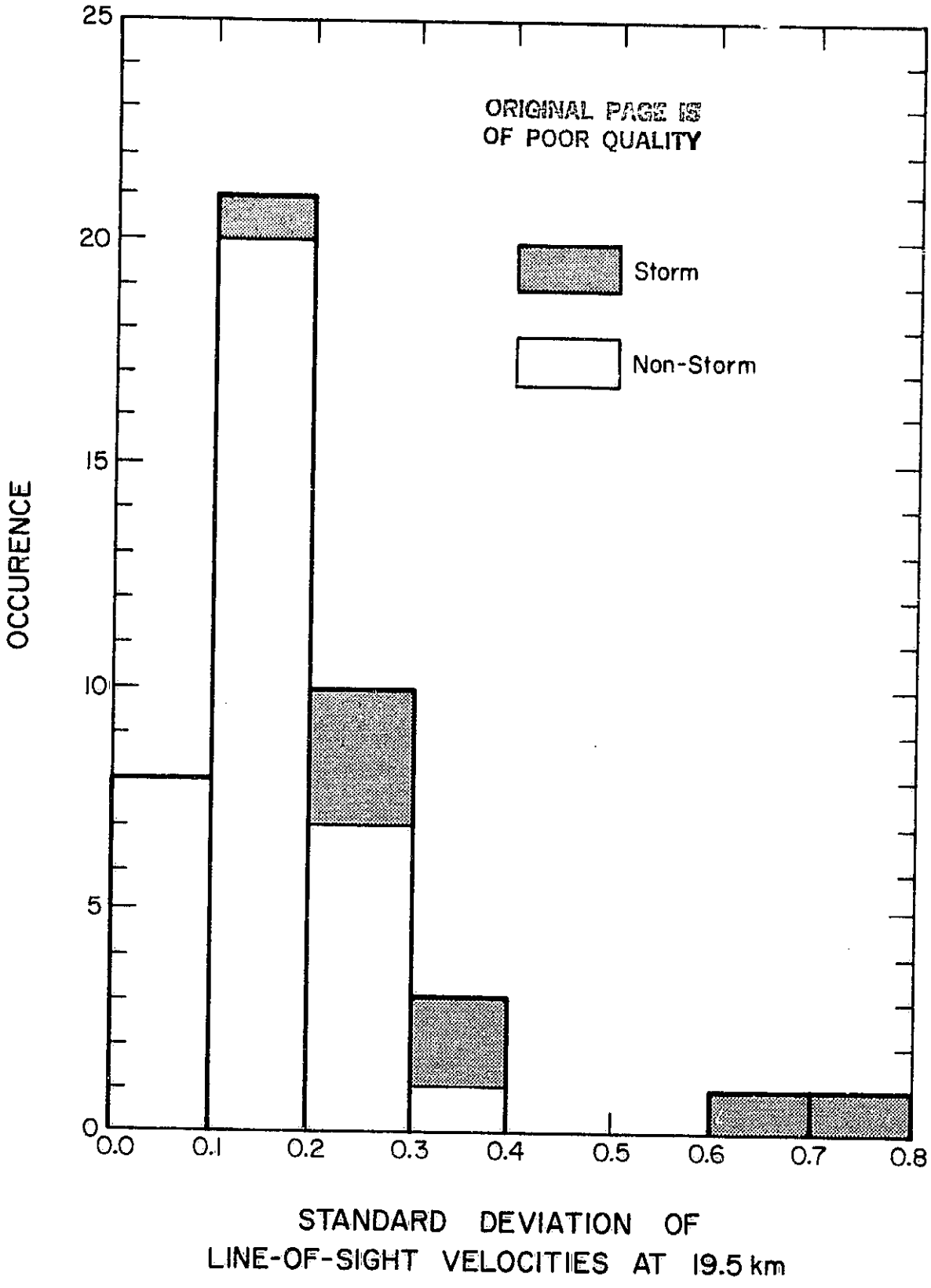

Figure 4.10 Standard deviation of line-of-sight velocities at 19.5 km for "storm" and "non-storm" conditions.

at least in part by the decreased wind variability over time in this region. Hour-to-hour changes in horizontal wind speed toward the southeast are calculated for each of the bottom eight height gates (9-19.5 km). The resulting 33 hour-to-hour changes are then averaged for each altitude. Figure 4.11 shows these averages as a function of altitude. There is a significant decrease in the hourly change above 13.5 km. This supports the observation made in Chapter 3 of better agreement between radar and balloon-measured winds above 13.5 km. Lack of wind variability in this region would lead to better agreement between the two measurements.

Fukao et al. [1982] suggest that differences between rawinsonde and radar-measured winds in the lower stratosphere are caused primarily by errors inherent to the rawinsonde technique. This error is also almost certainly present in the balloon data shown in Chapter 3. Fukao et al., also suggest that differences in the upper troposphere measurements can be accounted for by spatial and/or temporal variations in the wind field, whereas this effect is not as substantial in the lower stratosphere. Results shown in Figure 4.11 certainly support this hypothesis.

4.4 Effects of Gravity Waves on Specular Reflections

Power spectra of coherently integrated data provide a convenient method of observing short period fluctuations in the specularity of the received echo. At Urbana, a 64-point FFT is applied to sixty-four 1/8 second samples yielding power spectra of 8 seconds of coherently integrated data.

Data shown in this section was collected on July 15, 1982 from 13:35:20 CST to 13:37:10 CST. Minute-by-minute data were collected shortly prior to this time. Power and velocity plots of the minute-by-minute data are shown in Figures 4.12 and 4.13, respectively. These data are characteristic of a somewhat active day at Urbana, with line-of-sight velocity oscillations

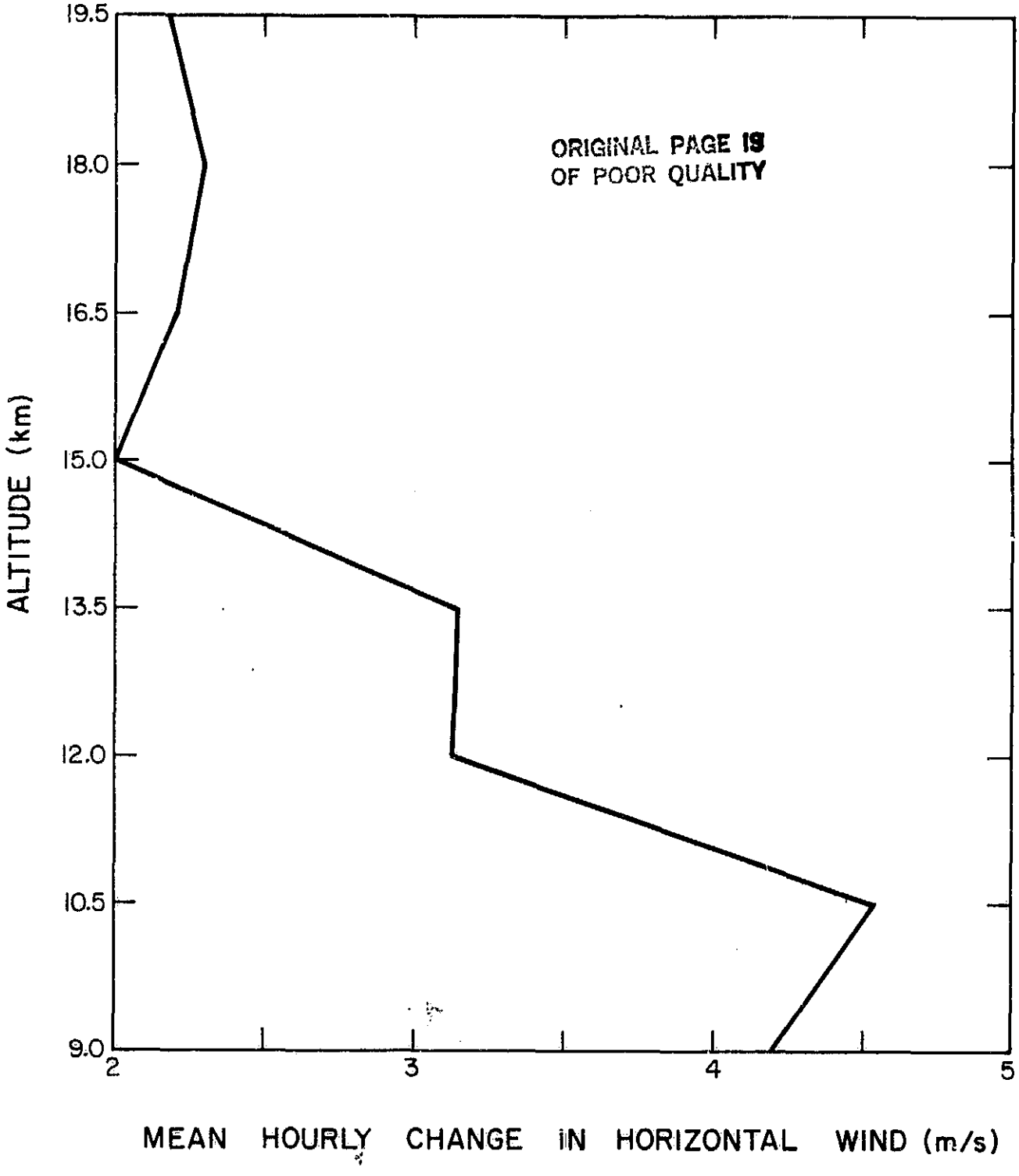

Figure 4.11 Profile of mean hourly change in horizontal wind toward the southeast versus altitude for a 36-hour period.

ORIGINAL PAGE IS
OF POOR QUALITY

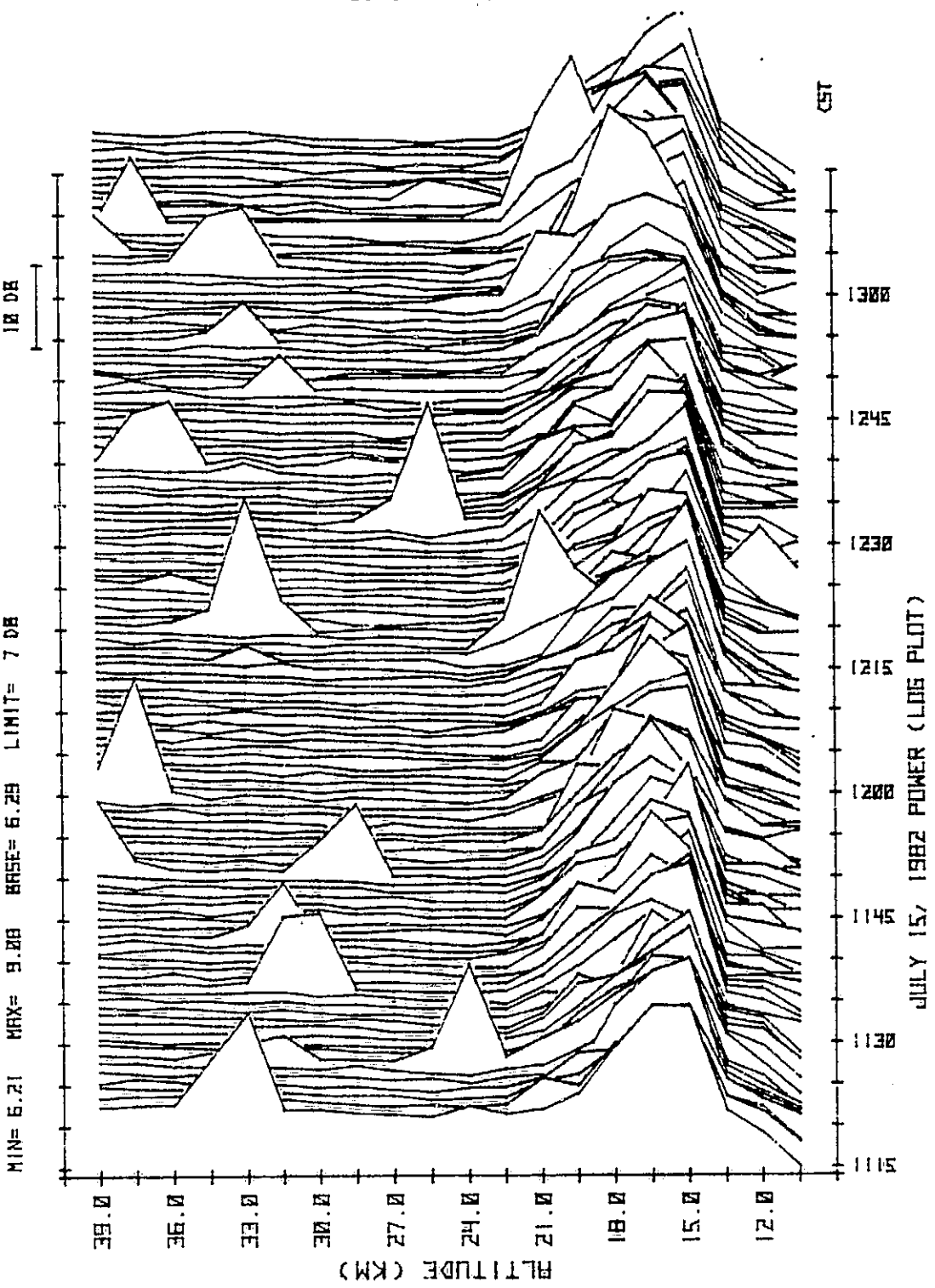

Figure 4.12 Vertical profile of scattered power beginning at 1115 CST on July 15, 1982.

ORIGINAL PAGE IS
OF POOR QUALITY

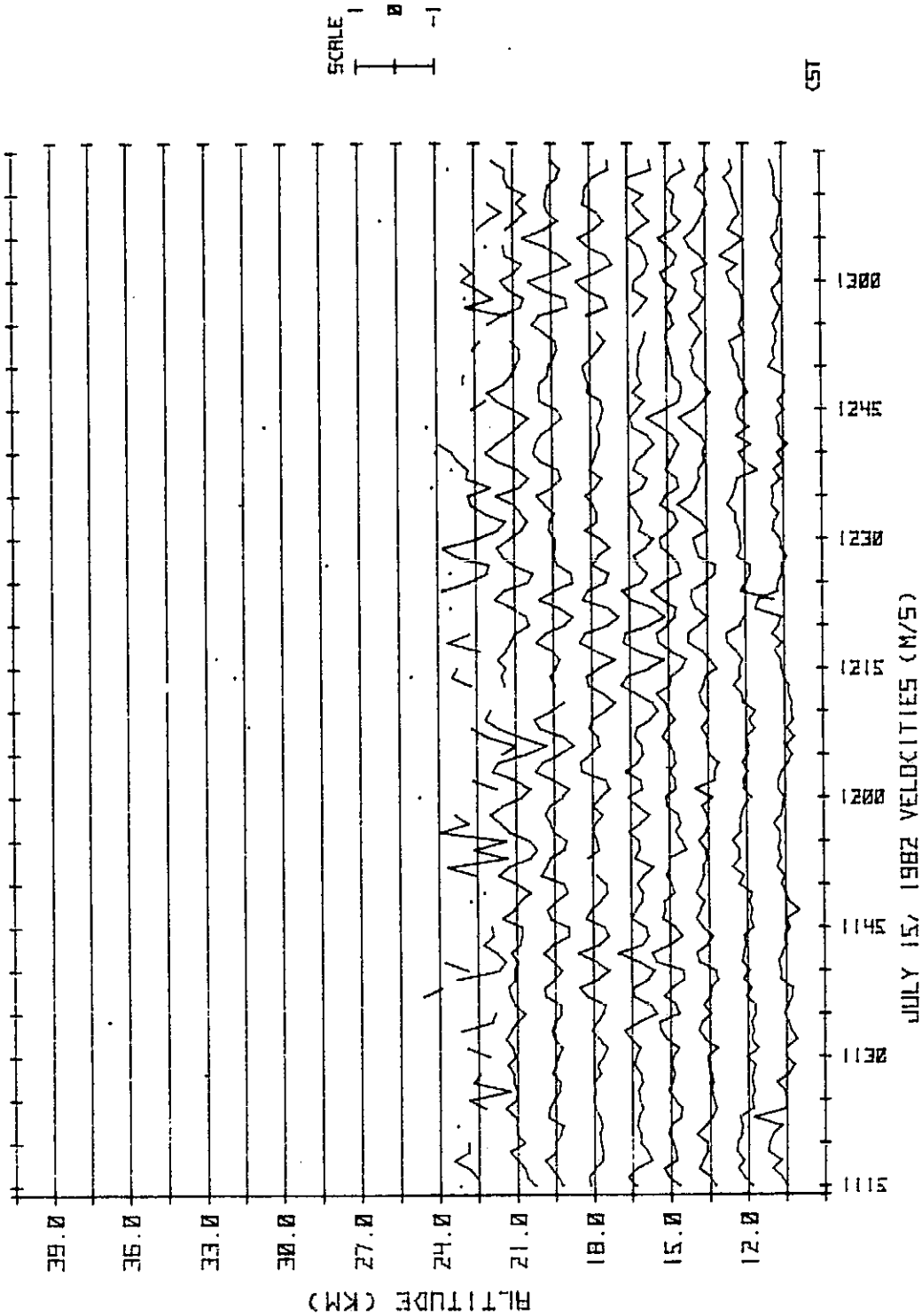

Figure 4.13 Line-of-sight velocity beginning at 1115 CST on July 15, 1982.

reaching amplitudes of ±0.5 m/s, peak-to-peak.

Power spectra for a two-minute period beginning at 13:35:20 CST at an altitude of 16.5 km are shown in Figures 4.14a - 4.19b. Plots are scaled such that the peak of the spectrum lies at full scale. All twelve plots show a strong return which is slowly changing from negative to positive Doppler frequency. This movement is attributed to gravity wave activity in the radar beam. The highest line-of-sight velocity reached is less then 1 m/s. This is consistent with the minute-by-minute observations shown in Figure 4.13.

Another interesting feature of the spectra is the variation in spectral width with time. The spectral width is large at 13:35:30 (Figure 4.14b), whereas it is quite small at 13:36:20 (Figure 4.17a). Another large spectral width occurs at 13:36:50 (Figure 4.18b). Gage et al. [1981] have observed similar spectral width fluctuations at Poker Flat, Alaska. They suggest two ways in which gravity wave activity can effect specular echoes such as those shown here. The first effect is a modulation in the received signal caused by the movement of the specular point with the phase of the wave. The second effect is that the structure responsible for the specular echo becomes incoherent, resulting in the disappearance of the specular echo.

The data shown here suggest the possibility of the presence of both effects. Evidence of the first effect, systematic modulation of the received signal caused by gravity wave tilting the coherent structure, can be seen in the second half of the data (Figure 4.17a to 4.19b). The scaling factor given on each plot, which is proportional to the maximum value of power plotted, first decreases almost two orders of magnitude and then increases during this period. If this modulation is caused by a tilting of the horizontal structure one would expect a maximum power return when the

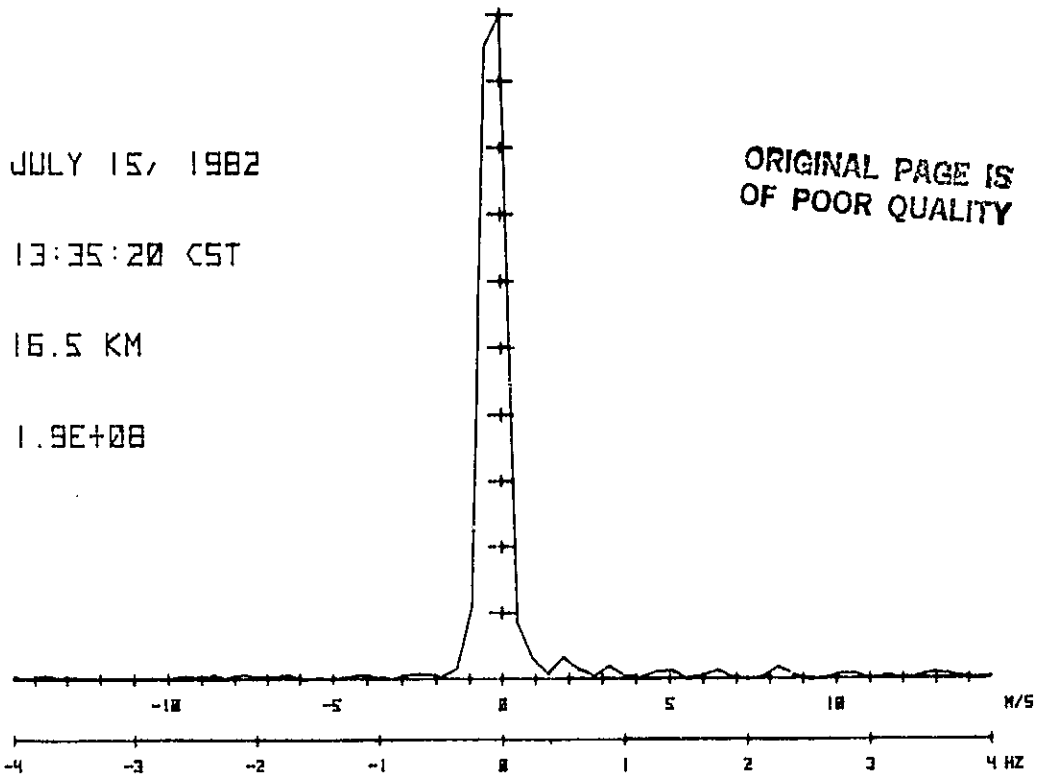

ORIGINAL PAGE IS
OF POOR QUALITY

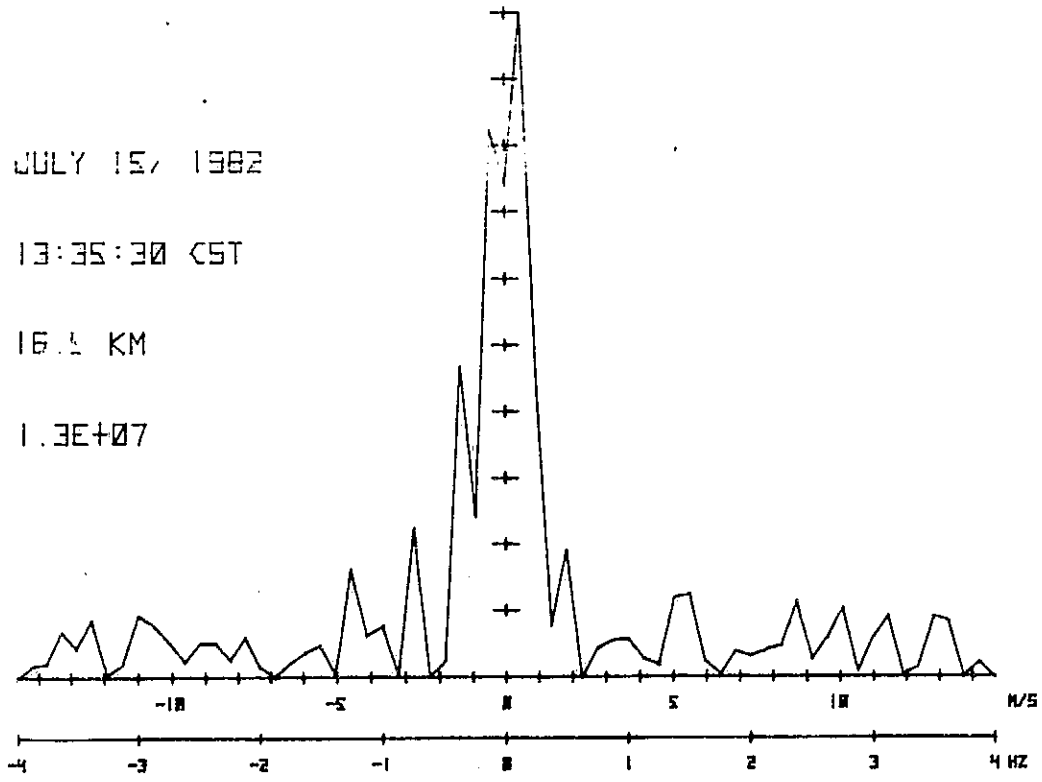

Figure 4.14(a&b) Power spectra of 8 seconds of coherently integrated data at 16.5 km for 13:35:20 and 13:35:30 CST on July 15, 1982.

ORIGINAL PAGE IS
OF POOR QUALITY

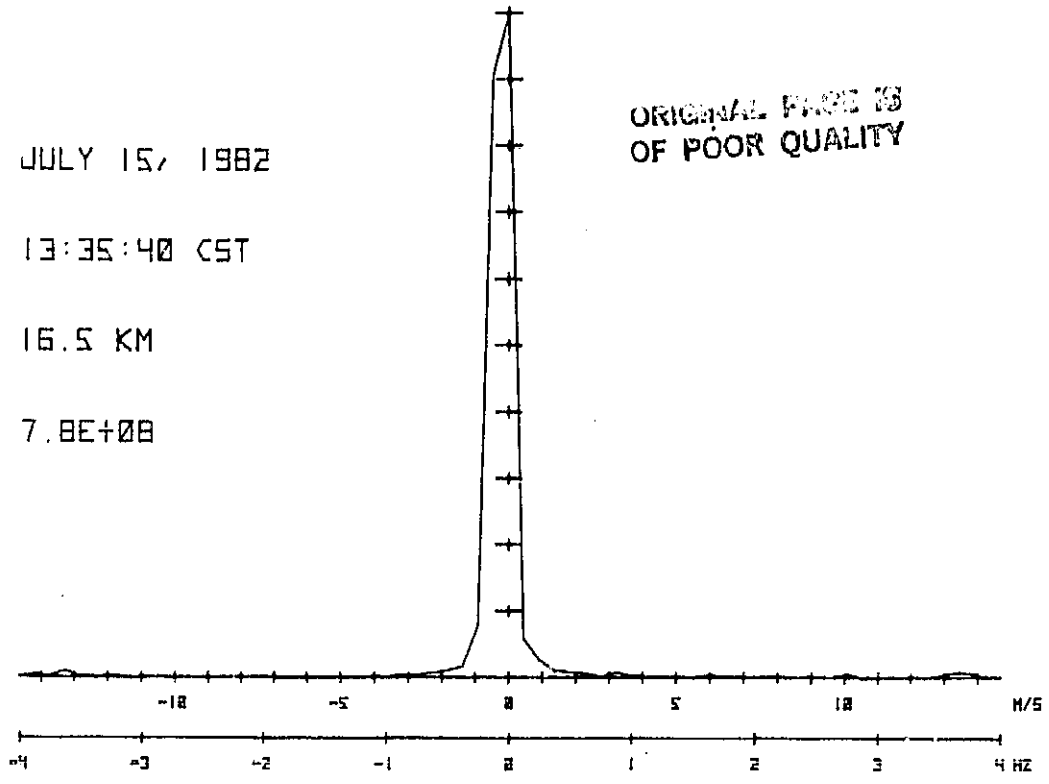

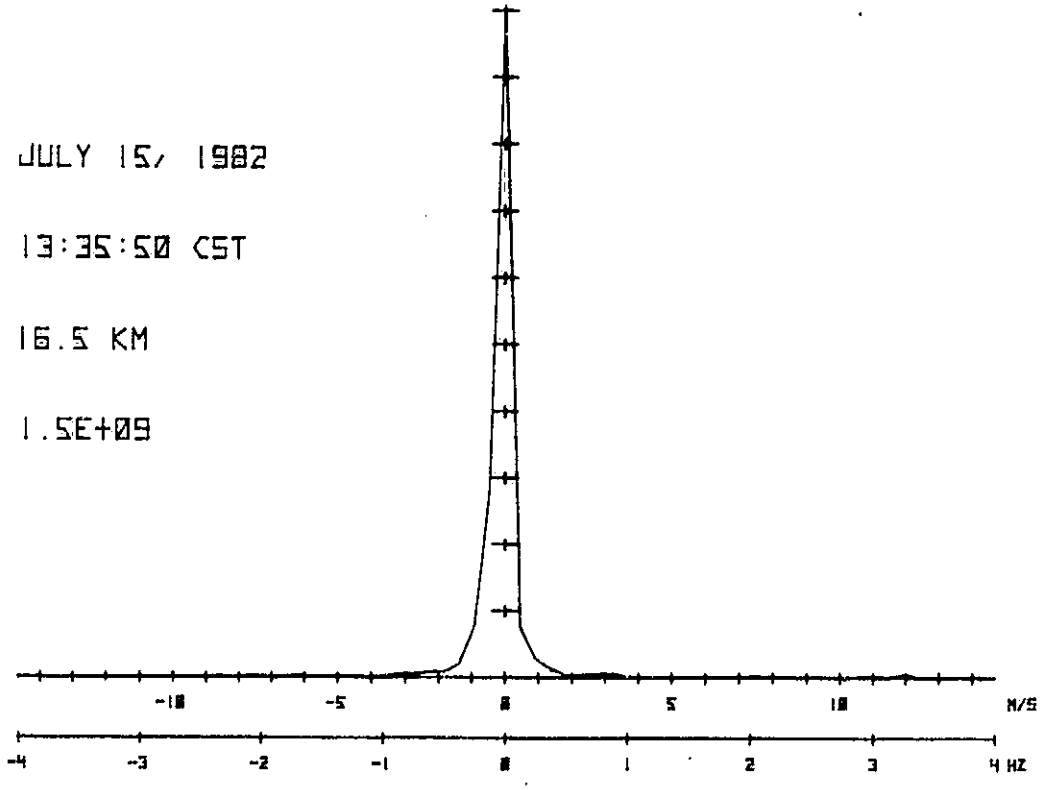

Figure 4.15(a&b) Power spectra of 8 seconds of coherently integrated data at 16.5 km for 13:35:40 and 13:35:50 CST on July 15, 1982.

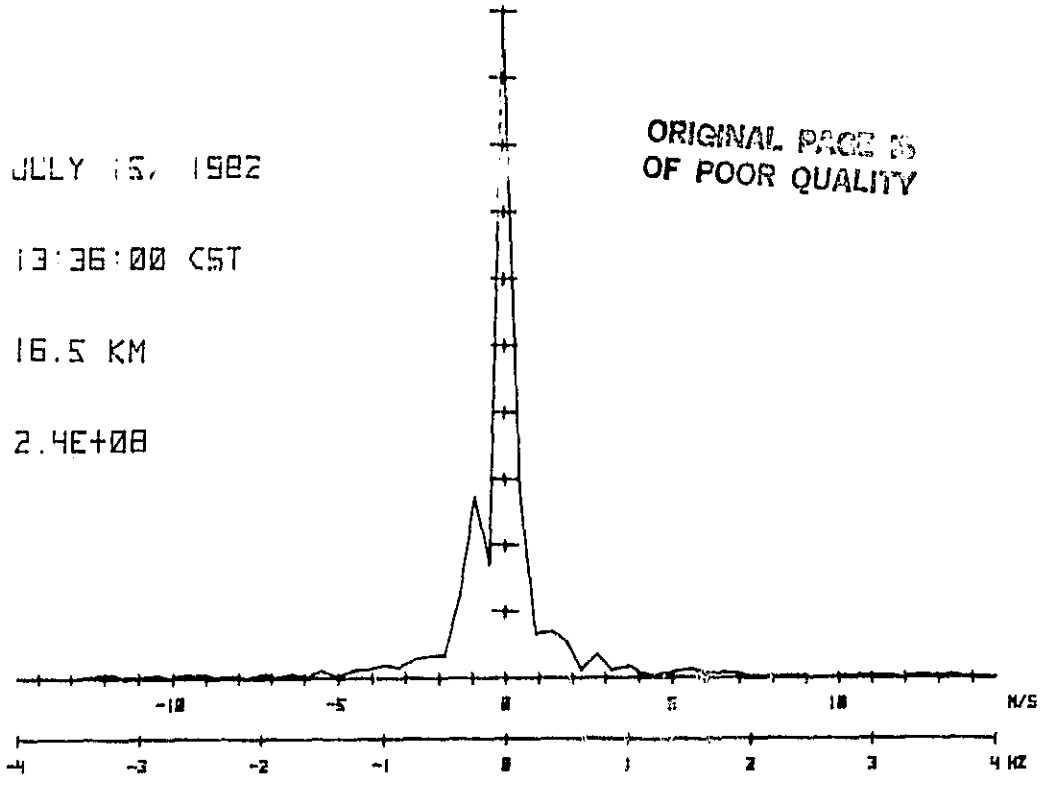

ORIGINAL PAGE IS
OF POOR QUALITY

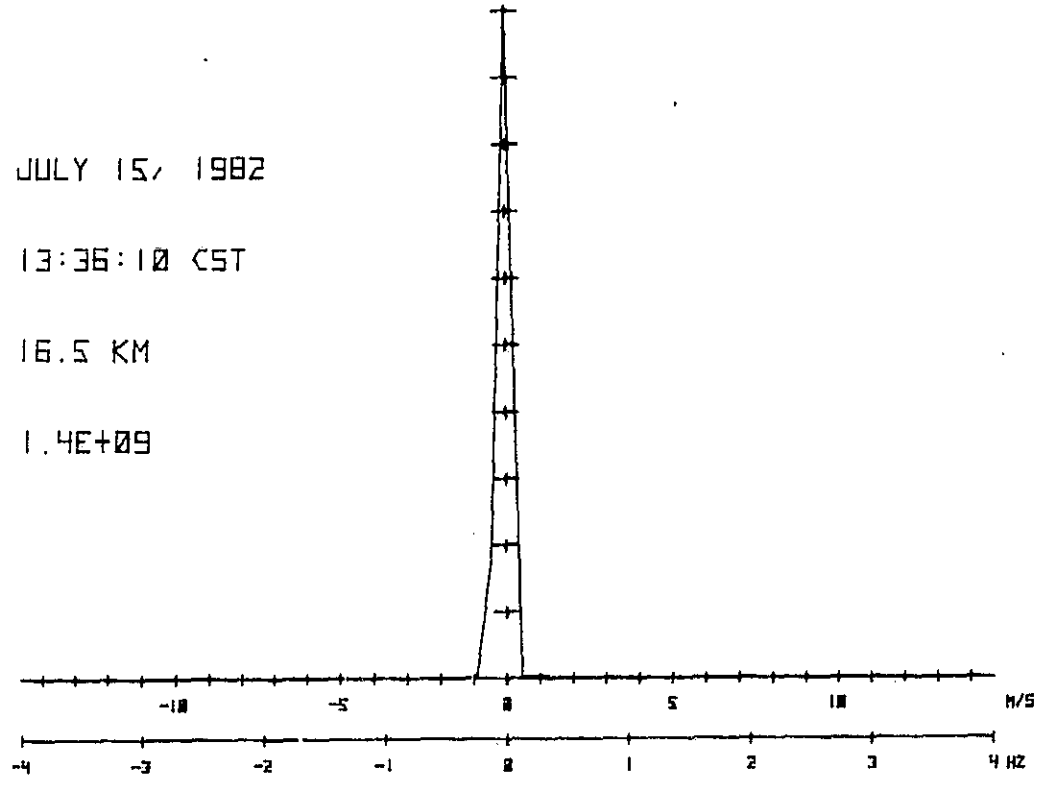

Figure 4.16(a&b) Power spectra of 8 seconds of coherently integrated data at 16.5 km for 13:36:00 and 13:36:10 CST on July 15, 1982.

ORIGINAL PAGE IS
OF POOR QUALITY

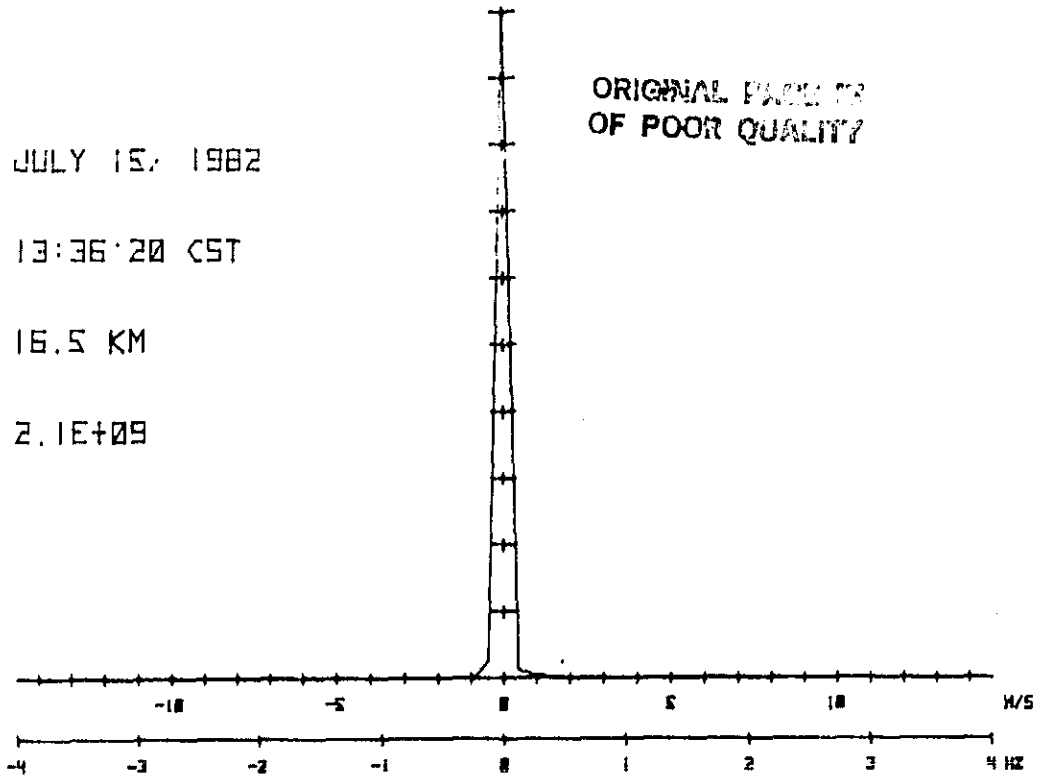

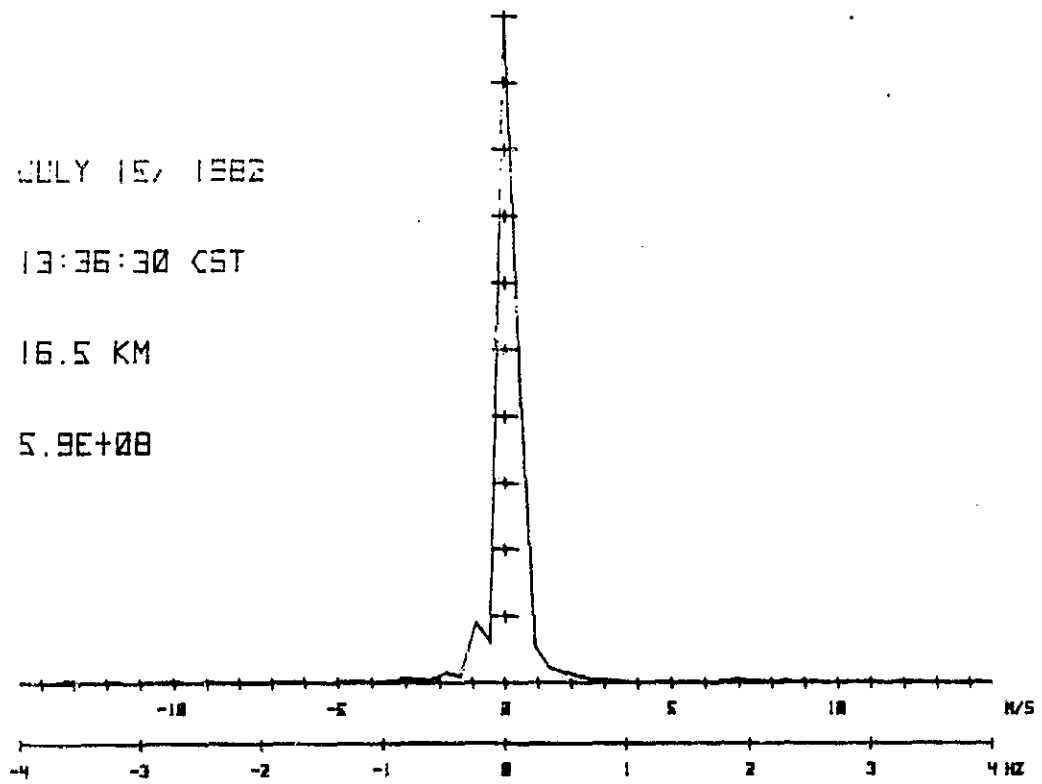

Figure 4.17(a&b) Power spectra of 8 seconds of coherently integrated data at 16.5 km for 13:36:20 and 13:36:30 CST on July 15, 1982.

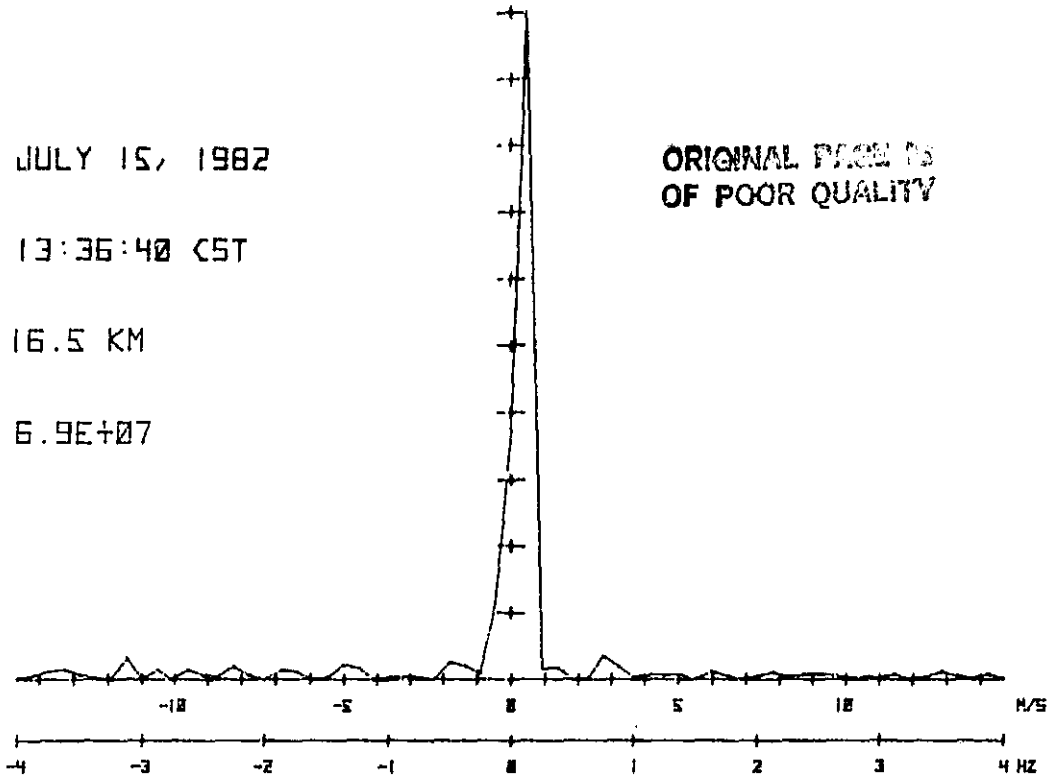

ORIGINAL PAGE IS
OF POOR QUALITY

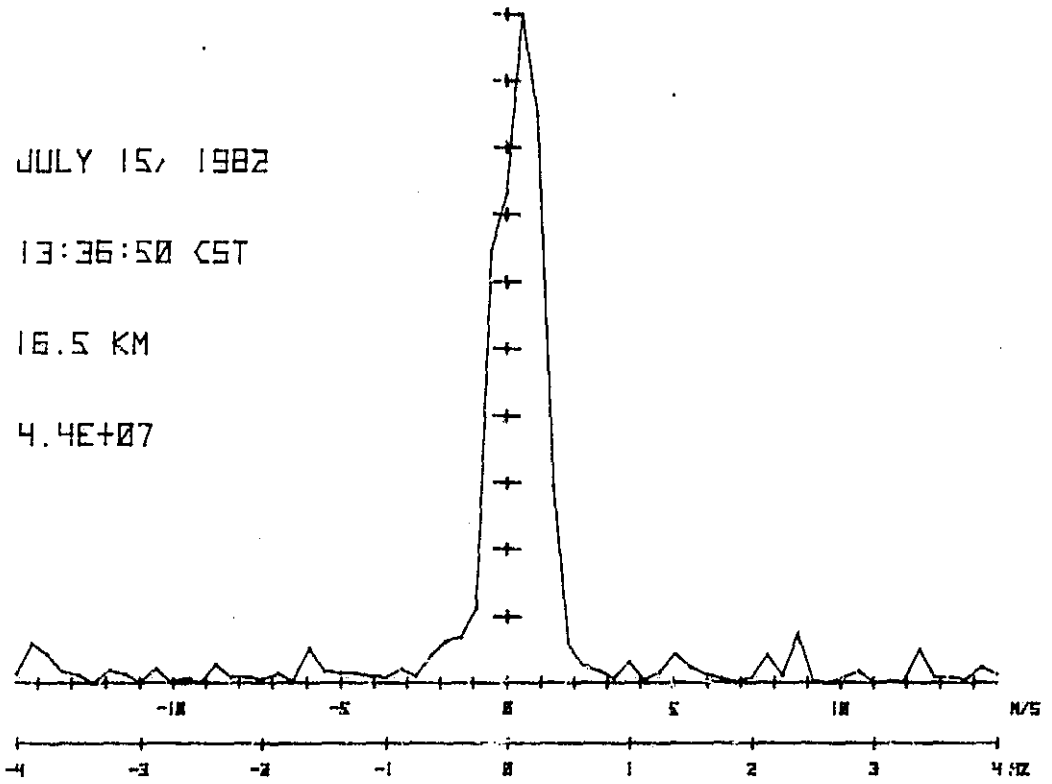

Figure 4.18(a&b) Power spectra of 8 seconds of coherently integrated data at 16.5 km for 13:36:40 and 13:36:50 CST on July 15, 1982.

C-2

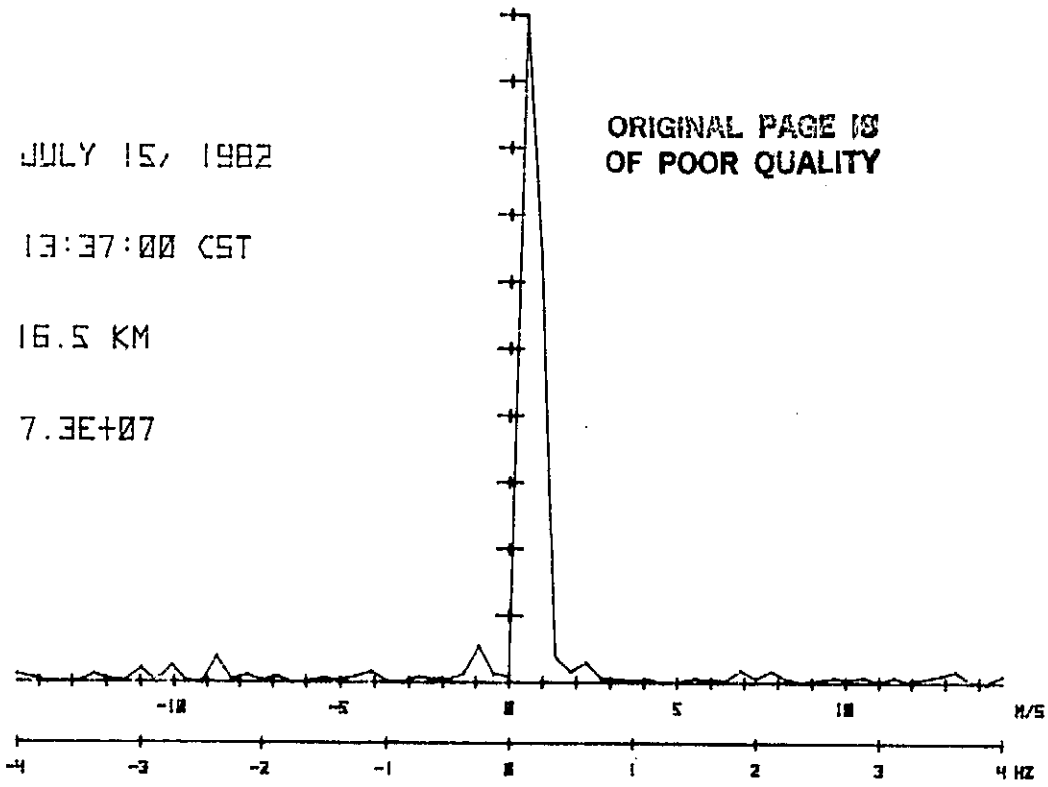

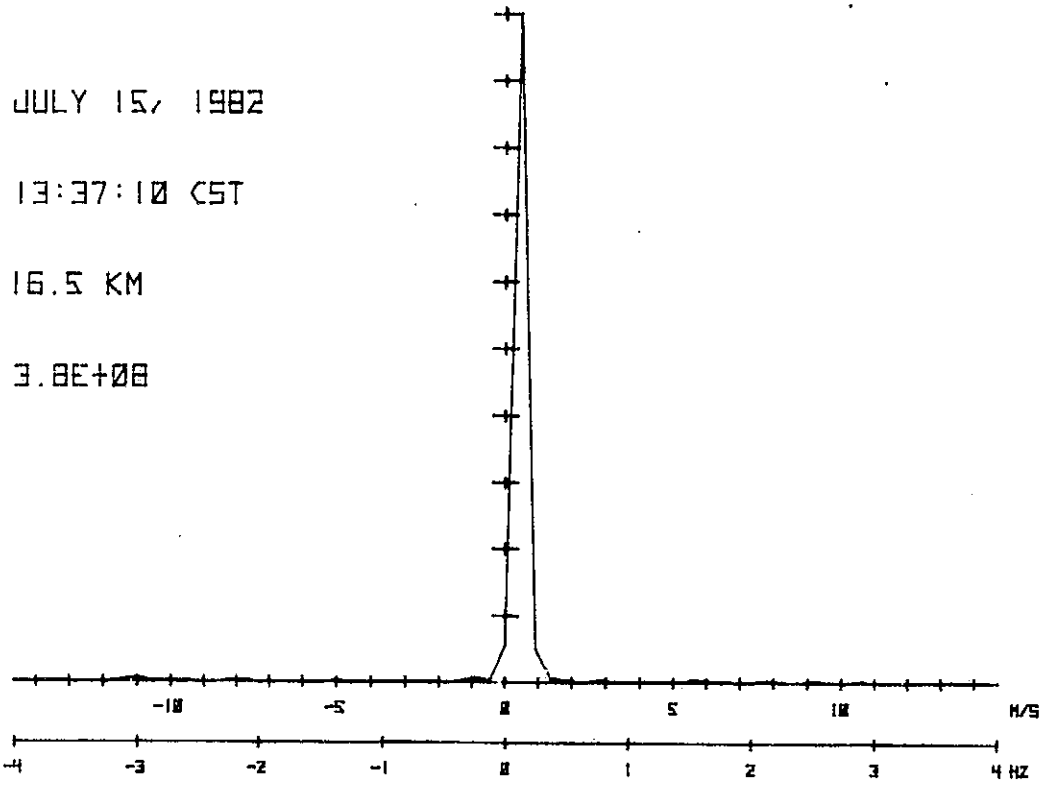

Figure 4.19(a&b) Power spectra of 8 seconds of coherently integrated data at 16.5 km for 13:37:00 and 13:37:10 CST on July 15, 1982.

structure is not tilted, i.e., zero vertical velocity, and a minimum power return when the structure is at maximum tilt, i.e., maximum vertical velocity, [Gage et al., 1981]. Thus, the power fluctuations should modulate at twice the frequency of the velocity fluctuations. Further analysis of these data to give simultaneous velocities will enable this point to be checked.

Evidence of the second effect, destruction of coherence by gravity wave-generated turbulence, is found in Figure 4.14b. The scaled power in this figure is more than an order of magnitude less than that of both the previous figure and the following figure. Since these figures are separated by only 10 seconds, this phenomenon is very short-lived. Comparison of Figure 4.14b with 4.14a and 4.15a shows that the slightly negative line-of-sight velocity apparent in Figures 4.14a and 4.15a is joined in Figure 4.14b by both a larger negative velocity and a positive velocity. It is suggested that turbulence associated with the gravity wave has produced the large spectral width seen in Figure 4.14b.

4.5 Relationship of Gravity-Wave Spectra to the Brunt-Vaisala Period

It is possible to determine the period of oscillation of the line-of-sight velocity by calculating the power spectra. These spectra vary significantly with both altitude and time.

Line-of-sight velocities for a two-hour period beginning at 0911 CST on July 15, 1982 is shown in Figure 4.20. Velocities for a second two-hour period beginning at 1115 CST were shown previously in Figure 4.13. Substantial short-period oscillations are present between 15 km and 21 km. Longer-period oscillations are apparent at the lower altitudes, due to the change in the Brunt-Vaisala frequency, ω_B. This is a characteristic oscillation frequency of a horizontally stratified atmosphere, and is given by $\omega_B = [(g/\theta)(\partial\theta/\partial z)]^{1/2}$. Here g is the acceleration due to gravity and θ is

ORIGINAL PAGE IS
OF POOR QUALITY

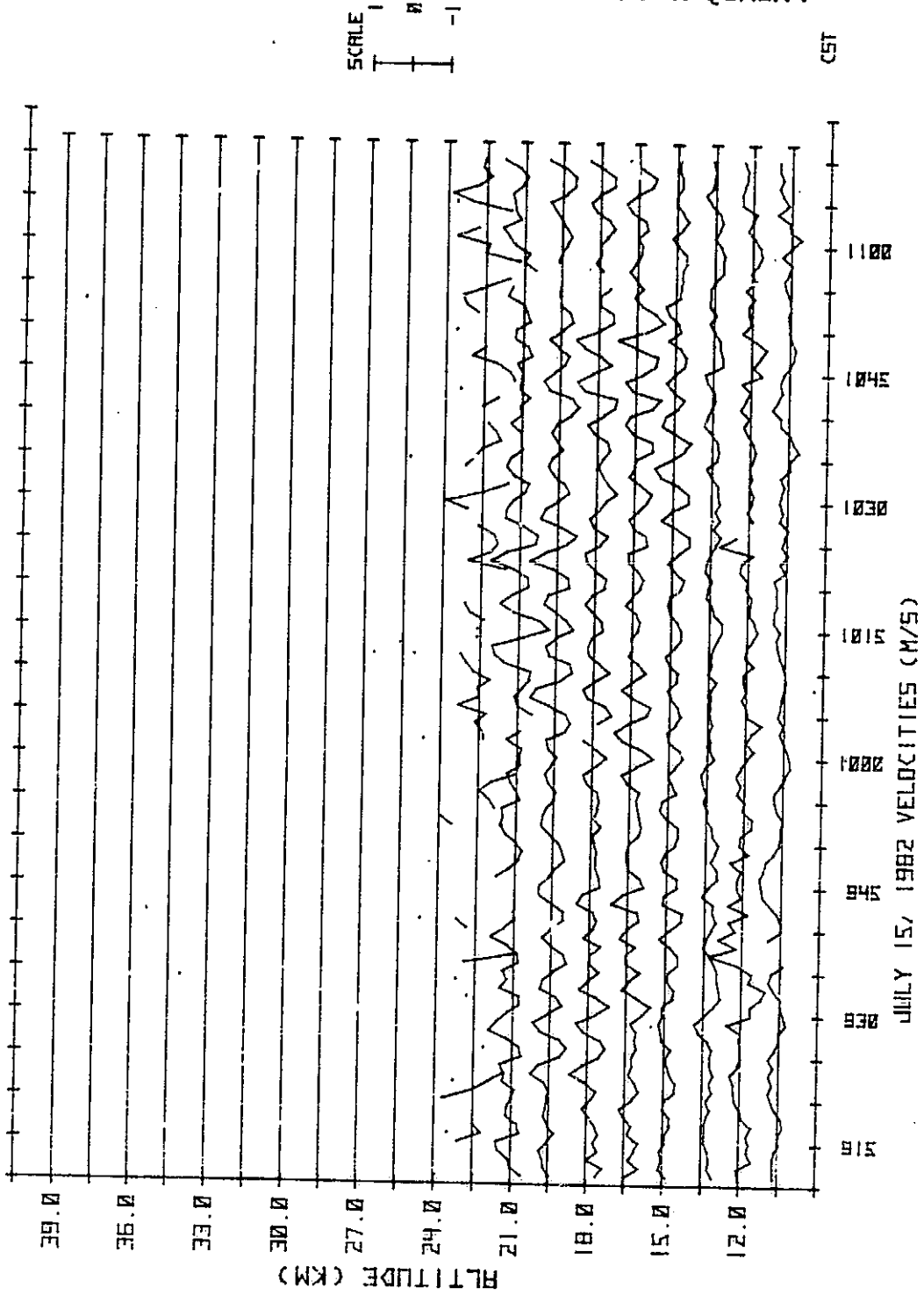

Figure 4.20 Line-of-sight velocity beginning at 911 CST on July 15, 1982.

the potential temperature. Therefore, the Brunt-Vaisala period, $2\pi/\omega_B$, decreases with increasing stability; and shorter-period oscillations are found in the stratosphere than in the troposphere.

The power spectra of the first two hours of velocity data are shown in Figures 4.21-4.23, one plot for each of three adjacent altitudes. The local Brunt-Vaisala period, calculated from data provided by the morning (0600 CST) radiosonde ascent, is shown on each plot. Note that the Brunt-Vaisala period is calculated as an average value over a rather large range of altitude, in the same way that potential temperature differences are calculated in Section 4.1.

In examining Figures 4.21-4.23, it is obvious that there are significant changes in the spectra with altitude. At 13.5 km, Figure 4.21, spectral peaks are located at 14.2 min and 12.8 min. A smaller peak is also located at 5.6 min, near the Brunt-Vaisala period of 5.8 min. Notice that short period oscillations of less than approximately 4 minutes are not present. This corresponds to the forbidden area of periodic wave motion, between internal gravity waves and acoustic waves [Beer, 1974]. The spectrum for 15 km is shown in Figure 4.22. The main spectral peak has moved to 4.9 min, quite close to the Brunt-Vaisala period of 5.0 min. The difference in oscillation period between 13.5 km and 15 km can easily be seen in Figure 4.20. The spectrum for 16.5 km is given in Figure 4.23. This spectrum is much cleaner than that of Figure 4.23, with a peak at 5.1 min, again very close to the Brunt-Vaisala period.

Power spectra corresponding to the line-of-sight velocities in Figure 4.13 are shown in Figures 4.24-4.27. The dominant periods at 10.5 km are 32 min and 18.3 min, as shown in Figure 4.24. The Brunt-Vaisala period at this altitude is approximately 12.9 min, somewhat shorter than the observed

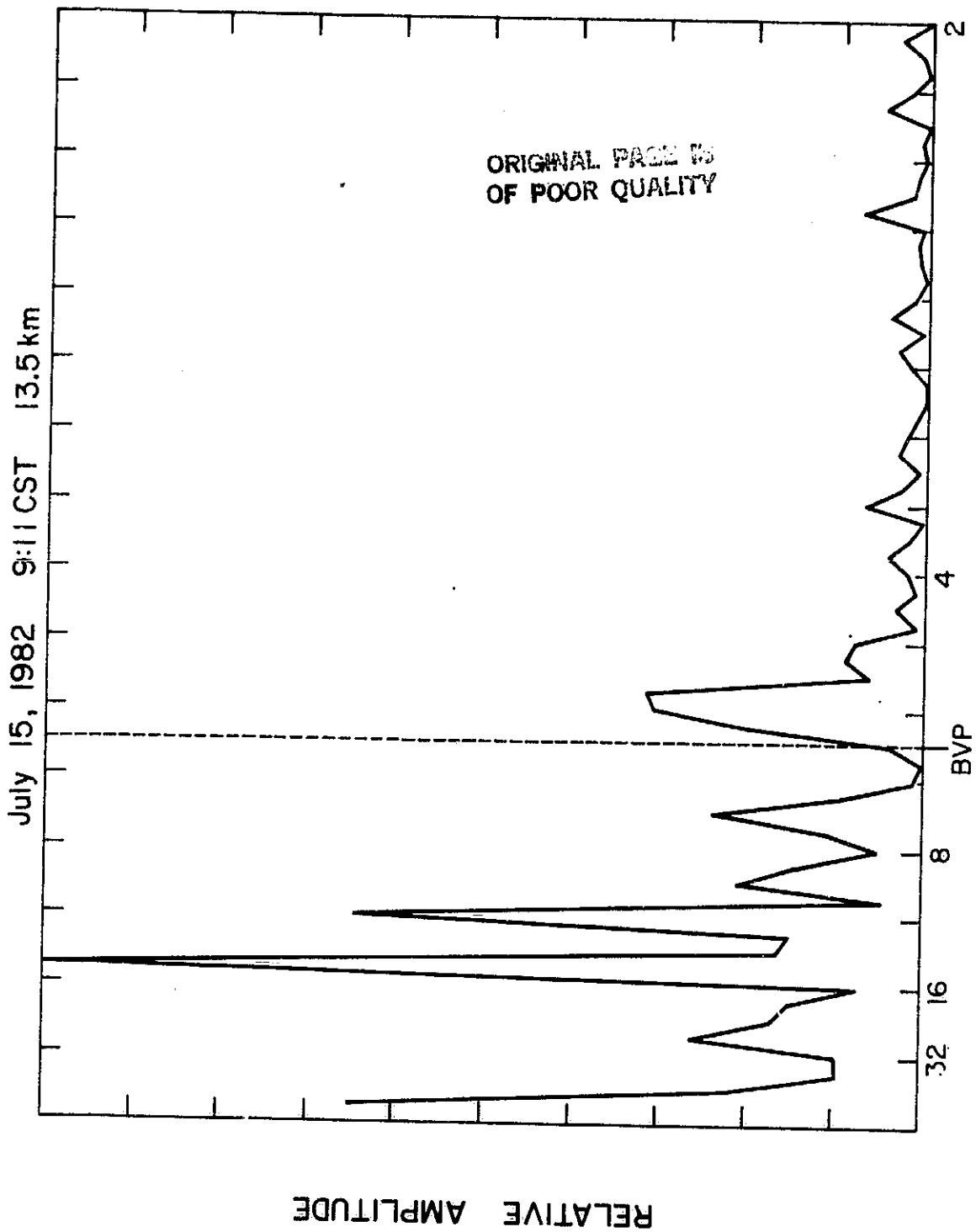

Figure 4.21 Power spectrum of two hours of line-of-sight velocities beginning at 911 CST on July 15, 1982 at 13.5 km. Calculated Brunt-Vaisala period is shown.

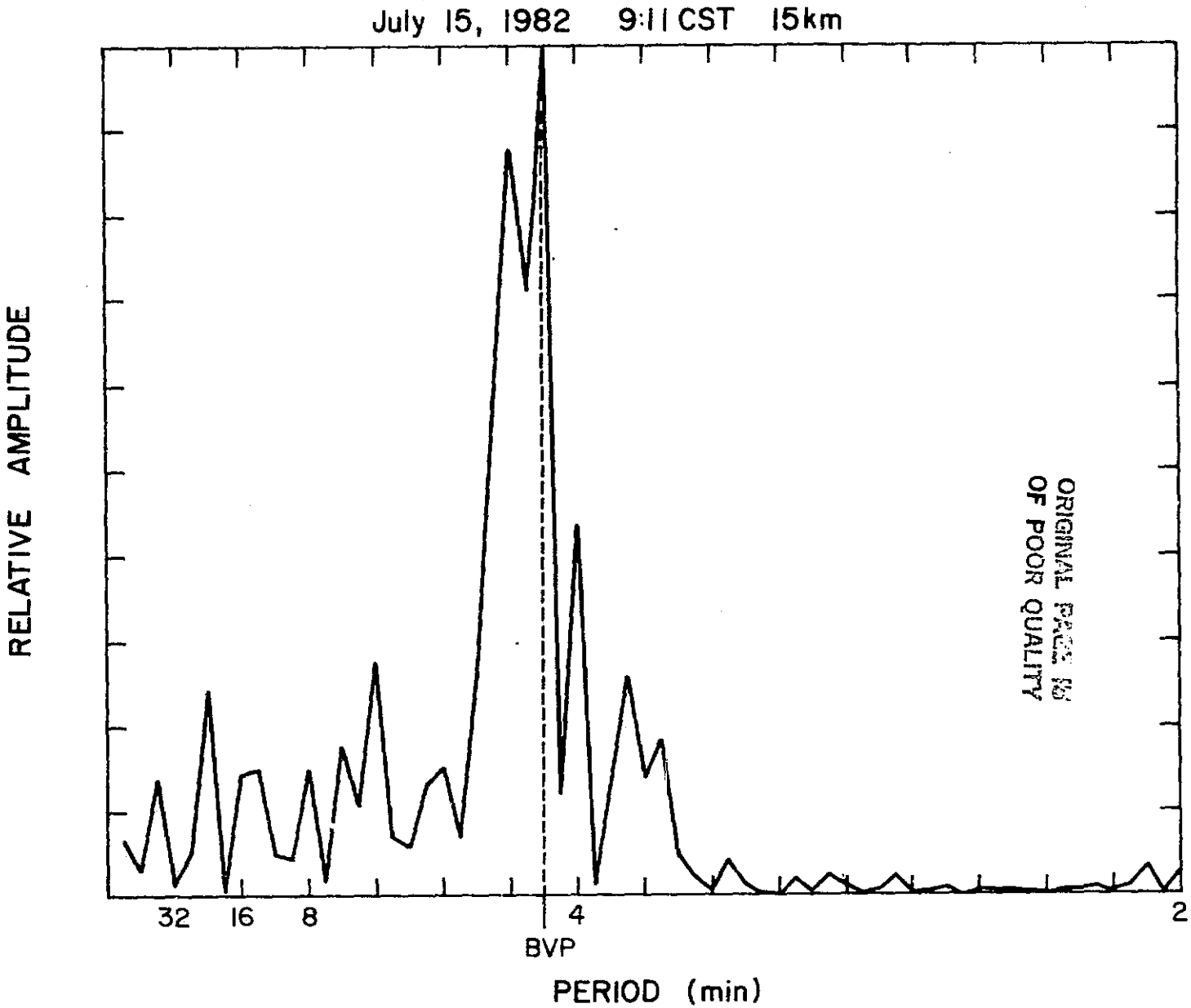

Figure 4.22 Power spectrum of two hours of line-of-sight velocities beginning at 911 CST on July 15, 1982 at 15 km. Calculated Brunt-Vaisala period is shown.

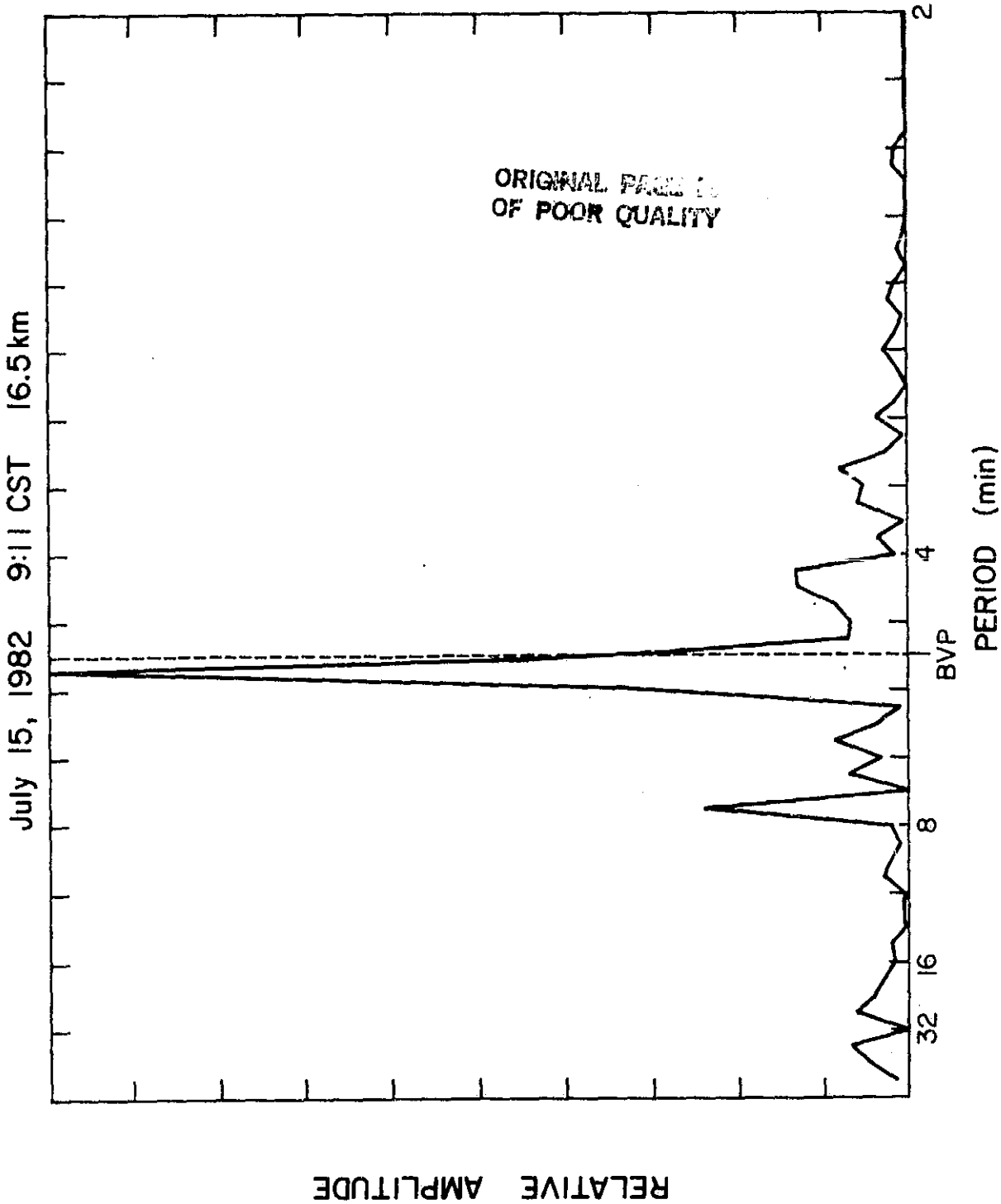

Figure 4.23 Power spectrum of two hours of line-of-sight velocities beginning at 911 CST on July 15, 1982 at 16.5 km. Calculated Brunt-Vaisala period is shown.

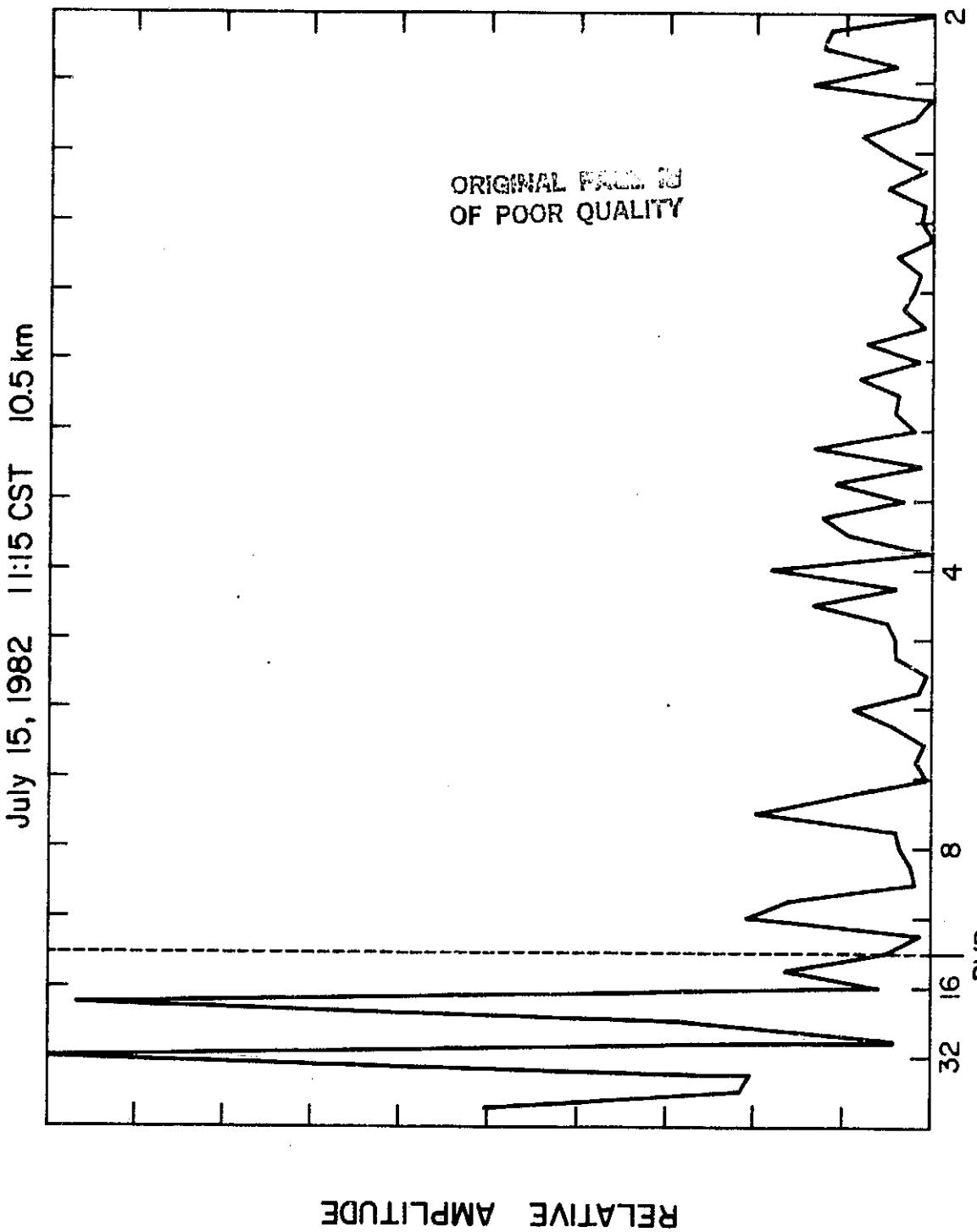

Figure 4.24 Power spectrum of two hours of line-of-sight velocities beginning at 1115 CST on July 15, 1982 at 10.5 km. Calculated Brunt-Vaisala period is shown.

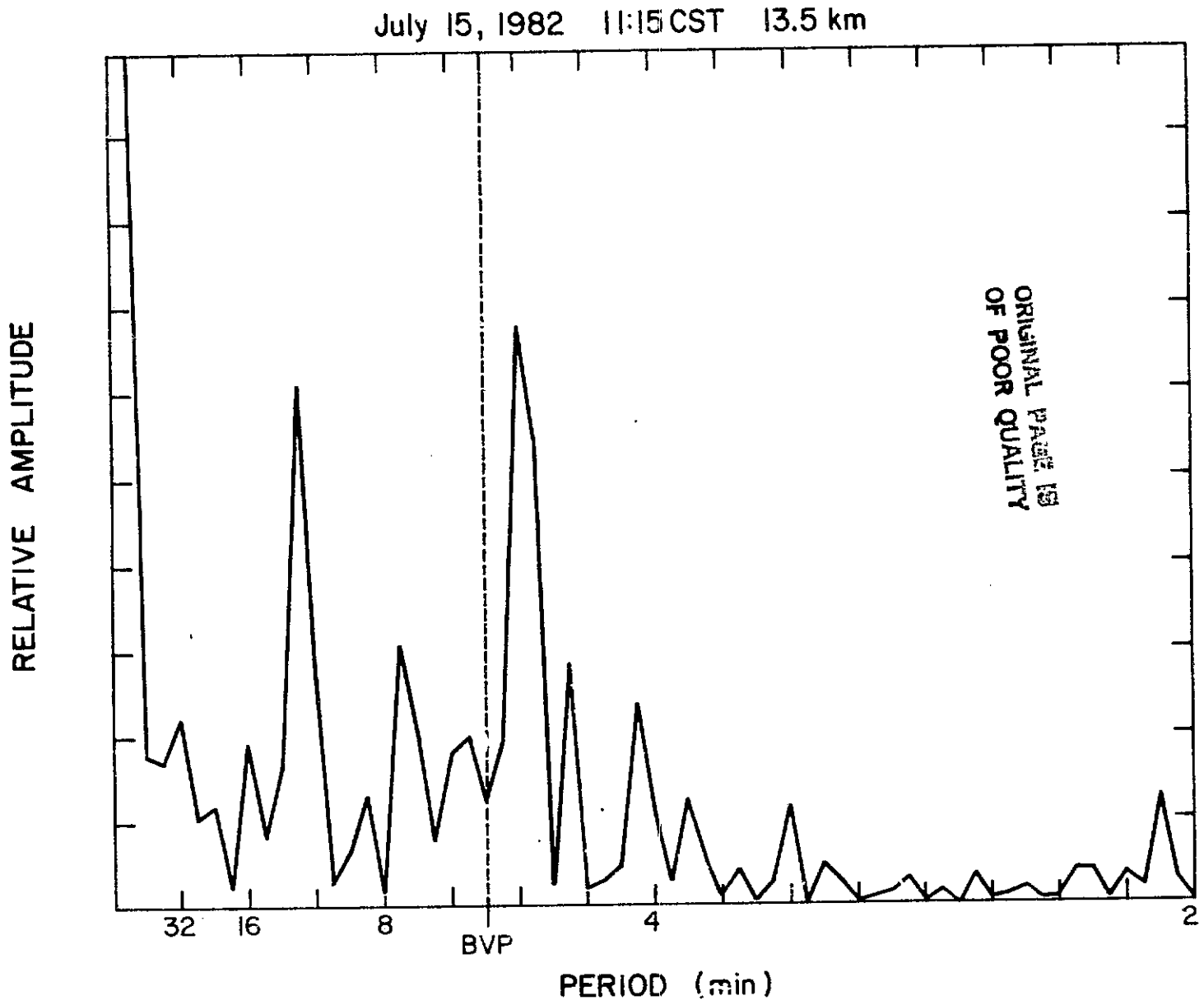

Figure 4.25 Power spectrum of two hours of line-of-sight velocities beginning at 1115 CST on July 15, 1982 at 13.5 km. Calculated Brunt-Vaisala period is shown.

ORIGINAL PAGE IS
OF POOR QUALITY

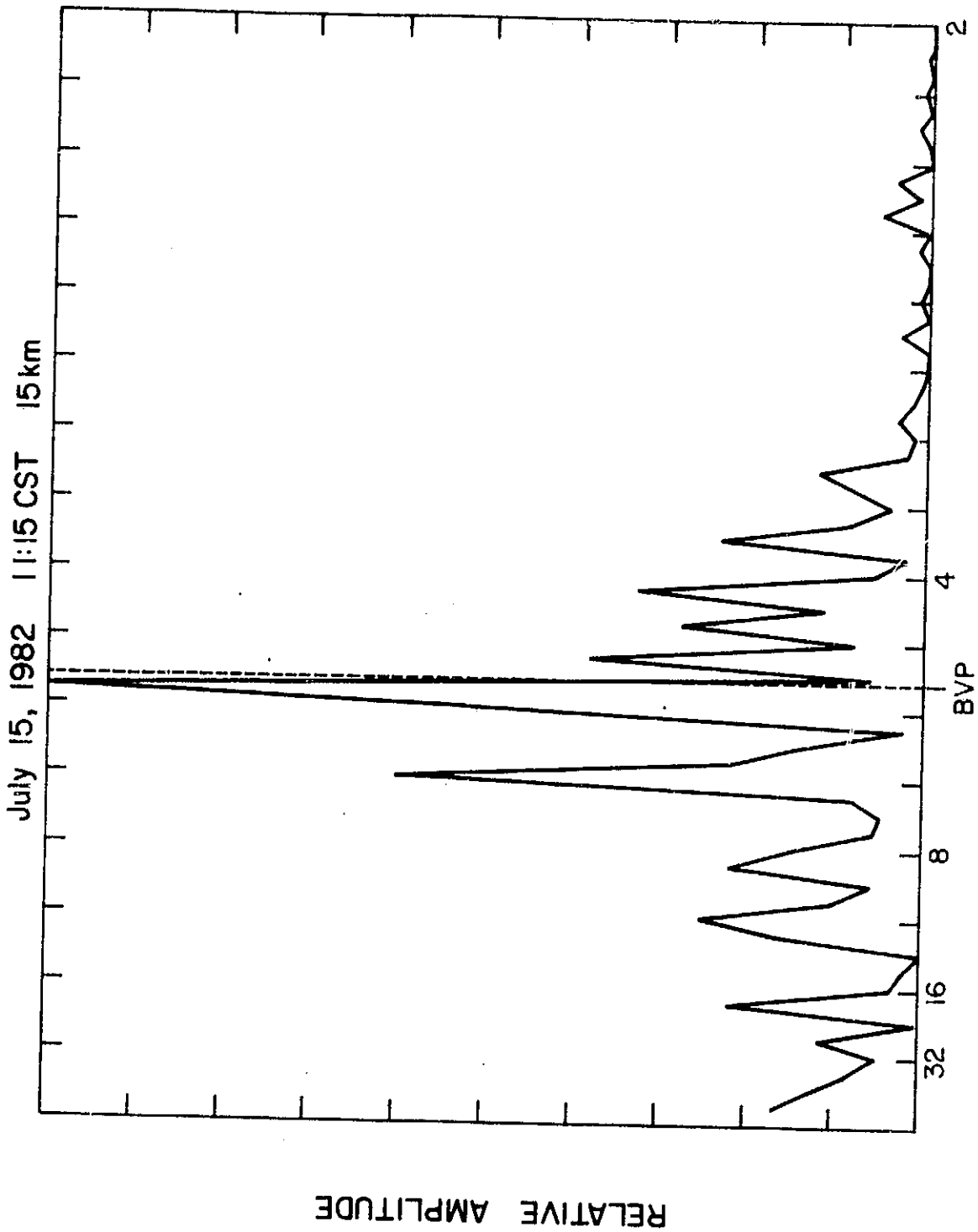

Figure 4.26 Power spectrum of two hours of line-of-sight velocities beginning at 1115 CST on July 15, 1982 at 15 km. Calculated Brunt-Väisälä period is shown.

ORIGINAL PAGE IS
OF POOR QUALITY

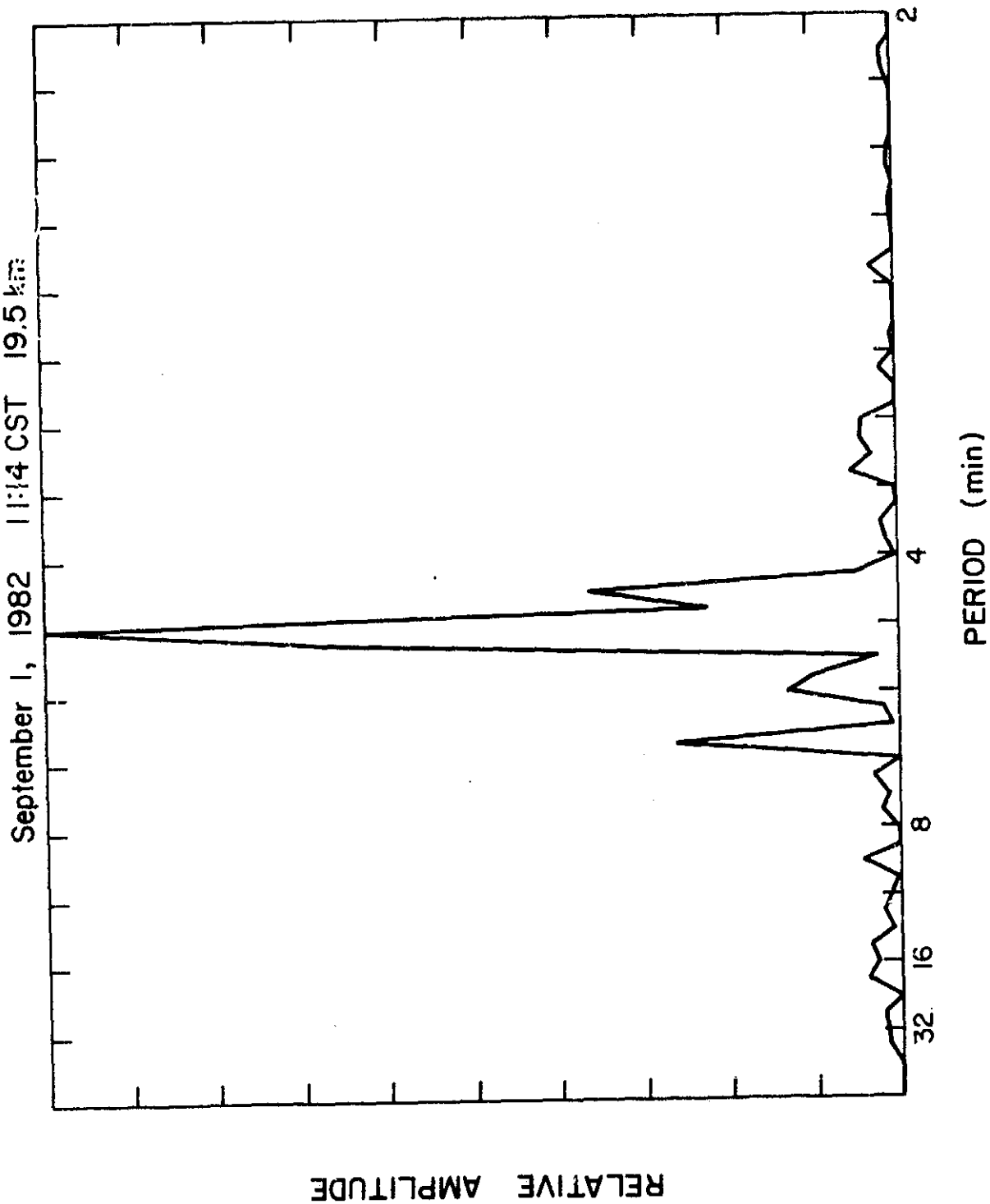

Figure 4.27 Power spectrum of two hours of line-of-sight velocities beginning at 1114 CST on September 1, 1982 at 19.5 km. Thunderstorms were nearby at the time.

dominant periods. This discrepancy is most likely caused by the temporal separation of the observations. When Figures 4.20 and 4.13 are compared, it is evident that the wave period became longer with time. In particular, periods prior to 1000 CST in Figure 4.20 are in the 10-12 min range, much closer to the observed Brunt-Vaisala period.

In contrast to the shift to longer periods at 10.5 km, Figure 4.25 indicates that at 13.5 km a shift to shorter periods is taking place. Spectral peaks are located at 11.6 min and 5.3 min, as compared to 14.2 min and 12.8 min for the previous two-hour time period (Figure 4.21). The spectrum at 15 km, Figure 4.26, shows a main spectral peak at 5.3 min, near the Brunt-Vaisala period of 5.0 min. A longer period component has also appeared at 6.4 min. Thus it seems as though a slight shift toward longer periods is occurring at 15 km. This contrasts with the shift toward shorter periods occurring at 13.5 km.

Minute-by-minute velocities for the spectrum shown in Figure 4.27 were given previously in Figure 3.16. These data were collected after thunderstorms had passed south of the radar site. This is a nearly monochromatic spectrum with a main peak at 4.6 min. This shows that when convective activity is present, one altitude may have line-of-sight velocity fluctuations which occur at nearly a single dominant period for as long as two hours.

5. SUMMARY AND SUGGESTIONS FOR FUTURE RESEARCH

5.1 Summary

The results of this work can be summarized as follows:

1) The Urbana coherent-scatter radar can be used to study the dynamics of the upper troposphere and lower stratosphere on a daily basis.

2) Comparisons of radar- and radiosonde-measured horizontal winds show good agreement. This agreement is generally better in the lower stratosphere where there is less temporal variation in the horizontal winds.

3) Observations in the vicinity of thunderstorms indicate that gravity wave amplitudes increase substantially during periods of intense convective activity. Also, updrafts and downdrafts associated with the storm can be observed.

4) Hourly-averaged scattered power levels are correlated with the hydrostatic stability of the upper troposphere and lower stratosphere.

5) Power spectra of coherently integrated data show changes in echo specularity over both short and relatively long time periods. This is evidence for at least two distinct mechanisms for these changes.

6) Power spectra of line-of-sight velocities clearly show the effects of the change in Brunt-Vaisala period with altitude. In the lower stratosphere, wave spectra can become nearly monochromatic for periods of at least two hours.

5.2 Suggestions for Future Research

5.2.1 Increased altitude resolution. During the course of this work, the Urbana radar was limited to an altitude resolution of 1.5 km for two reasons. First, the transmitter pulse width could not be made shorter than approximately 10 μsec. Second, on the receiving end, the conversion

time of the HP 5610 analog-to-digital converter (ADC) is 10 μsec.

There are many obvious advantages to improving the altitude resolution beyond 1.5 km. Stable layers could be studied in much greater detail. Detailed studies of the structure of turbulent layers would be possible. These turbulent layers are thought to have thicknesses on the order of 100 m [Woodman and Guillen, 1974]. Horizontal wind structure could be observed with much greater precision. At present, in the altitude range 9-16.5 km, radar profiles contain only 6 points while radiosonde profiles contain 13 or 14. Thus, with improved altitude resolution, a more accurate comparison of the two profiles could be made.

Improvements must be made at both the transmitting and receiving ends of the radar system in order to effectively increase altitude resolution. One method commonly used is phase-coding of the transmit pulse. One coding scheme, Barker code, is now available for the Urbana radar [Herrington and Bowhill, 1983]. This Barker code has a baud length of 6 μsec, corresponding to an altitude resolution of 900 m. On the receiving end, a dedicated preprocessor has been designed and built by Zendt and Bowhill [1982]. The preprocessor has two ADCs, one for each output channel of the phase detector. Each ADC has a conversion time of 1 μsec, corresponding to an altitude resolution (on the receiving end) of 150 m. In addition, the preprocessor performs a coherent integration of a user-selectable number of radar pulses.

These two improvements can be utilized to construct a system with an altitude resolution of 900 m. However, the phase-coding method holds a possible disadvantage for lower-atmospheric studies. In order to code the transmit pulse, the total pulse width must be lengthened. Consequently, the lowest observable altitude may increase.

A better alternative exists, however. The recent addition of a voltage overshoot filter on the primary of the pulse transformer allows the transmit pulse width to be decreased to 7 μsec (S. W. Henson, personal communication, 1983). Replacing the present pulse transformer with an available smaller one should allow the pulse width to be decreased to 3 μsec, which is the specified lower limit of the transmitter. Together with the preprocessor, this yields an altitude resolution of 450 m, more than 3 times the resolution used for this work.

5.2.2 Low altitude observations. Another important improvement to the present system would be a substantial decrease in the lowest observable altitude. The present lowest altitude of 9 km is still above the altitude at which most weather systems are located. Lower altitude capability would permit studies of many interesting phenomena. For example, frontal passages could be studied on a real-time basis. Of course, increased range resolution would also be essential to a study of this type. The temperature gradient at the frontal boundary will show up on the radar power returns. Another example would be a study of fair weather cumulus convection and how it affects the dynamics of the atmosphere above.

5.2.3 Faster data analysis. Finally, improvements are needed in the data analysis system. At the present time, collected data must be channeled through 4 separate computers at 2 different locations before it can be plotted. This process usually takes at least 2 full days to complete. A system which employs the same computer, or same type of computer, to do both the collection and processing of the data would be desirable. In addition, the computer used to collect the data could also provide some real-time analysis capability. This analysis could be displayed to aid the operator in pinpointing trouble with the radar system or in helping him make adjustments to the radar system so that the best possible data can be collected.

REFERENCES

Allman, M. E. and S. A. Bowhill [1976], Feed system design for the Urbana incoherent-scatter radar antenna, Aeron. Rep. No. 71, Aeron. Lab., Dept. Elec. Eng., Univ. Ill., Urbana-Champaign.

Balsley, B. B., W. L. Ecklund, D. A. Carter and P. E. Johnston [1980], The MST radar at Poker Flat, Alaska, Radio Sci., 15, 213-223.

Balsley, B. B. and K. S. Gage [1980], The MST radar technique: Potential for middle atmospheric studies, Pure Appl. Geophys., 118, 452-493.

Beer, T. [1974], Atmospheric Waves, Halsted Press, NY, pp. 54-56.

Booker, H. G. and W. E. Gordon [1950], Theory of radio scattering in the troposphere, Proc. IEEE, 38, 401-412.

Bowles, K. L. [1964], Radio wave scattering in the ionosphere, Advances in Electronics and Electron Physics, 17, 55-176.

Carlson, H. C. and N. Sundararaman [1982], Real-time jetstream tracking: National benefit from an ST radar network for measuring atmospheric motions, Bull. Amer. Met. Soc., 63, 1019-1026.

Czechowsky, P., J. Klostermeyer, J. Rottger, R. Ruster, G. Schmidt and R. F. Woodman [1976], The SOUSY-VHF-radar for tropo-, strato- and mesospheric sounding, Preprints, 17th Radar Meteor. Conf., 343-347.

duCastel, F. [1966], Tropospheric Radio Wave Propagation Beyond the Horizon, English ed., Pergamon, Oxford.

Ecklund, W. L., D. A. Carter and B. B. Balsley [1979], Continuous measurement of upper atmospheric winds and turbulence using a VHF doppler radar: preliminary results, J. Atmos. Terr. Phys., 40, 983-994.

Fukao, S., S. Kato, T. Aso, M. Sasada and T. Makihira [1980], Middle and upper atmosphere radar (MUR) under design in Japan, Radio Sci., 15, 225-231.

Fukao, S., T. Sato, N. Yamagaki, R. M. Harper and S. Kato [1982], Winds measured by a VHF Doppler radar and rawinsondes: Comparisons made on twenty-six days (August-September 1977) at Arecibo, Puerto Rico, J. Appl. Met., 21, 1357-1363.

Gage, K. S. [1983a], Jet stream related observations by MST radars, Preprints, MAP Workshop on Technical Aspects of the MST Radar, May 23-27, 1983, Urbana, IL.

Gage, K. S. [1983b], On the morphology of the scattering medium as seen by MST/ST radars, Preprints, MAP Workshop on Technical Aspects of the MST Radar, May 23-27, 1983, Urbana, IL.

Gage, K. S. and B. B. Balsley [1978], Doppler radar probing of the clear atmosphere, Bull. Amer. Met. Soc., 59, 1074-1093.

Gage, K. S. and B. B. Balsley [1980], On the scattering and reflection mechanisms contributing to clear air radar echoes from the troposphere, stratosphere, and mesosphere, Radio Sci., 15, 243-257.

Gage, K. S., D. A. Carter and W. L. Ecklund [1981], The effect of gravity waves on specular echoes observed by the Poker Flat radar, Geophys. Res. Lett., 8, 599-602.

Gage, K. S. and J. L. Green [1978], Evidence for specular reflection from monostatic VHF radar observations of the stratosphere, Radio Sci., 13, 991-1001.

Gage, K. S. and J. L. Green [1980], Prospects for a quantitative measurement of atmospheric stability using VHF radar, Preprints, 19th Radar Meteor. Conf., 605-612.

Gibbs, K. P. and S. A. Bowhill [1979], The Urbana coherent-scatter radar: synthesis and first results, Aeron. Rep. No. 90, Aeron. Lab., Dept. Elec. Eng., Univ. Ill., Urbana-Champaign.

Gibbs, K. P. and S. A. Bowhill [1983], An investigation of turbulent scatter from the mesosphere as observed by coherent-scatter radar, Aeron. Rep. No. 110, Aeron. Lab., Dept. Elec. Eng., Univ. Ill., Urbana-Champaign.

Green, J. L., K. S. Gage and T. E. Van Zandt [1979], Atmospheric measurements by VHF pulsed Doppler radar, IEEE Trans. on Geosci. Elec., GE-17, 265-280.

Green, J. L., J. M. Warnock, R. H. Winkler and T. E. Van Zandt [1975], A sensitive VHF radar for the study of winds, waves, and turbulence in the troposphere, stratosphere and mesosphere, Preprints, 16th Radar Meteor. Conf., 313-315.

Hardy, K. R., D. Atlas and K. M. Glover [1966], Multiwavelength backscatter from the clear atmosphere, J. Geophys. Res., 71, 1537-1552.

Harper, R. M. and W. E. Gordon [1980], A review of radar studies of the middle atmosphere, Radio Sci., 15, 195-211.

Herrington, L. J. and S. A. Bowhill [1983], Phase modulating the Urbana radar, Aeron. Rep. No. 109., Aeron. Lab., Dept. Elec. Eng., Univ. Ill., Urbana-Champaign.

Hess, G. C. and M. A. Geller [1976], The Urbana meteor-radar system: Design, development and first observations, Aeron. Rep. No. 74, Aeron. Lab., Dept. Elec. Eng., Univ. Ill., Urbana-Champaign.

Hines, C. O. [1960], Internal atmospheric gravity waves at ionospheric heights, Can. J. Phys., 38, 1441-1481.

Little, C. G. [1972], Status of remote sensing of the troposphere, Bull. Amer. Meteor. Soc., 53, 936-949.

Miller, K. L., S. A. Bowhill, K. P. Gibbs, and I. D. Countryman [1978], First measurements of mesospheric vertical velocities by VHF radar at temperate latitudes, Geophys. Res. Lett., 5, 939-942.

Rottger, J. [1980a], Structure and dynamics of the stratosphere and mesosphere revealed by VHF radar investigations, Pure Appl. Geophys., 118, 494-527.

Rottger, J. [1980b], Reflection and scattering of VHF radar signals from atmospheric refractivity structures, Radio Sci., 15, 259-276.

Royrvik, O., K. P. Gibbs and S. A. Bowhill [1982], VHF power scattered from the mesosphere at mid-latitudes, J. Geophys. Res., 87, 2501-2508.

Strauch, R. G., M. T. Decker and D. C. Hogg [1982], An automatic profiler of the troposphere, Preprints, 20th Aerosp. Sci. Meeting, January 11-14, 1982, Orlando, Florida.

Woodman, R. F. and A. Guillen [1974], Radar observations of winds and turbulence in the stratosphere and mesosphere, J. Atmos. Sci., 31, 493-505.

Zendt, F. and S. A. Bowhill [1982], A preprocessor for the Urbana coherent-scatter radar, Aeron. Rep. No. 102, Aeron. Lab., Dept. Elec. Eng., Univ. Ill., Urbana-Champaign.